

CCEER 88-1

A PRELIMINARY STUDY OF
ONE-WAY REINFORCED CONCRETE PIER
HINGES SUBJECTED TO SHEAR AND FLEXURE

J. Orié
M. Saiidi

A Report to
The National Science Foundation
Research Grants ECE-8317139

Civil Engineering Department
University of Nevada, Reno

January 1988

ACKNOWLEDGEMENTS

The study presented in this report was part of a continuing investigation at the University of Nevada, Reno (UNR) on the seismic response of highway bridges. The project was in part funded by Grant ECE-8317139 from the National Science Foundation. The statements in this report are those of the authors and do not necessarily present the view of the National Science Foundation.

Many thanks are due to Miss Chris Archer for her careful typing of this report.

Special thanks are given to Mr. Jesus Pedroarena, Civil Engineering technician, for his assistance and technical expertise during the testing stage of the project.

ABSTRACT

One-way reinforced concrete bridge column-to-foundation hinge connections were studied. Four specimens representing one-eighth scale models of the one-way hinges found on the Rose Creek bridge were built and tested. The specimens were subjected to uniaxial moment transfer in the strong direction.

Variables in the test were (a) shear-span to depth ratio and (b) monotonic versus cyclic behavior. Results from part (a) of the test indicated that shear resistance was primarily derived from aggregate interlock of the concrete within the compression zone, and not along the entire section depth as is assumed in the current design practice which is based upon shear friction theory. Results from part (b) of the test indicated that the reversal of load reduced the shear stiffness of the hinge considerably and that shear stiffness provided by the dowels was very small, thus reducing the energy absorption capacity of the hinge during earthquakes.

TABLE OF CONTENTS

	Page	
1	INTRODUCTION	
	1.1 Background.....	1
	1.2 Previous Work.....	3
	1.3 Object and Scope.....	6
2	EXPERIMENTAL	
	2.1 Introductory Remarks.....	8
	2.2 Test Specimens.....	8
	2.3 Materials and Fabrication.....	9
	2.4 Equipment.....	10
	2.5 Test Procedure.....	12
3	RESULTS FROM TESTING OF HINGED SPECIMENS	
	3.1 Introductory Remarks.....	17
	3.2 Load-Deflection Response.....	17
	3.3 Strain Distribution.....	21
4	INVESTIGATION OF BOND STRENGTH FOR PLAIN BARS	
	4.1 Introductory Remarks.....	22
	4.2 Test Specimens.....	22
	4.3 Test Setup.....	23
	4.4 Experimental Results.....	24
	4.5 Analysis of Test Results.....	24
5	ANALYSIS OF HINGED SPECIMENS	
	5.1 Introductory Remarks.....	27
	5.2 Flexural Analysis.....	28
	5.3 Shear Analysis.....	30
	5.4 Rotation Calculations.....	33
	5.5 Deflection Calculations.....	37
6	SUMMARY AND CONCLUSIONS	
	6.1 Summary.....	42
	6.2 Observations.....	43
	6.3 Conclusions.....	45
	REFERENCES.....	47
	TABLES.....	49

APPENDICES

Appendix A	
Mix Design.....	98
Appendix B	
Material Properties.....	99
Appendix C	
Instructions for Program AQUIREDAT.....	101
Appendix D	
Notation.....	111
Appendix E	
List of CCEER Publications.....	113

LIST OF FIGURES

	Page
2.1 Elevation of Rose Creek Interchange Pier and Hinge Cross Section.....	52
2.2 Test Specimens and Location of Reinforcing Bars and Strain Gages.....	53
2.3 Middle Segment After Curing.....	54
2.4 Flowchart for Data Acquisition Program AQUIREDAT.....	55
2.5 Location of Displacement Measuring Devices.....	56
2.6 Test Setup for Specimens CH4 and CH1.....	57
2.7 Specimen CH3 Midway Through the Test.....	58
2.8 Specimen CH4 in Early Stages of Testing.....	59
2.9 Specimen CH1 at End of Test.....	60
2.10 Hinge Region of Specimen CH3 at Later States of Testing..	61
2.11 Loading Cycle for Test Specimen CH4.....	62
3.1(a) Measured and Computed Load-Deflection Diagram for Specimen CH1.....	63
3.1(b) Measured and Computed Load-Deflection Diagram for Specimen CH2.....	64
3.1(c) Measured and Computed Load-Deflection Diagram for Specimen CH3.....	65
3.1(d) Measured and Computed Load-Deflection Diagram for Specimen CH4.....	66
3.2(a) Measured and Computed Load-Rotation Diagram for Specimen CH1.....	67
3.2(b) Measured and Computed Load-Rotation Diagram for Specimen CH2.....	68
3.2(c) Measured and Computed Load-Rotation Diagram for Specimen CH3.....	69
3.2(d) Measured and Computed Load-Rotation Diagram for Specimen CH4.....	70

LIST OF TABLES

	Page
5.1(a) Measured and Computed Yield Loads, Specimen CH1.....	49
5.1(b) Measured and Computed Yield Loads, Specimen CH2.....	49
5.1(c) Measured and Computed Yield Loads, Specimen CH3.....	50
5.1(d) Measured and Computed Yield Loads, Specimen CH4.....	50
5.2 Results from Shear Analysis.....	51

3.3(a)	Measured Load-Slip Deformation for Specimen CH3.....	71
3.3(b)	Measured Load-Slip Deformation for Specimen CH4.....	72
3.4	Response of Hinged Specimen when Subjected to Load Reversals.....	73
3.5	Load c. Cycle Number for a Ductility of 2.5.....	74
3.6	Load c. Cycle Number for a Ductility of 5.0.....	75
3.7	Strain Distribution in Right Side Gages, Specimen CH1.....	76
3.8	Strain Distribution in Left Side Gages, Specimen CH1.....	77
3.9	Strain Distribution in Right Side Gages, Specimen CH2.....	78
3.10	Strain Distribution in Left Side Gages, Specimen CH2.....	79
3.11	Strain Distribution in Right Side Gages, Specimen CH3.....	80
3.12	Strain Distribution in Left Side Gages, Specimen CH3.....	81
3.13	Strain Distribution in Right Side Gages, Specimen CH4.....	82
3.14	Strain Distribution in Left Side Gages, Specimen CH4.....	83
3.15	Strain Distribution in Left Side Gages, Specimen CH4.....	84
4.1	Elongation of a Steel Bar Embedded in Concrete.....	85
4.2	Bar Slip Mechanism in a Reinforced Concrete Element.....	85
4.3	Test Setup for Push-out Specimens.....	86
4.4	Measured Load vs. Slip Results for the Push-out Specimens.....	87
4.5	Assumed Typical Steel Stress and Bond Stress Distribution.....	88

4.6	Assumed Steel Stress and Bond Stress Distribution for Push-out Specimens.....	88
4.7(a)	Measured and Computed Load vs. Elongation, Push-out Specimen #1.....	89
4.7(b)	Measured and Computed Load vs. Elongation, Push-out Specimen #2.....	90
4.7(c)	Measured and Computed Load vs. Elongation, Push-out Specimen #3.....	91
5.1	Idealized Stress-Strain Curve for Concrete [12].....	92
5.2	Moment-Curvature Diagram of 2" x 12" Section.....	93
5.3	Mechanisms for Dowel Shear.....	94
5.4	Idealized Bond Stress Distribution for Hinged Specimens.....	95
5.5	Bar Slip Mechanism in a Typical Reinforced Concrete Base Element.....	96
5.6	Assumed Bar Slip Mechanism in Hinged Specimens.....	96
5.7	Cantilevered End Element.....	97
5.8	Idealized Curvature Distribution Along the Cantilevered Element.....	97
B.1	Idealized Stress-Strain Curve for #2 Plain Bars.....	100

CHAPTER 1

INTRODUCTION

1.1 Background

Reinforced concrete hinges have been used for well over half a century. They are frequently used in reinforced concrete bridges such as can be found on modern interstate highways throughout the world [17]. Hinges function as the connecting link between the bridge deck and the supporting column and as the connecting link between the column and the foundation.

The basic type of reinforced concrete (R/C) hinge that is most commonly used in short columns supporting multi-span bridges is the Freyssinet hinge. In the basic hinge, little or no reinforcement passes through the throat of the hinge and it is recognized that the strength of the concrete in the hinge is considerable, and is thus counted on for most of the strength of the hinge. Reinforcing steel is used to aid in providing shear resistance as well as increasing the bearing strength. This type of connection may also incorporate a shear key in the hinging region.

There are two types of column hinges, one-way and two-way (uniaxial and biaxial). One-way hinges are usually used in single column pier bents, whereas two-way hinges are often used in multicolumn pier bents.

The purpose of a hinge is to allow for relative rotation of connecting elements and prevent a build-up of flexural stresses. In a highway bridge with single column bents, the one-way hinge is positioned so that it allows for rotation about a transverse axis

(perpendicular to the road axis or nearly so). Hinging is needed in this direction to prevent a build-up of flexural stresses on the foundation systems. This is particularly important in bridges supported on soft soil. In the transverse direction the hinge must be designed to prevent a shearing or flexural failure such as could be caused by excessive wind or inertia forces due to an earthquake. Severe earthquakes subject a bridge to load reversals, therefore, connecting elements such as hinges must have adequate energy dissipating characteristics. Additionally, the hinge must be designed to support the axial compressive load of the bridge superstructure.

Two-way hinges allow rotation in the longitudinal and transverse direction of the bridge. Rotation in the longitudinal direction is needed for the same reasons as previously mentioned for one-way hinges. In addition, in the case of relative settlement of some of the foundations, the hinge action of two-way hinges prevent a build-up of forces in the superstructure.

Little is known about the behavior of bridge column-to-foundation one-way hinge connections subjected to a combined shear and flexure loading in their moment-resistant direction. However, there have been tests to determine the bearing, flexural, and shear capacity under monotonic and cyclic loading applied in the weak direction (direction of hinging). This type of connection is currently designed [5] based upon the axial compressive capacity of the section according to ACI 318-83 section 10.3.5. and designed for shear based upon the shear friction theory (ACI 318-83 section 11.7) [1]. Whether the shear friction theory is applicable to column hinges is not certain. Research is necessary, therefore, to increase the knowledge of hinge

design and to give insight into the behavior of hinges with the possibility of leading to a more rational design.

1.2 Previous Work

There appears to be no information regarding one-way hinges tested with a shear or flexural load applied transverse to the direction of hinging (the strong direction), however, there have been tests to determine the bearing, flexural, and shear capacity under monotonic and cyclic loading in the direction of hinging.

Base performed research on four prototype R/C hinges with loading in the direction of hinging [3]. Two were, essentially, Freyssinet hinges, with very little reinforcement through the throats, the third was designed as a Messenger hinge, and the fourth was a saddle bearing hinge. He applied a series of four different loadings: axial load only; combined axial load and shear load; axial load with cyclic flexural load. From the results of these tests he concluded that the specimens were able to carry design loads with ample factors of safety and permit rotations greatly in excess of design requirements. In addition, Base noted that the compressive stress in the concrete of the throats of the hinges reached values several times the cube strength of the concrete without causing crushing of the concrete. He also discovered that reinforcement through the throat appeared generally unnecessary. The static shear resistance of the hinges appeared to be more than adequate and only considerations of impact shear loading indicated a desirability for crossed bar reinforcement to aid in shear resistance.

Much research has been done on testing of shear transfer behavior

of shear friction type connections using "push-off" and "pull-off" tests [2,13,14,21]. Because the column-to-foundation R/C hinge connection is designed using the shear friction concept, this research was examined. The specimens used for the push-off tests (subsequently referring to push-off and pull-off specimens) are similar to the one-way hinge connections in that they consist of reinforcement distributed throughout the depth of the section across the shear failure line. Another point of similarity is that there is an initial crack at the interface of the column and foundation in the R/C hinge connection. Likewise, some of the push-off specimens had initial cracking at the connection interface. In both cases the crack was formed due to concrete on both sides of the crack interface being cast at different times. Most of the shear friction specimens had a shear span to depth ratio (l/h) less than or equal to 1, whereas hinge connections used in bridge columns typically have a nominal l/h ratio which may be 3 or higher.

It was discovered that when an initially cracked specimen is loaded monotonically in shear, slip will occur along the crack interface [2,13,14,21]. Since the crack tends to be rough, the sliding causes a separation which, in turn, causes tension in the reinforcement across the section. To maintain equilibrium, a compression force is produced in the section. This compressive force produces a frictional resistance to sliding at the interface. With sufficient separation, the reinforcement is stressed to yielding. At ultimate condition, therefore, the compression force exceeds the yield strength of the reinforcement due to strain hardening. The frictional

resistance to shear is then at least equal to the yield strength multiplied by a coefficient of friction at the concrete interface. Sliding along the crack face also subjects the reinforcing bars to a shearing action, sometimes referred to as dowel action.

Under load reversals an initially cracked specimen behaves slightly different. After one load reversal the specimen builds up residual tensile strains in the reinforcement which prevents the crack along the shear plane from closing immediately as the load is reversed [7,16,19]. As a result the shear is transferred by dowel action and some aggregate interlock. The shear stiffness is consequently much lower than in the first load cycle. The specimen exhibits slip equal to the previous maximum slip until asperities again come into bearing. The resistance of asperities to deformation results in a sharp increase in resistance to shear. Further load reversals result in similar behavior until the surfaces in contact are abraded and become smoother, reducing the resistance to shear.

As noted, some shear along the crack interface, or shear plane, is resisted by dowel action; i.e. direct resistance of the bars to shearing action. Dowel strength can be developed by three mechanisms: the flexure of the reinforcing bars, the shear strength across the bars, and the kinking of the reinforcement. The yield strength of the bar in flexure and shear, however, cannot be fully utilized for dowel action if the bar is to provide a clamping or compressive force, as well [15]. Tests by Pauley, et al. [16] indicate that kinking is likely to be the major source of dowel strength, particularly when small size bars are used. In these tests it was observed that for large dowel forces to be developed, large shear slip must occur. At

smaller values of slip (0.01 inch considered acceptable within limits of structural usefulness) there is considerably larger shear resisted by aggregate interlock than dowel action.

1.3 Object and Scope

The primary objective of this investigation was to carry out a pilot study of the behavior of bridge column-to-foundation one-way hinge connections subjected to uniaxial moment transfer with loading applied transverse to the direction in which the hinge is designed to rotate. The effect of axial force was excluded to simplify the testing. This would lead to a conservative estimate of the shear strength. In practice, the case of zero axial force in columns could occur during strong earthquakes. Four column-to-foundation subassemblages were built and tested. Three of the specimens were tested monotonically with a varying shear-span to depth ratio of 1, 2, or 3, while the fourth specimen was tested cyclically. In this test a ratio of 3 which closely represents actual single height to width ratios was used. The specimens were built in the form of a beam with adjacent end sections representing single column piers connected to a middle section representing a foundation. A point load was applied in the middle at the foundation section. By applying a point load in the center and simply supporting the ends, this produced the same effect as loading one end of a cantilevered column with the other end attached to a fixed base. The applied load created a combined shear and flexural loading on the hinge connection.

The object of one portion of the investigation was to determine the effect of varying the shear span on the shear and flexural

capacity of the hinge and to determine a limiting shear span to produce a shear failure. By decreasing the shear span, the shear effect became dominant.

During the cyclic tests, slow reversals of load up to and beyond yield capacity were applied. The object of this portion of the investigation was to obtain a general insight into the effect of load reversals on shear and flexural strength and give an indication of the energy dissipation.

Calculations were performed to determine deflection and rotation. Also included was an examination of the current method of analysis and design to try and determine any improvements that could be made.

During testing of the hinge connections, appreciable bar slippage was observed. This prompted a study in which tests were performed on 3 "push-out" specimens to determine the bond characteristics between the plain reinforcing bars and the concrete in order to better predict the load-deflection characteristics of the specimens.

CHAPTER 2

EXPERIMENTAL STUDIES ON HINGE SPECIMENS

2.1 Introductory Remarks

Four model column-to-foundation connections representing one-eighth scale replicas of the hinges used in piers 2 and 3 of the Rose Creek bridge were built and tested (Fig. 2.1). The specimens consisted of two end elements representing single column bridge piers and a center portion representing the foundation (Fig. 2.2). The specimens were cast and tested in the horizontal position with no axially applied loads at the end of the column sections. They were loaded in combined shear and flexure in the strong direction.

Three specimens were tested monotonically and one cyclically. The shear-span to depth ratio (l/h) was different in each test. This chapter describes the test specimens, equipment, and procedure used for testing.

2.2 Test Specimens

The hinge specimens (Fig. 2.2) consisted of three separate concrete segments; two 6"x12"x39" end segments and one 6"x12"x17" center segment linked together with 6 #2 plain reinforcing bars. The reinforcement was placed along the length of the specimen and were spaced 2 inches o.c. with one inch of cover on the top and bottom. The reinforcement was centered within the 6 in. width of the specimen. The middle portion represented a model foundation and the two end portions represented single column bridge piers. At the junction between the end and middle sections there was a hinge region that was formed by a 2"x12"x1/4" keyway. The hinging region was formed by casting a 1/4" by

2" keyway in the middle section adding 1/4" styrofoam inserts, and scraping the hinge throat area to a roughness amplitude of 1/4" before the end sections were cast. Figure 2.3 is a picture of the middle segment after curing. The reinforcing bars and the strain gage wires coming out of the center are shown. This created a cross-sectional area of 24 sq. in. with a reinforcement ratio of 1.25% at the hinge throat. The steel ratio in piers 2 and 3 of the Rose Creek bridge was 1.27%.

2.3 Materials and Fabrication

Grade 40 plain #2 (0.25 in. dia.) bars with a yield stress of 43 ksi were used in all of the specimens. Deformed #2 bars would be more representative of the actual steel but they were not available at the time of fabrication.

The proportion of the concrete mix, (given in ratios of cement: fine aggregate: coarse aggregate by weight) was 1.0:2.44:2.31 for all specimens. Type I-II low alkali cement was used. Aggregate was obtained from a local pit and was sieved to remove any particles larger than 1/2 inch. The coarse aggregate used in all hinge specimens was well graded and conformed to grading size number 8 of ASTM C33. The fine aggregate was not well graded and had a fineness modulus of 4.3.

Concrete was mixed in a 4 cubic foot revolving drum mixer with a mixing time of approximately 10 minutes. Three 6 x 12 in. concrete cylinder were prepared for each of the middle sections and also for the end sections. Compression testing was done at 14 days, 28 days, and on the day each specimen was tested. Mix Design and material

properties are presented in Appendices A and B.

Formwork was built from 2x4's and 3/4 in. plywood. The forms were cleaned and coated with oil prior to casting to facilitate stripping.

The three sections were poured separately to model in-situ practices of first casting the foundation and then the piers. The middle section of each specimen was cast first and placed in a moist cure room (Fig. 2.3). After one day of moist curing, the concrete in the 2 in. wide hinge regions was roughened to an amplitude of approximately 1/4" to ensure a good bond between concrete cast at different times. The middle portion was moist cured for a total of three days to allow for sufficient hardening at which time the end sections were cast and the entire specimen was moist cured for one week. At this time the forms were struck and the specimens were cured at room temperature and humidity until time of testing.

The four specimens were labeled CH1 through CH4. The following table indicates the l/h ratios, and the type of loading used for each specimen.

Specimen	l/h	Load Type
CH1	3	monotonic
CH2	2	monotonic
CH3	1	monotonic
CH4	3	cyclic

2.4 Equipment

A Hewlett Packard 9000 series microcomputer along with a 3054 data acquisition system were used to record data from the electrical sensing devices. The purpose of the data acquisition unit is to record

a change in voltage in the electrical or electro-mechanical measuring device. Through computer software this information is recorded and converted to information such as strain or displacement [4]. The computer is the controller for the data acquisition unit and is also useful for storing and processing the data, such as producing plots of load vs. strain or load vs. displacement. Figure 2.4 illustrates a flow chart of the computer program that was developed and used for acquiring data. The instructions to execute the program are presented in Appendix C.

Eight Micromeasurements type EA-06-140LZ-120 quarter bridge strain gages were mounted on reinforcing bars within each specimen (Fig. 2.2). The gages were bonded to the side of the rebar and located in the center of the 1/4 in. hinging region. Gages were bonded to the reinforcing bars with Devcon 5-minute epoxy cement. At points where gages were applied the bars were sanded smooth and the surface was cleaned with Budd cleaning solvent #1. The gages were then sealed with a layer of electrical tape and a coat of clear silicon rubber sealant.

A Celesco displacement transducer was used to measure centerspan deflection and two Schaevitz type 2000 DC-D linear variable differential transformers (LVDT's) along with two micrometer dial gages were used as a means of recording rotation of the center portion of the model relative to the end sections. The LVDT's were mounted on the pier section of the specimen by epoxy bonding the LVDT support to the concrete. One end of an aluminum rod was connected to the inner core of the LVDT and the other end was connected to a bracket that was epoxy bonded to the foundation section. This bracket allowed for rotation so that the aluminum rod would not bend and cause the LVDT

core to bind with the rod, thus giving a possible erroneous electrical output signal. A dial gage was also used as a back-up to the Celesco. In tests of specimens CH3 and CH4 two dial indicators were used to measure vertical slip between the middle and end sections. Figure 2.5 shows a typical set-up of the location of the displacement measuring devices. The Celesco displacement transducer and the dial gage for the center displacement are not shown. Figure 2.6 shows a picture of the test setup used for specimen CH4. Specimen CH1 was also tested in this frame. The computer and data acquisition unit can be seen on the right side of the picture. This picture also indicates the location of dial gages and LVDT's along with the loading ram and the dial gage just to the right of the loading ram that was used for measuring centerspan deflection. Figures 2.7 and 2.8 are photographs of specimens CH2 and CH3, respectively. These photos depict the testing apparatus and location of measuring devices used for these tests.

2.5 Test Procedure

Testing procedure varied in each test due to the different support position and test set-ups. The general procedure of loading to a predetermined load and pausing to record data was followed in each test. As soon as the load was reached the data acquisition unit was triggered to record the electrical strain and displacement data. Dial gage readings were then taken and recorded on data sheets. An outline of the loading procedure, support conditions, and failure mode for each specimen is as follows.

Specimen CH1

In this test an l/h ratio of 3, which approximates the nominal aspect ratio of the Rose Creek bridge columns, was used. CH1 was set up on simple supports that consisted of a one inch diameter bar welded to the top of a built up steel section. This did not allow the hinge specimen to rotate freely about the ends, therefore, the rotation and separation at the hinges in both sides of the specimen was not completely symmetrical.

Since this was the first specimen tested it was not certain how much deflection would occur. A space of 3 inches was allowed between the bottom of the specimen and the test frame.

After a mini-cycle in which a preload of 840 lbs. was applied, the specimen was loaded continuously until there was no room for further travel on the load ram. At this point the specimen still exhibited reserve capacity, therefore, the specimen was unloaded and steel plates were placed in between the load ram and specimen to increase the travel of the ram. The specimen was again loaded until there was little room left for further displacement. Figure 2.9 is a photo of specimen CH1 at the end of the test. Notice the large rotations that occurred. Also, notice that the concrete began to crush at the very top of the hinge region, and that unsymmetrical rotations occurred indicated by the different crack widths on both sides of the middle segment.

The failure mode in CH1 was dominated by flexure, with crushing of concrete in the compression zone and all but the top bar yielding in tension. The large hinge rotations that were observed were dominated by bond slip rotations. Separation occurred along the crack

interface between the foundation and column portions with no other shear or flexure cracks occurring. The cracks at both interfaces initially began opening in the tension zone and progressively opened as the neutral axis moved to within one inch of the extreme compression fiber by the end of the test.

Specimen CH2

The supports were moved in to provide an $l/h=2$. By moving the supports in, the effect of shear was increased. The simple supports used for CH1, were again used in this test, however, oil was placed between the roller support and bearing plate on CH2.

This specimen was preloaded to 500 lbs. to test instrumentation. It was then continuously loaded until the load dropped to 88% of peak load. The specimen had a centerspan displacement of almost 6 in. at this point.

The supports again did not allow for symmetric hinge rotations, and as a result, the right column rotated and separated much more than the left. Specimen CH2 also had large flexural deformations and large hinge rotation dominated by bond slip rotation. The strain gages indicated that all bars yielded, the lower five bars in tension and the uppermost bar in compression. There was sufficient slip between the foundation and column portions to engage the shear key. As a result, near the end of the test an approximately 45° crack was formed in the top corner of the foundation section.

Specimen CH3

The supports were moved in to provide an $l/h=1$, further

increasing the effect of shear. The supports were altered slightly by removing the welded bar and replacing it with a small (approx. 1 in. wide) steel channel. A steel roller was then placed in the channel, thus, allowing for freedom of movement. This worked well until the roller was pushed against the side of the channel, at which time, unsymmetrical rotation began to occur in the hinge regions.

A preload of 1000 lbs. was applied to test the instrumentation. The specimen was then continuously loaded until it was observed on the load-deflection curve that an increase in displacement does not increase the load appreciably. The specimen was then loaded using displacement control at intervals of 0.1 in. of centerspan deflection until the load dropped significantly.

After yielding CH3 exhibited very large slip deformation between the foundation and column portions. Again the shear key was engaged and a 45° crack formed in the top corner of the foundation portion and by the end of the test the corner block of concrete completely broke off. This can be seen in Fig. 2.10 which also indicates the large amount of separation that occurred. Specimen CH3 also exhibited major flexural deformation with at least the two bottom bars yielding in tension. As in the tests of CH1 and CH2 there were large hinge rotations.

Specimen CH4

A slow cyclic loading was applied to specimen CH4 to observe the effects of load reversal and examine the energy absorption capacity of the hinge region. An $l/h=3$ was used since this more closely represents the nominal aspect ratio in the Rose Creek bridge. In order to apply

load reversals, different supports were required. Supports were made by vertically mounting two pieces of steel channel to a base and slots were cut into the channels for the pinned end of the specimen to fit into. A pinned end was provided for by manufacturing a steel bracket that fit snugly around the column portion of the specimen. Dowels that fit into the slots were welded to these brackets. This support mechanism worked very well, allowing for rotation as well as horizontal displacement of the specimen ends.

Specimen CH4 was loaded using displacement control. It was initially preloaded through a cycle of 0.05 in. displacement and then loaded using the load history shown in Fig. 2.11.

The failure mode of CH4 was dominated by flexural deformations. Upon initial loading to yield, CH4 behaved the same as CH1, with a separation occurring in the tension zone along the hinge interface, and little slip deformation occurring. However, upon successive reversals of load, CH4 exhibited a reduction in shear stiffness as indicated by larger slip deformations. When the load was reversed the crack opened and slip occurred until compression was developed.

CHAPTER 3

RESULTS FROM TESTING OF HINGED SPECIMENS

3.1 Introductory Remarks

The results from the tests of four model hinge specimens are presented in this chapter. Observations of the specimen behavior are outlined. Curves of load vs. centerspan deflection and load vs. average rotation between the middle and end portions are presented for all the specimens along with, load-slip deformation curves for specimens CH3 and CH4. These curves represent the most important data recorded from the tests and give an indication of the rate of stiffness and strength decay in each specimen. Diagrams of strain distribution, recorded from strain gages in the hinge region, are also presented.

3.2 Load-Deflection Responses

Since the hinge was not very strong in the weak direction, there was concern that the hinge might be damaged while removing the specimens from the forms and placing them in the test apparatus. However, this did not happen. Prior to testing it was observed that each specimen appeared to be in very good condition. Minor cracks were visible at the bottom of the hinge throats, but it was not clear how far the cracks extended inside each joint. There were very minimal shrinkage type cracks in the areas outside of the joint region.

Upon loading, all specimens exhibited initial vertical cracks in the tension zone along the hinge interfaces on both sides of the middle stub portion. As the load was increased up to yielding, these cracks continued to open and extend further into the upper portion of

the section, thus moving the neutral axis up. The extent of cracking and separation varied in each test due to varying shear spans and cyclic instead of monotonic loading for specimen CH4. As expected, there were no other flexural cracks occurring in any of the specimens. Large hinge rotations due to bond slip between the reinforcing bars and concrete were observed in every test.

The load-deflection curves for each specimen including measured and calculated values are presented in Figs. 3.1(a) through 3.1(d) and load vs. average rotation curves are presented in Figs. 3.2(a) through 3.2(d). Points at which bars yielded are marked on both the measured and calculated curves. Also included is the calculated ultimate point. The number indicates which layer yielded from the bottom layer (layer 6), to the second layer from the top of the section (layer 2). Note, that no clear cracking point can be observed in the load-deflection diagrams. This indicates that the throat regions were initially cracked. These curves give an indication of the rate of stiffness and strength decay in each specimen. The measured curves will be discussed in Chapter 5. Figures 3.3(a) and 3.3(b) show plots of load-slip deformation for specimens CH3 and CH4.

From the load-deflection curves for specimens CH1, CH2, and CH3 (Figs. 3.1(a-c)) it can be seen that, as the shear span was reduced, the amount of applied load on the specimen and subsequent shear on the hinge region increased. This resulted in a lower applied moment for a given load and an increase in the stiffness of the specimen. This can be observed from the initial linear portion of the curves. The curves show that the yielding of reinforcement is more gradual for CH1 than

for CH2 or CH3, with almost 1 in. of deflection in CH1 before reaching the yield plateau compared to 0.5 in. for CH2 and 0.25 in. for CH1.

Also from the load-deflection curves it can be seen that for specimen CH1 the curve is relatively smooth after yielding. However, as the shear span is reduced for specimens CH2 and CH3 the portion of the curve after yielding becomes more jagged. This reflects the shear and resulting slip of the middle block relative to the side elements. As slip occurred between the middle and end segments the rough concrete asperities in the compression zone at the interface began to crush and grind away. This resulted in slight increases and decreases of load. From Figs. 3.1(c) and 3.3(a) for specimen CH3 the effect of the shear key on the load carrying capacity of the hinge section can be noted. After yielding, the load began to drop initially, but started to increase again. The second increase in load capacity reflects the engagement of the shear key until the sudden drop in load when the corner block of concrete completely broke free from the center portion.

From the load-deflection curve of specimen CH4, the pinching of the hysteresis loops can be noted indicating a reduction in the energy absorption capacity of the hinge region. The load-deflection and load-slip curves indicate that load reversals reduced the shear stiffness of the hinge region substantially. When loaded in one direction after yielding had occurred, a crack opened in the tension zone. When the load was reversed there was a large amount of deflection and slip with a little increase in shear capacity until the crack was closed and compression was developed. The compression resulted in frictional resistance that was the reason for the increase in shear capacity and

in overall stiffness. This is best illustrated in Fig. 3.4. In the negative load region of the final cycle (Fig. 3.1(d), it is noticed that on the portion of the hysteresis curve between 1 in. and -1 in. deflection there is a very small increase in load (=900 lbs.). During this portion of the loading there was a slight separation between the middle and end segments. Thus, the specimen was relying primarily on the shear resistance of the reinforcing bars (known as dowel action) for shear resistance, with slight frictional resistance of the concrete asperities at the hinge interface. This slight increase in capacity suggests that the dowel action does not contribute significantly to the shear strength of the hinge connection.

Figures 3.5 and 3.6 show that for each cycle there was a reduction in load for a given displacement reflecting a reduction in stiffness and in energy absorbing capacity. The positive load side of Fig. 3.5 indicates that the biggest drop in load occurred after the first complete cycle. On the initial cycle the load reached 3600 lbs., however, on the second cycle a load of only 2400 lbs. was reached representing a 33% reduction in load. In the negative load region the drop in load was not as severe. For example, on cycle 2 a load of 3360 lbs. was reached for a deflection of 0.5 in. (displacement ductility of 2.5). On the next cycle the load reached 3050 lbs. A reduction in load of only 9.2%.

Figure 3.6 indicates that at a displacement amplitude of 1.0 in. (displacement ductility of 5) the hinge deteriorated rapidly with each cycle of loading. Between cycles 3 and 5 the load in the hinge was reduced by 50% at an amplitude of 1.0 in. displacement for the

positive load region.

3.3 Strain Distribution

Figures 3.7 through 3.15 show the strain distribution within the hinge section as recorded by strain gages located on the reinforcing bars. Tensile strains are shown as positive quantities. It should be noted that gages were located on the top two and bottom two bars within the section. There were two gages per bar and each was located at the hinge interface on each side of the middle stub portion. The recorded strain values are marked by an asterisk (*) and straight lines are used to connect the recorded strain values at different steel layers. The strain gages give an indication of when various layers of steel have yielded. Linear interpolation is used to determine when the middle two layers of steel yielded. These plots also give an estimate of the location of the neutral axis. The strain gages appeared to be very reliable for strain values up to and slightly past yield strains. However, after significant yielding, most gages displayed a significant jump in strain upon the next load increment instead of a slow increase. This is especially noticeable in the gages located on the bottom bar. At higher values of strain many of the diagrams indicate an erratic strain distribution throughout the section. After yield strains have been reached, the gages may indicate local bending or slippage occurring in the bars.

CHAPTER 4

INVESTIGATION OF BOND STRENGTH FOR PLAIN BARS

4.1 Introductory Remarks

This chapter describes tests that were performed to determine the bond force between plain #2 bars and concrete.

If we consider a steel bar with sufficient development length, subjected to tension, the bar will slip and elongate as shown in Figure 4.1. When a reinforced concrete beam element is subjected to a moment, rotation will occur at the joint face. In addition, the beam may rotate due to the slip between the tensile reinforcement and concrete as shown in Figure 4.2. This additional rotation due to slip between the steel and concrete (referred to as bond slip rotation) can be significant.

During testing of the hinged specimens described in previous chapters, large rotations and deflections were observed. To account for these large rotations and deflections, the effect of bond slip was examined. The method by which the deflection and rotation due to bond slip were calculated are presented in Chapter 5. Small diameter plain bars were used in the hinged specimens. A review of literature showed a scarcity of available information concerning the bond stress distribution between plain bars and the concrete. As a result three push-out test specimens were built to study the effect of bond slippage, and quantify bond strength for #2 plain bars. This chapter describes these tests.

4.2 Test Specimens

Three identical push-out test specimens consisting of a plain #2

bar embedded in a 3.5x3.5x8 in. concrete prisms were built and tested. The bar was 11.75 in. long with a full embedment length of 8 in. The bar stuck out 1 in. at the top of the specimen and 2.75 in. at the bottom. A flat was ground at the top and bottom of the bar and a small aluminum tab was epoxy bonded to the bottom of the bar to provide a larger area to support the tip of the dial gage. The test was performed by pushing on the bar to simplify the test set-up. Bars were used from the same stock as used in the model hinges and had the same properties as outlined in Chapter 2. The concrete had the same mix as the concrete used in the hinged specimens and had a concrete compressive strength of 3310 psi on the day of testing. The compressive strength was determined from tests on standard 6x12 in. cylinders.

The specimens were cast horizontally in wood forms and the concrete was vibrated using an internal vibrator. The specimens were moist cured for three days in the form, at which time the forms were struck. The specimens were moist cured for four additional days and then cured at room temperature until the time of testing.

4.3 Test Set-up

The test set-up was simple. It consisted of two very stiff steel supports with a 6x10x1 in. plate placed over the top of the supports. The plate had a 1-1/2 in. diameter hole in the center. The test specimen was placed in a vertical position on top of the plate with the 2.75 in. length of bar sticking through the hole. This entire testing apparatus was placed on the base of a Reihle 300,000 lb. capacity testing machine. Figure 4.3 shows a diagram of the test set-

up. Prior to testing, the loading head of the Reihle machine was lowered until it touched the end of the top bar. One dial gage was mounted to measure the displacement of the loading head at the top of the specimen, thus giving a measurement of strain in the bar, and a second dial gage was mounted at the other end of the bar below the specimen to measure slippage. A dial gage with a sensitivity of 0.0001 in. was used to measure slippage until peak bond strength was reached. It was then replaced with a gage of 0.0001 in. sensitivity. The gage for measuring movement of the loading head had a sensitivity of 0.001 in.

The specimens were loaded in 100 lb. increments until peak bond strength was reached. Displacement-controlled testing was used beyond that point. After applying each load increment the load and dial gage readings were recorded.

4.4 Experimental Results

A graph of applied load vs. slip for the three specimens is presented in Fig. 4.4. The bond stress is defined as the bond force divided by the surface area of the bonded length. In the tests an 8 inch bonded length was used. The results were similar in that all three specimens reached peak bond stress at a slip of approximately 0.02 in. The average bond strength was 197 psi.

4.5 Analysis of Test Results

Since the concrete strength of the push-out specimens was different from that of the hinged specimens, the measured bond strength of 197 psi could not be used directly for the hinged

specimens. Assuming that bond strength is proportional to the concrete compressive strength, the following empirical relationship was found to match the measured strength.

$$u = 3.4 \sqrt{f'_c} \quad (4.1)$$

in which u = bond strength, psi; and f'_c = concrete compressive strength, psi.

In calculating bond slip, the bond stress is assumed to be uniformly distributed along the bonded length and an average bar stress is assumed to calculate elongation [19] (Fig. 4.5). The elongation (or slip) of the reinforcement is computed from:

$$e = \frac{f_s l_d}{2E} \quad (4.2)$$

Based on an equilibrium relation between the bar force and the bond force, l_d is determined from:

$$l_d = \frac{f_s d_b}{4u} \quad (4.3)$$

where:

l_d = length of reinforcement to develop a stress of f_s

d_b = diameter of tensile steel reinforcement

f_s = steel tensile stress

E_s = modulus of elasticity of steel

u = assumed average bond stress

P = applied load on the bar

Based on equation 4.2 the slip of the bars for the push-out

specimens was computed using the steel stress distribution shown in Fig. 4.6. The measured and computed values of load-slip are presented in Figs. 4.7(a-c). Notice that the calculated slip is less than the measured slip. This indicates that the assumed steel stress distribution could be different from a linear relationship, thus resulting in a higher average stress, f_s .

In Chapter 5 the bond slip for the hinged specimens is presented along with the bond-slip rotation and deflection. Bond-slip of the hinged specimens is also calculated based upon a linear steel stress distribution. Thus, the results from the push-out tests suggest that the computed slip and subsequent rotation and deflection in the hinged specimens may be underestimated. This point is further discussed in Chapter 5.

CHAPTER 5

ANALYSIS OF HINGED SPECIMENS

5.1 Introductory Remarks

This chapter covers the analysis of the hinged specimens which included calculations of the flexural and shear strength and calculations of the centerspan displacement and rotation of the column element relative to the foundation element.

Flexural analysis of the hinge in the strong direction was carried out using a moment-curvature analysis program called IAL. This program calculated moments required to cause yielding in different steel layers along with the ultimate moments and corresponding curvature at these points. The constitutive relationship for concrete is based on the Hognestad model [12] and for steel is a trilinear relationship consisting of an elastic yield plateau, and a strain hardening branch.

Several formulas were used to calculate the shear capacity. These included (a) the ACI shear-flexure formulas (ACI EQ's. 11-3 and 11-6), (b) the shear-friction formula (ACI EQ. 11-26) [1], (c) shear strength calculated based upon a coefficient of friction multiplied by the net compression force in the section, and (d) the dowel action of the reinforcement using empirical formulas discussed in Ref. 15.

The area-moment method was used to calculate the deformation which included the plastic deformation of the hinge throat and the elastic deformation of the end segments. The deformation due to bond slip was calculated and added to the elastic deformation to get the total deformation. Also, the total concentrated rotation of the hinge

was calculated by adding the inelastic rotation of the hinge section to the rotation developed from bond slip.

5.2 Flexural Analysis

Results of a flexural analysis of each specimen based upon measured properties of steel and concrete (see App. B) are presented in Tables 5.1a-d. The load required to cause yielding at various steel layers, and at the ultimate point when concrete reaches a strain of 0.004 at the extreme compressive fiber, is computed using program IAI and is compared to the measured load at these points.

IAI is a reinforced concrete moment-curvature analysis computer program that computes the interaction at the yield and ultimate points for a specified layer of steel, along with the values at varying concrete strains. It is assumed that plane sections before bending remain plane after bending and that the stress-strain curves for concrete and steel are known. IAI computes curvatures associated with a range of bending moments and axial loads based upon the material properties and the requirements of strain compatibility and equilibrium of forces. The program used the Hognestad model [12] to idealize the stress-strain curve for concrete. The Hognestad model is a function consisting of a parabola and a linear segment (Fig. 5.1). A bilinear approximation which includes the effect of strain hardening but ignores the yield plateau was used for idealization of the stress-strain curve for steel.

The input required for this program includes the steel and concrete properties, section dimensions, arrangement of reinforcement, and applied axial load. By using IAI with zero axial load, the

capacity of the hinge section under pure moment was determined. The moment-curvature diagram for a model hinge cross-section was developed by running IAL five times; once for each of the five bottom layers of steel. A typical moment-curvature diagram is presented in Fig. 5.2. The corresponding yield loads at each layer were determined from equilibrium on the simply supported specimen with an applied yield moment.

Measured load was defined as the load causing yielding as indicated by strain gages. In the case of layers 3 and 4, where no gages were attached, linear interpolation between loads was used to estimate the yield load. For specimen CH1 the displacement increments were too large and, as a result, the load at yielding of layer 6 was missed. Two ratios of calculated to measured load are presented in Table 5.1a for specimen CH1. In this test the load was recorded from two strain gages mounted on the load ram acting as a "mock" load cell. The load was also determined from the pressure gage reading of the load ram pressure. The load from the mock load cell indicates a much higher load than calculated. Subsequent tests, in which an actual load cell was used, showed that the readings from the mock cell were not reliable due to its low sensitivity. The load determined from the pressure gage readings appears more reasonable as can be seen from the calculated to measured load ratios given in Table 5.1a. The calculated load compares well with the measured load determined from the pressure gage except in the early stages of yielding in which steel layers 5 and 6 yielded.

Specimens CH2 and CH3 were tested on the Reihle machine which had a built-in load indicator. A better agreement between the calculated

and measured loads was observed for these specimens. In the test of CH4 a load cell was added to the loading ram. The load cell appeared to be much more reliable than the mock load cell used for CH1.

A comparison of calculated to measured load ratios given in Tables 5.1b-d indicates that program IAI gave a good estimate of the moment for specimens CH2, CH3, and CH4. The largest discrepancy between calculated and measured loads occurred at the yielding of layers 2 and 6.

The calculated ultimate load is the load at which concrete in the extreme compressive fiber reaches a strain value of 0.004, whereas, the measured ultimate load is the peak load that was reached during testing. The calculated ultimate load was very close to the measured load for specimens CH2 and CH3 but was overestimated for specimen CH4. It should be pointed out that the measured ultimate load for CH4 was reached after three major cycles of loading, thus producing some strength degradation at this point. Had the specimen been loaded monotonically to failure the ultimate measured load probably would have been higher, giving a better correlation with the calculated load.

5.3 Shear Analysis

Results from shear strength calculations are presented in Table 5.2. The results indicate that the different formulas for shear give varying results for shear capacity. As explained in Chapter 3 it was observed that the shear strength of the hinge was primarily derived from the frictional resistance within the compression zone of the hinge interface. This suggests that the shear resistance can be

computed from the friction formula:

$$V_n = \mu C \quad (5.1)$$

where $\mu = 1.0 \lambda$ for concrete placed against hardened concrete with the surface intentionally roughened and $\lambda = 1.0$ for normal weight concrete (Ref. 1). In calculating the shear strength of the hinged specimens with the above formula, the compressive force, C , was determined by

$$C = 0.85f'_c b a \quad (5.2)$$

in which $a = \beta_1(x)$ (5.3)

and $\beta_1 = 0.8$ and x = distance from the neutral axis to the extreme compressive fiber.

Table 5.2 indicates that the model hinge section attained a shear force of at least 6895 lbs. This, however, is not the ultimate shear capacity of the section since major flexural yielding had taken place. However, because of the large slippage of the middle segment relative to the end segments, the load dropped quickly after yielding, thus indicating an imminent shear failure. The shear formula given in Eq. 5.1 overestimates the shear capacity in this case by 44%.

Another point to note is the increase in applied shear from CH1 to CH3. This is because the shear span-to-depth ratio was decreased from 3 to 1. As the shear span-to-depth ratio is decreased, the moment arm from the support to the hinge is decreased, thus requiring a larger applied load to cause yielding and consequently an increase in the applied shear and moment.

The ACI equations for shear-flexure (ACI EQ's 11-3 and 11-6) considerably underestimate the shear capacity of the hinged section.

This was expected since a shear-flexure (diagonal tension) failure was not observed nor anticipated in any of the tests. These equations were attempted for the sake of completeness.

As mentioned in Chapter 1, the shear-friction method is currently used to determine the shear capacity of the hinge. Using the ACI shear-friction formula (ACI EQ's 11-16) shear strength was computed considering (a) all bars contributing to shear transfer, (b) one bar contributing, and (c) for two bars contributing. These results, presented in Table 5.2, are labeled SFr1, SFr2, and SFr3, respectively.

If it is assumed that all the reinforcement across the hinge interface contributes to shear transfer, then the shear capacity is overestimated by almost 50% for CH3. By considering all the bars as contributing, then there is an assumed shear plane along the entire depth of the section. In the hinged specimen tests there was considerable separation along the crack interface, thus only the concrete within the compression zone contributed to the frictional resistance. The observed depth of the shear plane was approximately 1 inch. This suggests that only one bar had any significant contribution to the shear friction resistance. The compressive force due flexure, of course, also provided for friction forces. The conventional shear friction theory incorporating all the bars does not seem to be the means by which shear was transferred. A more realistic approach would be to consider the compressive force caused by flexure multiplied by a friction factor as the shear strength.

In addition to the above mechanisms, shear forces may be resisted

by dowel action across the shear plane. Dowel strength can be developed by three mechanisms: the flexure of the reinforcing bars, the shear strength across the bars, and by kinking of the reinforcement [15]. These three mechanisms along with formulas for calculating dowel shear are illustrated in Fig. 5.3. In the R/C hinge tests, the observed mechanism for dowel action included a slight kinking in the bars. The extent of kinking varied in different tests and was not always clear. Shear strength results from dowel action due to kinking are based upon measured angles of bar deformation at the end of each test. For specimen CH3 the calculated value for shear due to kinking was 4400 lbs., which is almost 2/3 of the measured ultimate shear. From the cyclic test of CH4 it is recalled in Chapter 3 that the estimated contribution of dowel action to shear capacity was 900 lbs. After examining the first and second tests (specimens CH1 and CH2) it was determined that dowel action due to flexure was not the observed mode of dowel action, therefore, this value is not calculated for specimens CH1, CH3, and CH4.

5.4 Rotation Calculations

The calculation procedure used for determining the rotation of the pier or, end portion, relative to the foundation or, middle stub, is presented in this section. The calculated rotation consisted of rotation due to plastic deformation of the hinge throat plus rotation due to bar slip. Calculated load-rotation curves are presented in Figs. 3.2(a-d) and are superimposed on the measured curves. Both calculated and measured results display the concentrated rotation within the hinge region.

The rotation due to inelastic deformation of the hinge throat was calculated by spreading the yield curvature over the length of the hinge. The rotation at yielding of each bar layer is

$$\theta_y = \phi_y \times 1/4" \quad (5.4)$$

where ϕ_y equals the curvature at yielding of the particular bar layer computed by program IAI for the weak section. A hinge length of 1/4" was used, however the actual hinge length varied along the section depth due to the roughness at the hinge interface, and could well be about 1/2".

Bond-slip rotation was computed with respect to the location of the neutral axis using the following formula

$$\theta_s = \frac{e}{d - kd} \quad (5.5)$$

where d is the distance from the rebar to the extreme compressive fiber and e is bar elongation due to bar slip. The distance from the extreme compressive fiber to the neutral axis equals kd , and was computed from:

$$kd = \frac{\epsilon_c}{\phi_y} \quad (5.6)$$

The strain in the concrete at the extreme compression fiber, ϵ_c is computed from strain compatibility for yielding of each layer. A concrete strain of 0.004 was used for the ultimate point.

Bar elongation due to bond slip, e , is computed from Eq. 4.2

using the bond stress distribution shown in Fig. 5.4. The total development length was calculated from:

$$l_d = \frac{f_y d_b}{4u} + 6" \quad (5.7)$$

where 6" is added to account for the bond slip of the bar within the middle stub portion. The above development length is different from what is commonly used in R/C connections. Bar slippage in an ordinary connection primarily takes place in the anchorage in the column [19] as shown in Fig. 5.5. The slippage in the beam is small due to the distributed cracking and beam flexibility. In the hinge specimens, there are two rigid blocks rotating relative to each other with no cracking occurring in either block, thus, slip takes place in both portions. In the middle block the bar is pulled from both ends, and thus, only half of the length of the bar is added to the development length used in calculating slippage. This is shown in Figure 5.6. In Eq. 5.7, d_b is the bar diameter. The bond stress, u , was determined from Eq. 4.1.

The load-rotation curves for specimens CH2, CH3, and CH4 (Figs. 3.2(b-d)) indicate a general trend, in that, as the shear span is reduced, the calculated rotations compare more closely to the measured results. In all cases the calculated ultimate rotation greatly underestimates the actual rotations. This is because for calculation purposes the ultimate point was considered to occur at a concrete compressive strain of 0.004 at the top compressive fiber, but, the specimens failed at a local strain of approximately 0.2 over the hinge

throat.

For specimens CH1, CH2, and CH3, measured rotation results are plotted up to the point in which one of the rotation measuring dial gages was out of range. For specimen CH4 measured results are plotted only up to yielding of layer 2 because after this point the load was reversed.

In the case of specimen CH1, the initial linear portions of the calculated and measured curves match closely. Figure 3.2(a) indicates, however, that both the loads and deflections at various layers were underestimated. As previously mentioned a mock load cell was used to record the load. The low sensitivity of the mock cell is the most likely reason for the overestimation of loads. From the measured curve it is noticed that the initial portion of the curve remains linear up to approximately 3100 lbs. then begins to become less steep as the bars yield. This suggests that layer 6 was yielding sooner than indicated by the strain gages, thus the strain gages at this level may have malfunctioned. Another explanation is that since the end supports did not allow for freedom of rotation it is possible that compression may have developed in the section causing the gages to indicate yielding at higher loads and rotations.

Figure 3.2(b) indicates that the calculated load-rotation for specimen CH2 resembles the measured curve. The strain gages appeared to work very well in this test as can be seen by the smooth rounding of the yielding portion of the measured curve between yielding of layer 6 and layer 2. The calculated curve indicates a stiffer hinge section than was actually observed. Calculated loads compare well with

measured loads as can be seen in Table 5. 1b, but, calculated rotations are underestimated by 50% for layers 6, 5, and 4, 40% for layer 3, and 30% for layer 2.

Calculated load-rotation results most closely match measured results (Fig. 3.2(c)) for specimen CH3, especially at yielding of layers 3, 4, and 5. The calculated rotations at layers 2 and 6 are also close to the measured rotations but the loads are overestimated. The strain gages again appeared to be working properly with the measured curve rounding out as the bars yield.

In the test of specimen CH4, layer 4 yielded in between load increments and thus, the measured rotation for this point is not defined. Calculated load-rotation results overestimate the initial stiffness of the hinge section by about 50%. In this test the specimen was loaded through an initial pre-cycle to test the transducers. Since the section was not very strong, this may have initially weakened the section by introducing some bond slip. Specimen CH4 appeared to be weaker than specimen CH1 which had the same shear span of 3. This may reflect the difference in concrete strengths of the middle segment, with the concrete in the middle segment of CH4 having much lower strength than that of CH1 (Appendix B).

5.5 Deflection Calculations

This section outlines the procedure used to calculate centerspan deflection. The calculated deflection consisted of deflection due to plastic deformation of the hinge throat and elastic deformation of the end elements, plus deflection due to bond slip. Shear deformations were not included in the calculations because they were considered

negligible relative to inelastic flexural deformations. Figure 3.3(a) shows that even for specimen CH3 with a shear span of only one the measured vertical slip between the middle and end segments was negligible in the elastic state of loading. However, the vertical slip was noticeable for the yielding and post-yielding stages. Calculated load-deflection curves are presented in Fig. 3.1(a-d) and are superimposed on the measured load-deflection curves to determine the applicability of the analytical procedure.

Deflection due to flexure was calculated using the area-moment theorem. As described in Chapter 2 the hinged specimens consisted of three segments. It was assumed that the middle segment was very stiff and did not contribute to the flexural deformation. The calculations were simplified by modeling the hinged specimen as consisting of a fixed middle segment with two cantilevered end segments. Therefore, by applying the area-moment theorem to only one cantilevered segment the elastic deformation of the free end, and consequently, the centerspan deflection was determined. The cantilevered portion was made up of a 6"x12" element connected to the fixed based by a 2"x12"x1/4" hinge section as shown in Fig. 5.7. The length of the element for calculation purposes depended upon the support length. The curvature (M/EI) varied along the length of the element as follows. For the 6"x12" portion the curvature varied from zero at the free end to M_y/EI , where the moment of inertia, I was based upon the uncracked moment of inertia of a 6"x12" section and the concrete modulus of elasticity, E was calculated from [1]:

$$E = 57000 \sqrt{f'_c} \quad (5.8)$$

The curvature over the 1/4" plastic hinge length was taken from program IAI for a 2"x12" section. The idealized curvature distribution is shown in Fig. 5.8. Deflection was calculated at yielding of the different layers of steel, with the value of M_y used in the calculations determined from IAI, based upon a 2"x12" section.

Deflection due to bond slip was calculated from:

$$\delta_s = \theta_s * L \quad (5.9)$$

where θ_s is the rotation due to bond slip calculated in Eq. 5.5 and L is the length from the support to the hinge throat.

The calculated and measured load-deflection results presented in Figs. 3.1(a-d) are similar to the load-rotation results in that there is a general trend of improvement in correlation for specimens CH2, CH3, and CH4 as the shear span is decreased.

The measured load-deflection curve for specimen CH1 (Fig. 3.1(a)) resembles the load-rotation curve (Fig. 3.2(a)) and indicates that yielding occurred sooner than indicated by the strain gages. The calculated response matches the measured response but underestimates the actual yield deflections.

From Fig. 3.1(b) it can be seen that for specimen CH2 the calculated deflection underestimates deflection in the initial linear, elastic range. The calculated deflection at yielding of layer 2 gave a reasonable estimate of the actual deflection.

There is an inconsistency in the measured deflection for specimen CH3. There was less centerspan deflection at the yielding of layer 4 than for yielding at layer 5. This indicates a possible error in the displacement transducer for that particular point. A comparison of the

rotation on both sides indicates that rotations at this state of the test were symmetric. As the displacements increased, the rotations became unsymmetrical relative to the center. Unsymmetrical rotations cause the middle segment to rotate, thus affecting the centerspan displacement.

The load-deflection response for specimen CH4 (Fig. 3.1(d)) shows similar results as the load-rotation response (Fig. 3.2(d)) with the initial flexural stiffness being overestimated.

A possible explanation for the lack of close agreement between the computed and measured deformations could be that the effect of bond slip may have been underestimated. By referring to Figs. 4.7(a-c) it is seen that the empirical formulas used for calculating slip in the push-out specimens underestimate the actual slip. Since the same procedure was used to calculate slip in the slip specimens as in the hinged specimens, this indicates that the calculated bond slip in the hinged specimens may also be underestimated.

The difference between the calculated and measured slip may have been even greater had the bars in the push-out tests been pulled in tension for the following reason. When a material is loaded in one direction it undergoes strain in the direction of loading as well as strain perpendicular to the direction of loading due to the Poisson effect. In the case of a bar loaded in tension or compression the bar elongates or shortens and consequently decreases or increases in diameter. The bars in the push-out tests were subjected to compression which caused the bars to increase in diameter upon loading. The bars in the hinged specimens, however were subjected to tension which

caused the bars to decrease in diameter upon loading. When a steel bar surrounded in concrete is loaded the surface adhesion between the steel and concrete is broken due to slippage of the bar. For a bar in tension the surface adhesion may also be broken from the reduction in diameter of the bar due to the bar pulling away from the surrounding concrete. Analogous to a wooden chair leg that loosens due to drying and shrinkage of the wood. In contrast, for a bar in compression the adhesion would be broken only by the slippage of the bar. The increase in bar diameter would actually cause a tighter fit between the steel and concrete which could reduce slippage. Plain bars are especially sensitive to the above phenomena.

The above hypothesis would lead to an actual bond stress value that is lower than that determined from the tests results of the pushout specimens and, in turn, would lead to higher calculated rotations and deflections in the hinged specimens. Because the steel used in the hinged specimens consisted of plain bars, and because plain bars are rarely used in the actual construction of bridge piers, the bond slip computations were not refined any further.

CHAPTER 6

SUMMARY AND CONCLUSIONS

6.1 Summary

This report presents a study of one-way Fresyssinet type reinforced concrete hinges subjected to uniaxial moment transfer in the strong direction of the hinge. This type of connection is typically used at the base of highway bridge columns to provide a "pinned" detail, therefore eliminating transfer of moment to the foundation in the weak direction. For the purpose of this study four 1/8th scale models of the one-way hinge connections found on the Rose Creek bridge were constructed and tested. The primary variable in the test was the shear-span to depth ratio. A limited study of the cyclic behavior was also carried out.

Two of the specimens (CH1 and CH4) were tested with a shear-span to depth ratio of three which is the nominal value for the Rose Creek bridge columns. CH1 was subjected to monotonic loading while CH4 was loaded cyclically. The purpose of this portion of testing was to determine the effect of cycling load on the flexural and shear stiffness of the hinge.

The effect of varying the shear-span to depth ratio involved specimens CH1, CH2, and CH3. The ratio for these three specimens was three, two, and one, respectively. By reducing the shear span, the effect of shear was increased. This portion of the testing also was done to try and determine a limiting shear span to produce a shear failure.

Analysis of the hinged specimens was discussed in Chapter 5 and

involved calculation of the flexural and shear strength, the concentrated hinge rotation, and the center-span displacement of the element. Flexural analysis was performed using a moment-curvature program called IAL. The comparison between calculated and measured results are presented in Tables 3.1a-d. Various formulas based upon different mechanisms of shear failure were used to determine the shear capacity of the hinge. These included the equations presented in the ACI code for shear-flexure (ACI Eq's. 11-3 and 11-6), and the equation for shear-friction (ACI Eq's. 11-26) [1]. Also, shear strength due to friction within the compression zone was considered and the contribution of dowel action to shear was examined. These results are presented in Table 5.2 and indicate a wide variation of shear capacities.

Concentrated hinge rotation and centerspan deflection consisted of two components, flexure and bond slip. Flexural deformation was computed from the curvature distribution along the element and included the elastic deformation of the column element and the plastic deformation of the hinge.

During testing of the hinged connections, appreciable bar slippage was observed. This prompted a study in which tests were performed on 3 push-out specimens to determine the bond characteristics between the plain reinforcing bars and the concrete in order to better explain the load-deflection characteristics of the specimens.

6.2 Observations

In the course of the study presented in this report, the

following important points were noted.

1. Cyclic loading of specimen CH4 showed that the reversal of load reduced the shear stiffness of the hinge region substantially until closing of the crack on the compression side.
2. Shear resistance was primarily derived from the frictional forces at the compression zone and not along the entire depth of the section as assumed in the shear-friction method.
3. The maximum applied shear was attained during the testing of specimen CH3 which had a shear-span to depth ratio of 1. This, however, did not represent the limiting value of shear strength in the section, since the maximum value was attained after the specimen had yielded in flexure. The shear span would have to be reduced further to produce a limiting value of shear.
4. Significant flexural deformations occurred in all the specimens. Even for specimen CH3, which had a shear span to depth ratio of 1, a reasonable amount of ductility was noted.
5. The moment-curvature program IAI produced a good estimate of the flexural capacity of the hinge in the strong direction of bending.
6. In specimen CH3 (shear span to depth ratio of 1) where shear was relatively large, the engagement of the shear key provided additional strength and ductility at larger displacement amplitudes.
7. The effect of bond slip was very significant in rotation and deformation that occurred.

6.3 Conclusions

The following conclusions are based on the tests and analyses presented in this report.

1. A different arrangement of reinforcing bars could produce a more efficient hinge in the strong direction of bending while still providing the required ductility in the weak direction. One possible arrangement would be to bundle the bars near the edges of the cross section. This would provide more strength in flexure, and would result in smaller crack widths, thus increasing shear resistance. With a higher amount of flexural steel near the edges there would be less separation at the interface, thus providing a larger contact area for aggregate interlock between the base of the hinge and the foundation.
2. The current method of analysis based upon shear-friction for determining shear capacity of the hinge section did not give a reasonable estimate of the shear strength. Friction forces were primarily developed within the compression zone of the hinge interface.
3. Use of deformed bars would have resulted in less bond slip, resulting in less rotation and deformation.
4. The trend towards better agreement between calculated and measured rotations and centerspan deflections as the shear span was reduced suggests that the results could be modified by a factor that includes the effect of the shear span (l/h).
5. The effect of dowel action was noticed only after large deflections had occurred. Until significant deflection and separation, shear resistance was provided by frictional

resistance from aggregate interlock within the compression zone. After significant deflection the depth of the compression zone became smaller, thus limiting the frictional resistance and increasing the shear stress on the reinforcing bars. Results from specimen CH4 indicate that the shear stiffness provided by dowels alone was very small, thus reducing the energy absorption capacity of the hinge during earthquakes.

REFERENCES

1. ACI Committee 318, " Building Code Requirements for Reinforced Concrete (ACI 318-83)," American Concrete Institute, Detroit, Michigan, 1983, pp. 44-50.
2. ACI-ASCE Committee 426. "The Shear Strength of Reinforced Concrete Members - Chapters 1 to 4," Journal of the Structural Division, ASCE, Vol. 99, No. ST6, June 1973, pp. 1091-1187.
3. Base, G.D., "Tests on Four Prototype Reinforced Concrete Hinges," London, Cement and Concrete Association, Research Report No. 17, May 1965, pp. 1-28.
4. Collins, T.H., "Data Collection and Transmission for Civil Engineers Using Microcomputers," Proceedings 2nd National Conference on Microcomputers in Civil Engineering, Florida, 1984, pp. 246-249.
5. Department of Transportation, State of California. Column Key Design Calculations by J.C. Moese, pp. 9-10.
6. Gavlin, N.L., "Bond Characteristics of Model Reinforcement," Report # UILU-ENG-76-2007, Department of Civil Engineering, University of Illinois at Urbana-Champaign, Urbana, Illinois, 37 pp.
7. Gosain, N.K., R.H. Brown, and J.O. Jirsa, "Shear Requirements for Load Reversals on RC Members," Journal of the Structural Division, ASCE, Vol. 103, ST7, July 1977, pp. 1461-1475.
8. Hewlett-Packard, "Basic 4.0 Programming Techniques for HP 9000 Series 200/300 Computers," Programming Manual, Hewlett-Packard Company, 1985.
9. Hewlett-Packard, "3054 A (Series 200 Basic) Data Acquisition Control System Library," Operating and Programming Manual, Hewlett-Packard Company, 1982.
10. Higdon, A., Ohlsen, E.H., Stiles, W.B., Weese, J.A., and Riley, W.F., Mechanics of Materials, John Wiley & Sons, 1976, pp. 383-393.
11. Hoedajanto, D., "A Model to Simulate Lateral Force Response of Reinforced Concrete Structures with Cylindrical and Box Sections," Doctoral Dissertation, Graduate College, University of Illinois, Urbana, 1983.
12. Hognestad, E., "A Study of Combined Bending and Axial Load in Reinforced Concrete Members," University of Illinois Experimental Station, Bulletin Series No. 399, November 1951, 128 pp.

13. Mattock, Alan H., "Cyclic Shear Transfer and Type of Interface," Journal of the Structural Division, ASCE, Vol. 107, No. ST10, Oct. 1981, pp. 1945-1963.
14. Mattock, A.H. and N.M. Hawkins, "Shear Transfer in Reinforced Concrete - Recent Research," PCI Journal, Vol. 17, March/April 1972, pp. 55-75.
15. Pauley, T., and R. Park, Reinforced Concrete Structures, John Wiley & Sons, 1975.
16. Pauley, T., R. Park, and M.H. Phillips, "Horizontal Construction Joints in Cast in Place Reinforced Concrete," Shear in Reinforced Concrete, ACI Special Publication 42, Vol. 2, Detroit, 1974, pp. 599-616.
17. Podolny, W. Jr., and J.M. Muller, Construction and Design of Prestressed Concrete Segmental Bridges, John Wiley & Sons, 1982, pp. 357, 365.
18. Portland Cement Association, "Design and Control of Concrete Mixtures," 12th Edition, Portland Cement Association, 1979, pp. 55-65.
19. Sozen, M.A., "Hysteresis in Structural Elements," Applied Mechanics in Earthquake Engineering, ASME, MMD, Vol. 8, November 1974, pp. 63-98.
20. Wang, C.K. and C.G. Salmon, Reinforced Concrete Design, Fourth Edition, Harper & Row, 1985.
21. Wight, J.K. and M.A. Sozen, "Strength Decay of RC Columns under Shear Reversals," ASCE, Journals of the Structural Division, Vol. 101, No. 5, May 1975, pp. 1053-1065.

TABLE 5.1a MEASURED AND COMPUTED YIELD LOADS,
SPECIMEN CH1

CH1						
Load No.	Layer	Meas. Load	Meas. Load from Pressure*	Calc. Load	Calc. Meas.	Calc. Meas.*
16	6	4280	3550	2160	0.50	0.61
16	5	4280	3550	2580	0.61	0.73
17	4	4400	3600	2960	0.67	0.82
17	3	4400	3600	3350	0.76	0.93
19	2	4718	4200	3940	0.84	0.94
29	ult.	5004	4700	4220	0.84	0.90

TABLE 5.1b MEASURED AND COMPUTED YIELD LOADS,
SPECIMEN CH2

CH2				
Load No.	Layer	Meas. Load	Calc. Load	Calc. Meas.
15	6	3875	3485	0.90
21	5	4625	4110	0.89
25	4	5125	4695	0.92
28	3	5500	5285	0.96
32	2	6000	6215	1.04
42	ult.	6525	6560	1.01

TABLE 5.1c MEASURED AND COMPUTED YIELD LOADS,
SPECIMEN CH3

CH3

Load No.	Layer	Meas. Load	Calc. Load	Calc. Meas.
10	6	6500	7525	1.16
15	5	9000	8780	0.98
18	4	10500	9950	0.95
20	3	11500	11140	0.97
23	2	12500	13025	1.04
40	ult.	13650	13670	1.00

TABLE 5.1d MEASURED AND COMPUTED YIELD LOADS,
SPECIMEN CH4

CH4

Load No.	Layer	Meas. Load	Calc. Load	Calc. Meas.
6	6	1678	2125	1.27
10	5	2959	2540	0.86
--	4	3100	2930	0.95
11	3	3362	3325	0.99
12	2	3605	3950	1.10
85	ult.	3824	4175	1.09

TABLE 5.2 RESULTS FROM SHEAR ANALYSIS

Formula	Specimens			
	CH1	CH2	CH3	CH4
SF1	2795	2590	2540	2580
SF2	2745	2385	2350	2280
SFr1	12900	12900	12900	12900
SFr2	2150	2150	2150	2150
SFr3	4300	4300	4300	4300
DA	shear	7500	7500	7500
	kinking	1020	1870	4400
	flexure	2640	--	--
F	11440	11270	11250	11260
Max. Applied shear	2570	3330	6895	1870

SF1 - Shear Flexure (ACI Formula 11-3) [1]

SF2 - Shear Flexure (ACI Formula 11-6) [1]

SFr1 - Shear Friction based on all bars

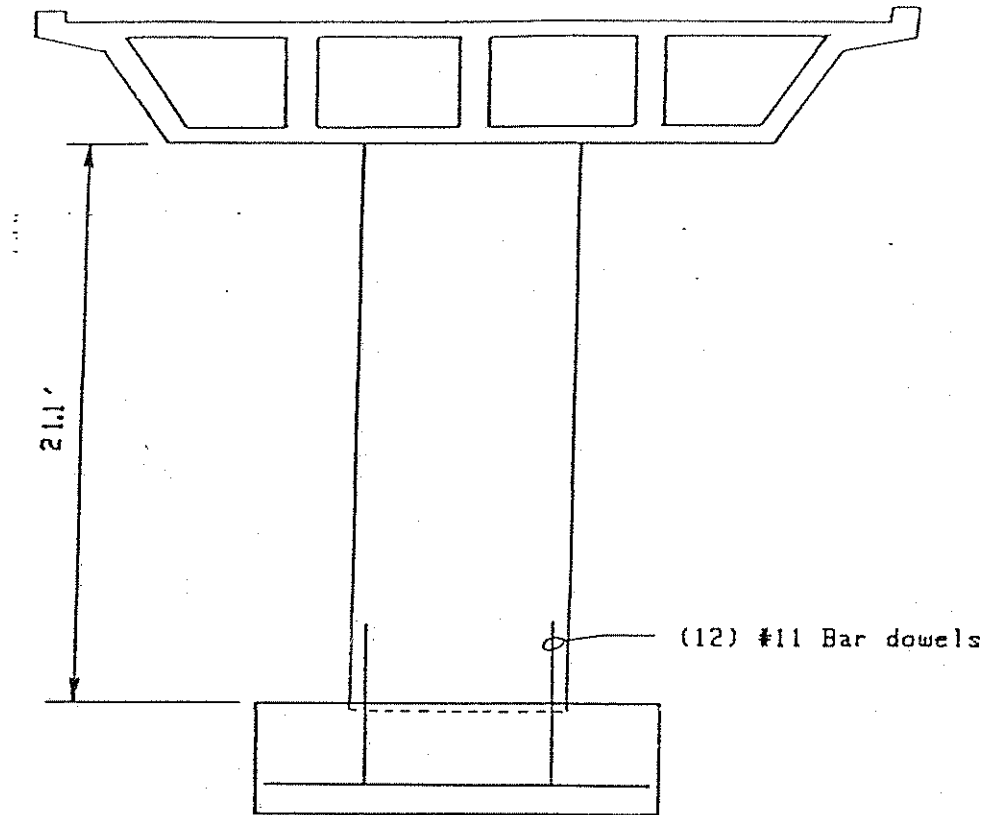
SFr2 - Shear Friction based on 1 bar } (ACI Formula 11-26) [1]

SFr3 - Shear Friction based on 2 bars }

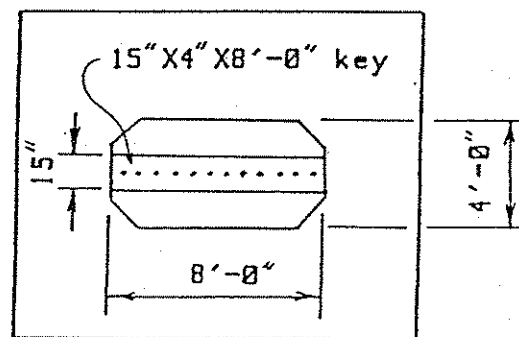
DA - Dowel Action (Formulas by Park & Paulay [15])

F - Coefficient of Friction X Compressive Force

Note: Shear results from Dowel Action due to kinking is based upon measured angles of bar deformation at the end of test.



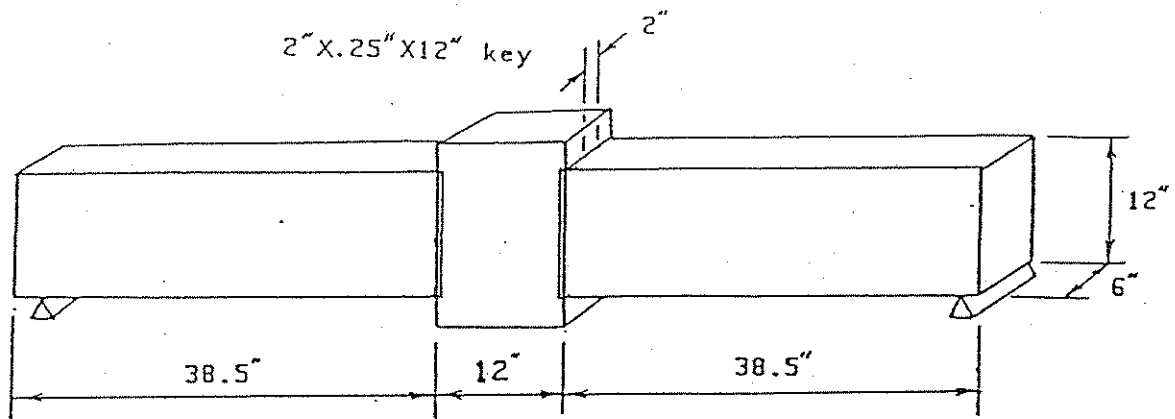
Elevation



Footings Plan

Fig. 2.1. Elevation of Rose Creek Interchange Pier and Hinge Cross Section.

Test Specimens



Location of Strain Gages and Reinforcing Bars

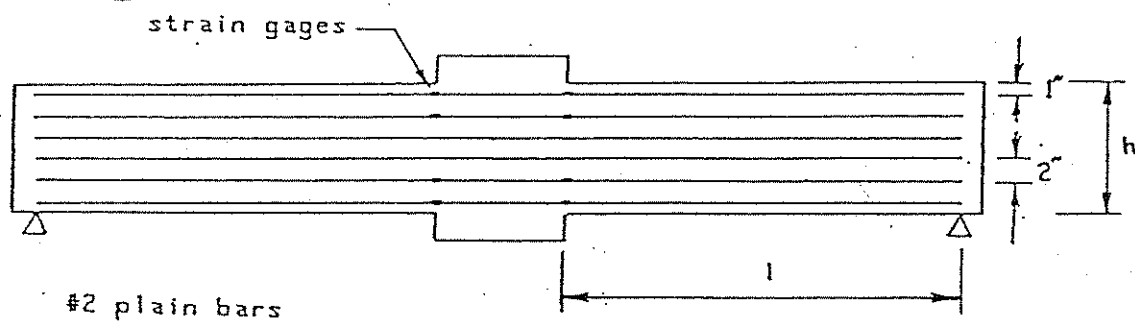


Fig. 2.2. Test Specimens and Location of Reinforcing Bars and Strain Gages.



Fig. 2.3 Middle Segment After Curing.

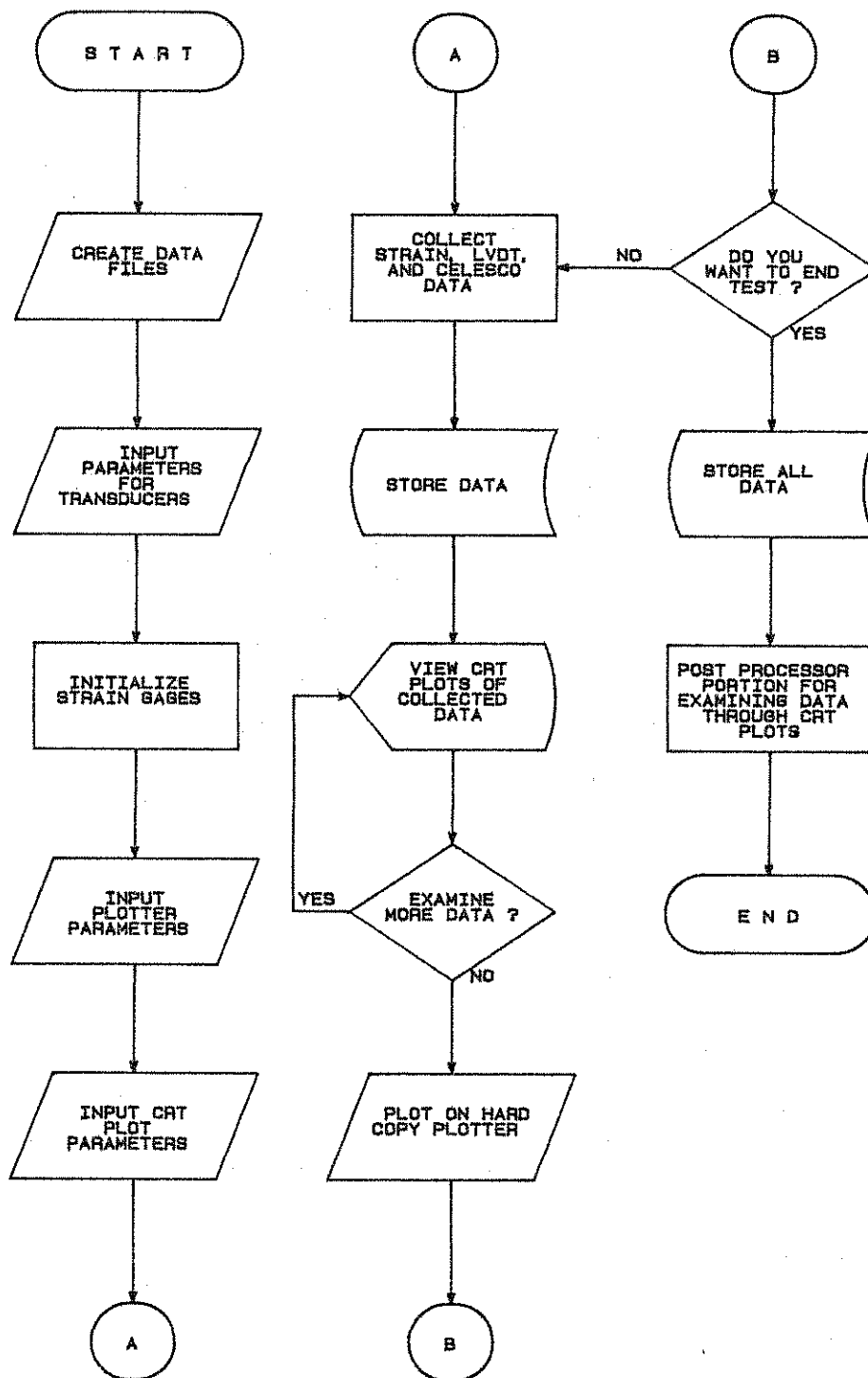
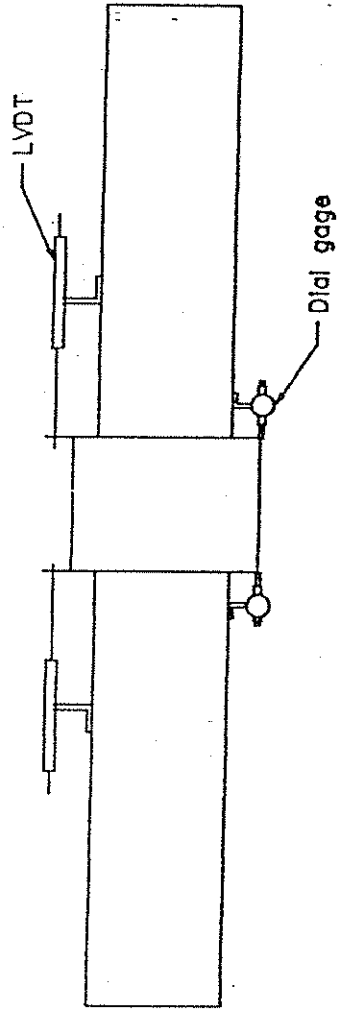


Fig. 2.4 Flowchart for Data Acquisition Program AQUIREDAT.

Rotation measuring devices



Gages to measure slip

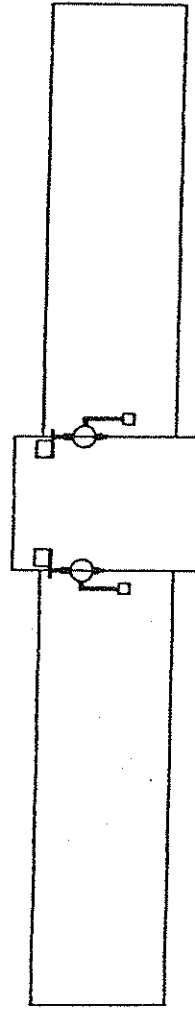


Fig. 2.5 Location of Displacement Measuring Devices.

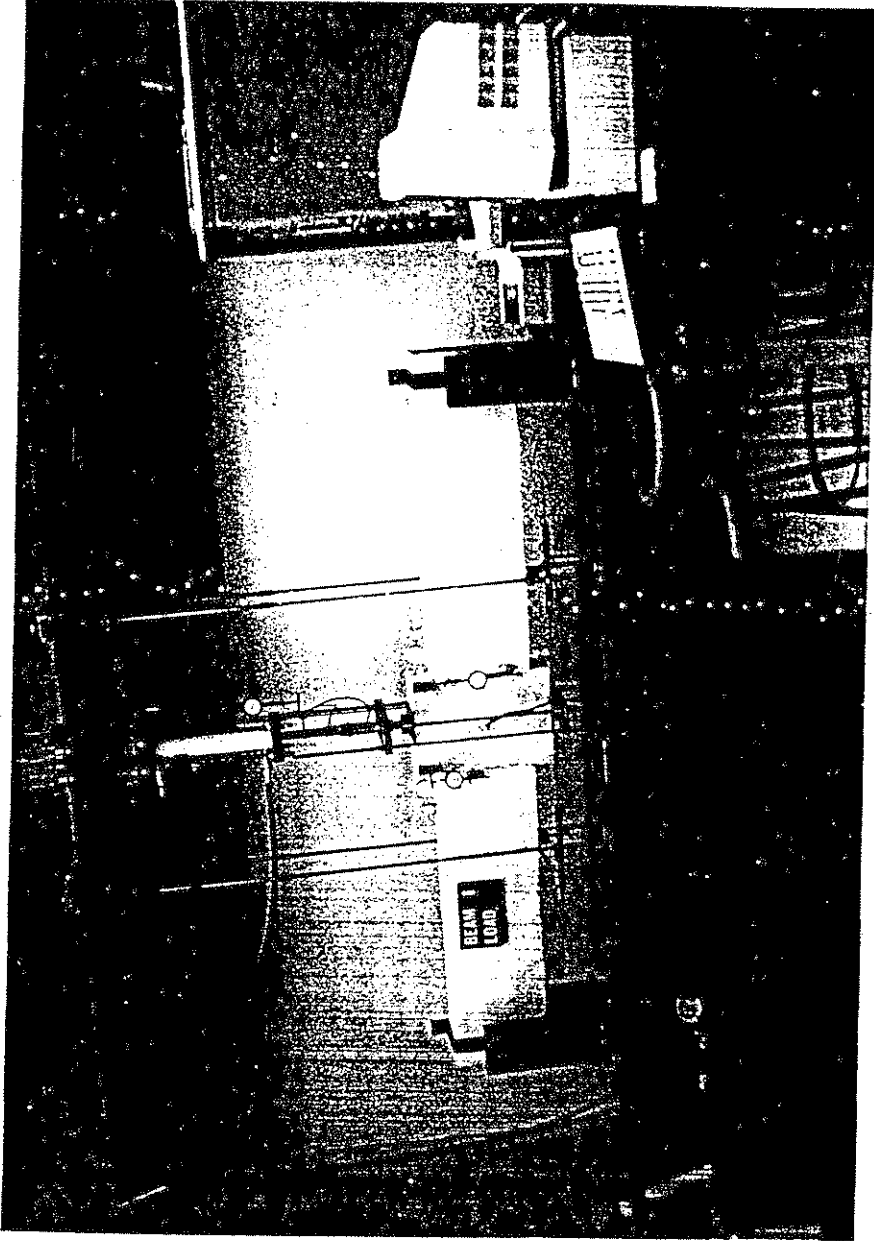


Fig. 2.6 Test Setup for Specimens CH4 and CH1.

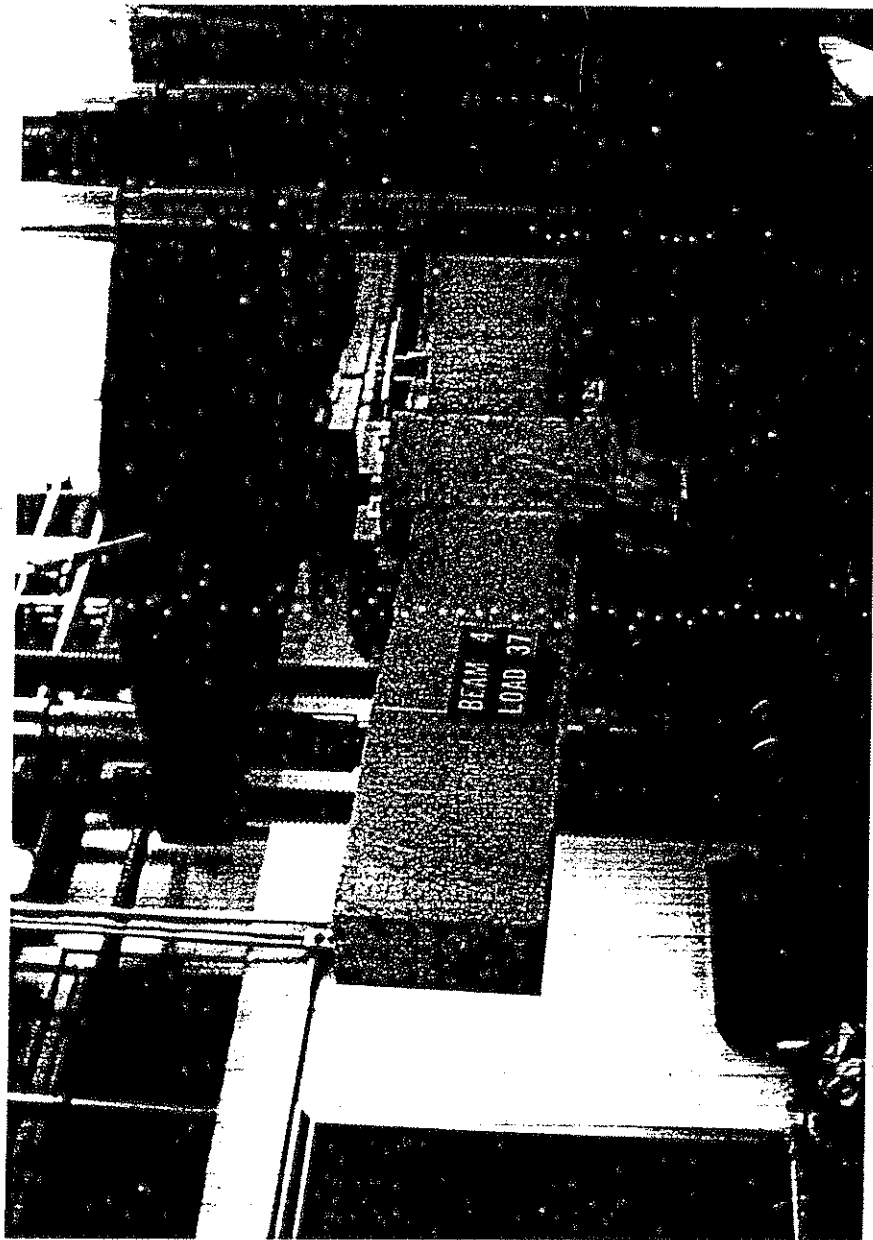


Fig. 2.7 Specimen CH3 Midway Through the Test.

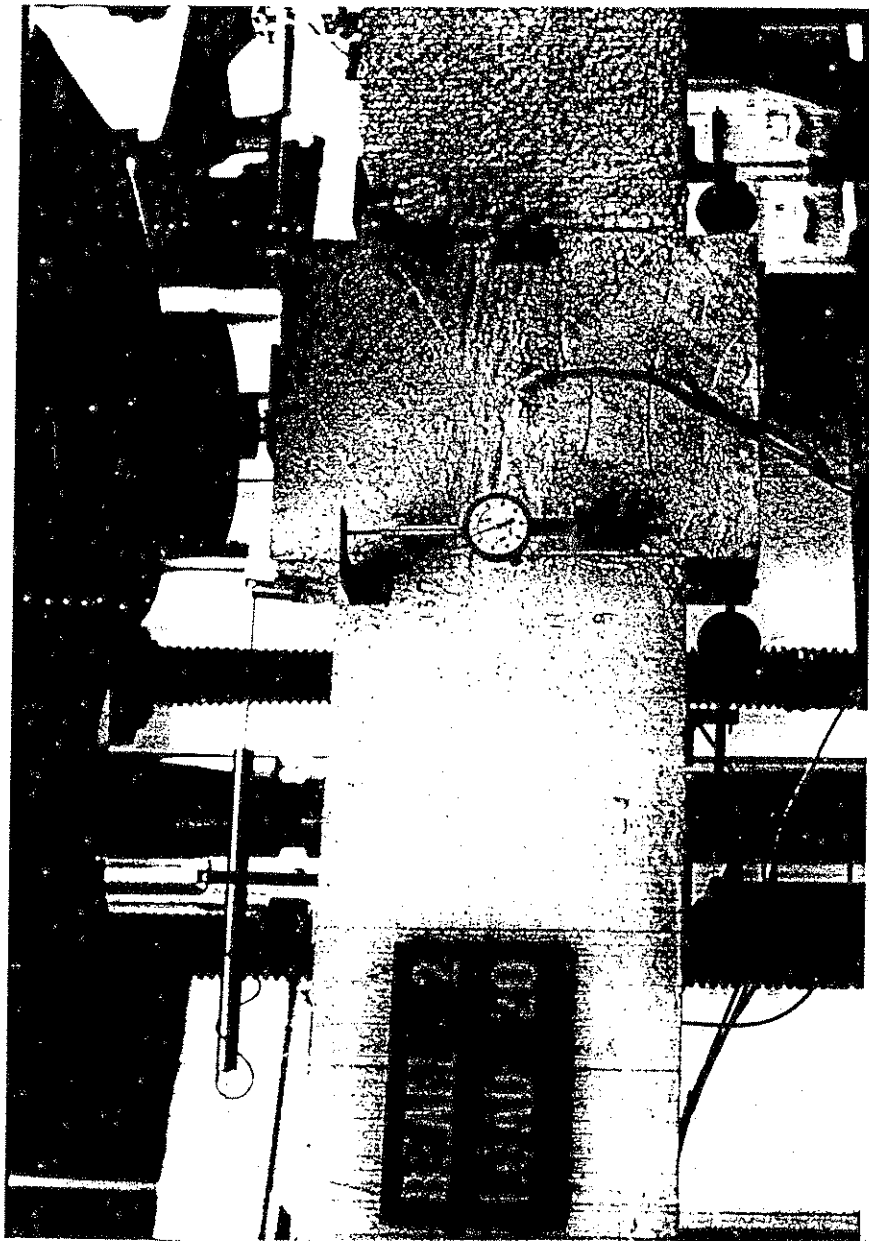


Fig. 2.8 Specimen CH4 in Early Stages of Testing.

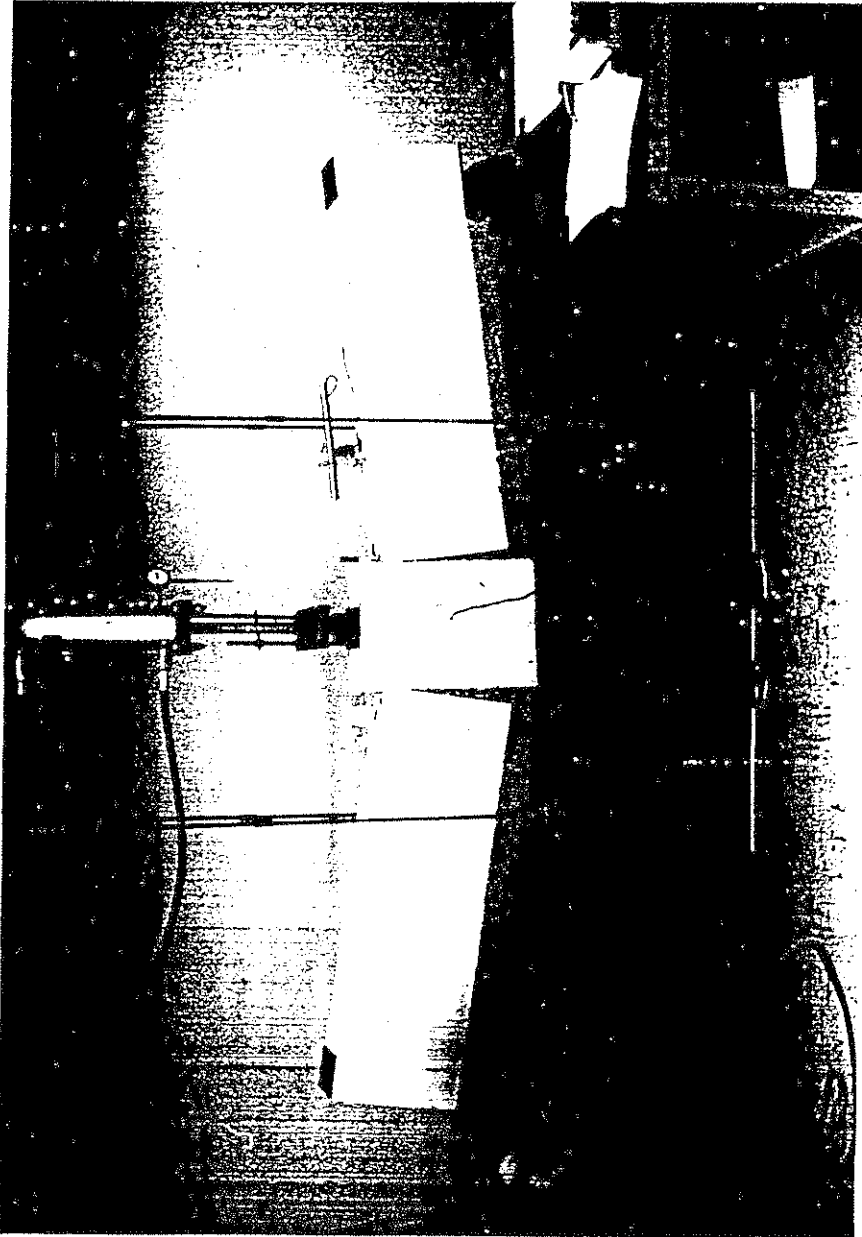


Fig. 2.9 Specimen CH1 at End of Test.

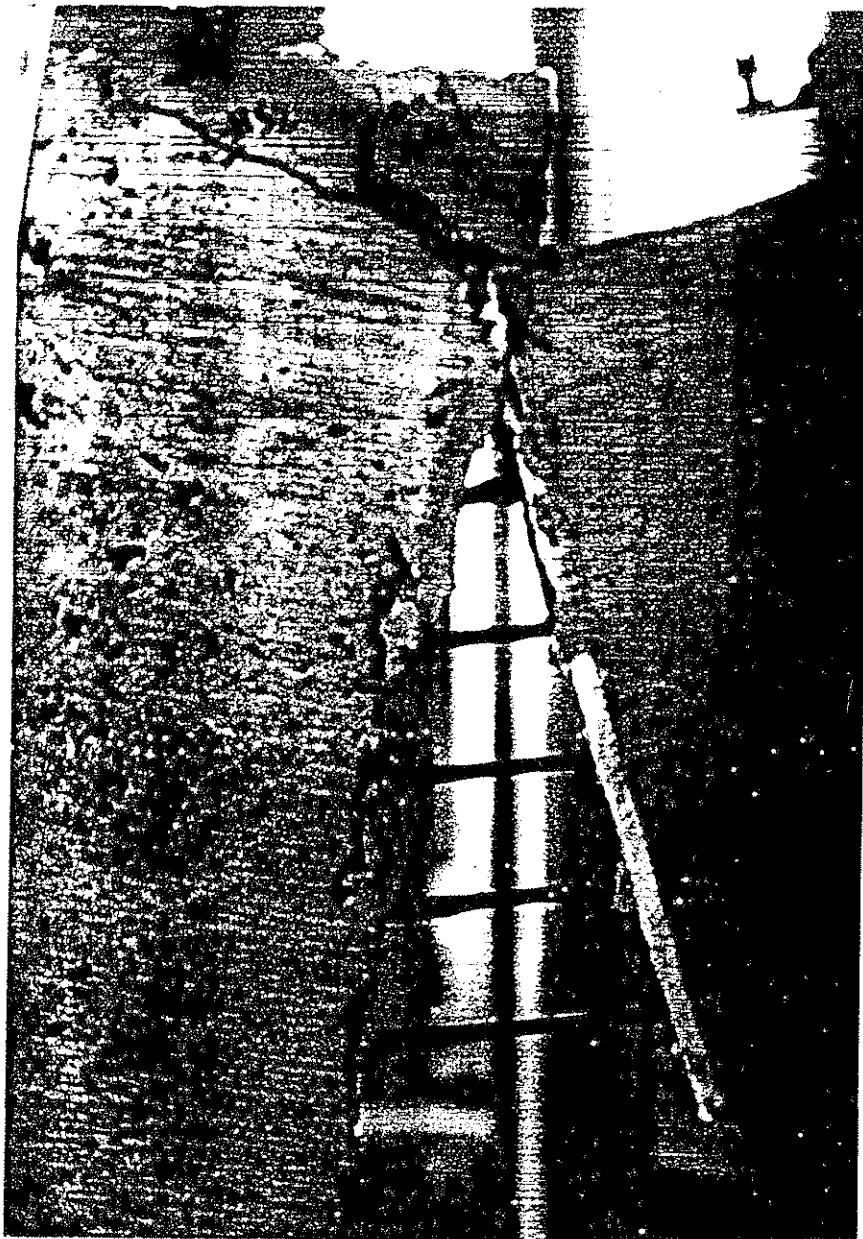


Fig. 2.10 Hinge Region of Specimen CH3 at Later Stages of Testing.

LOADING CYCLE (CH4)

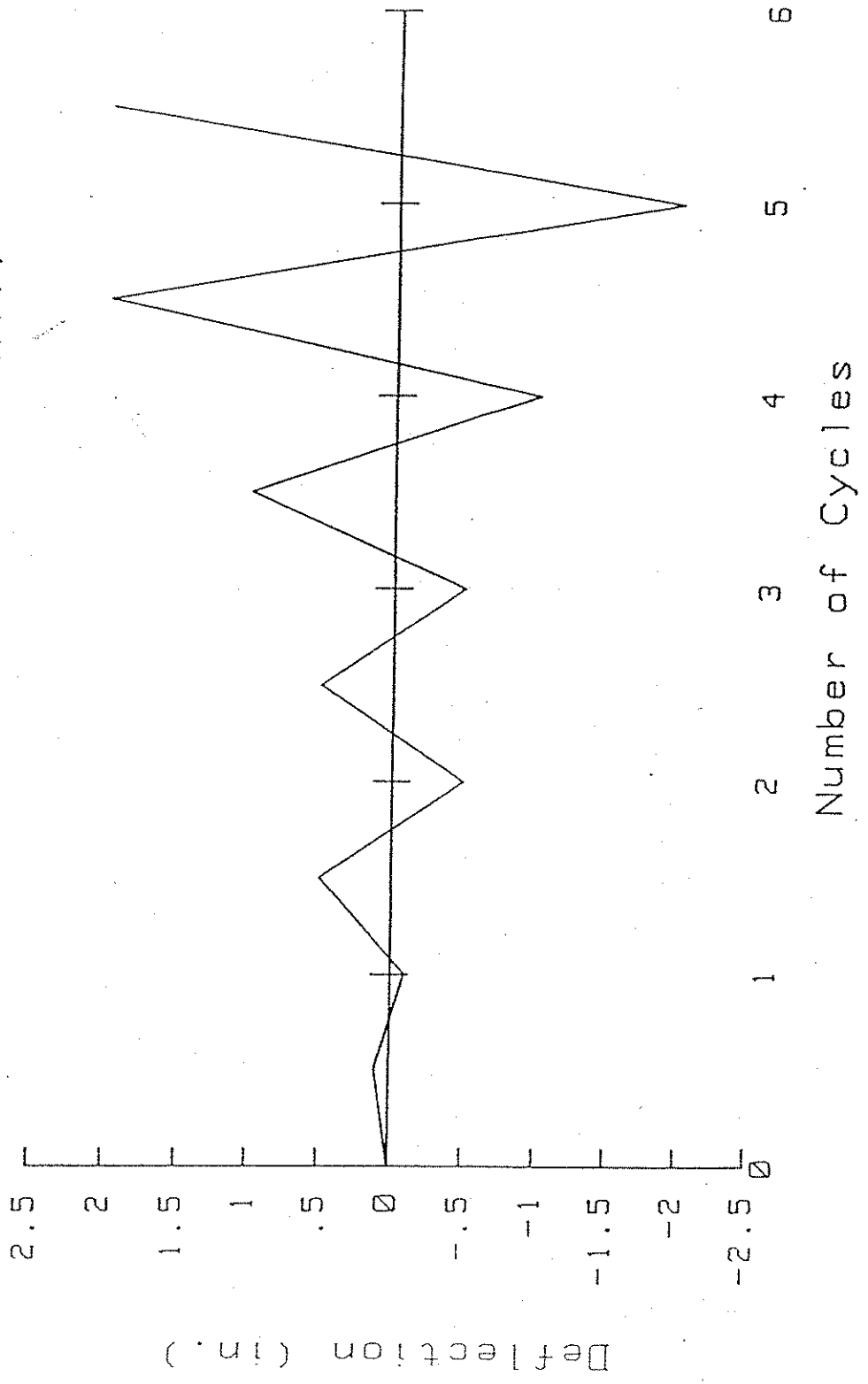


Fig. 2.11 Loading Cycle for Test Specimen CH4.

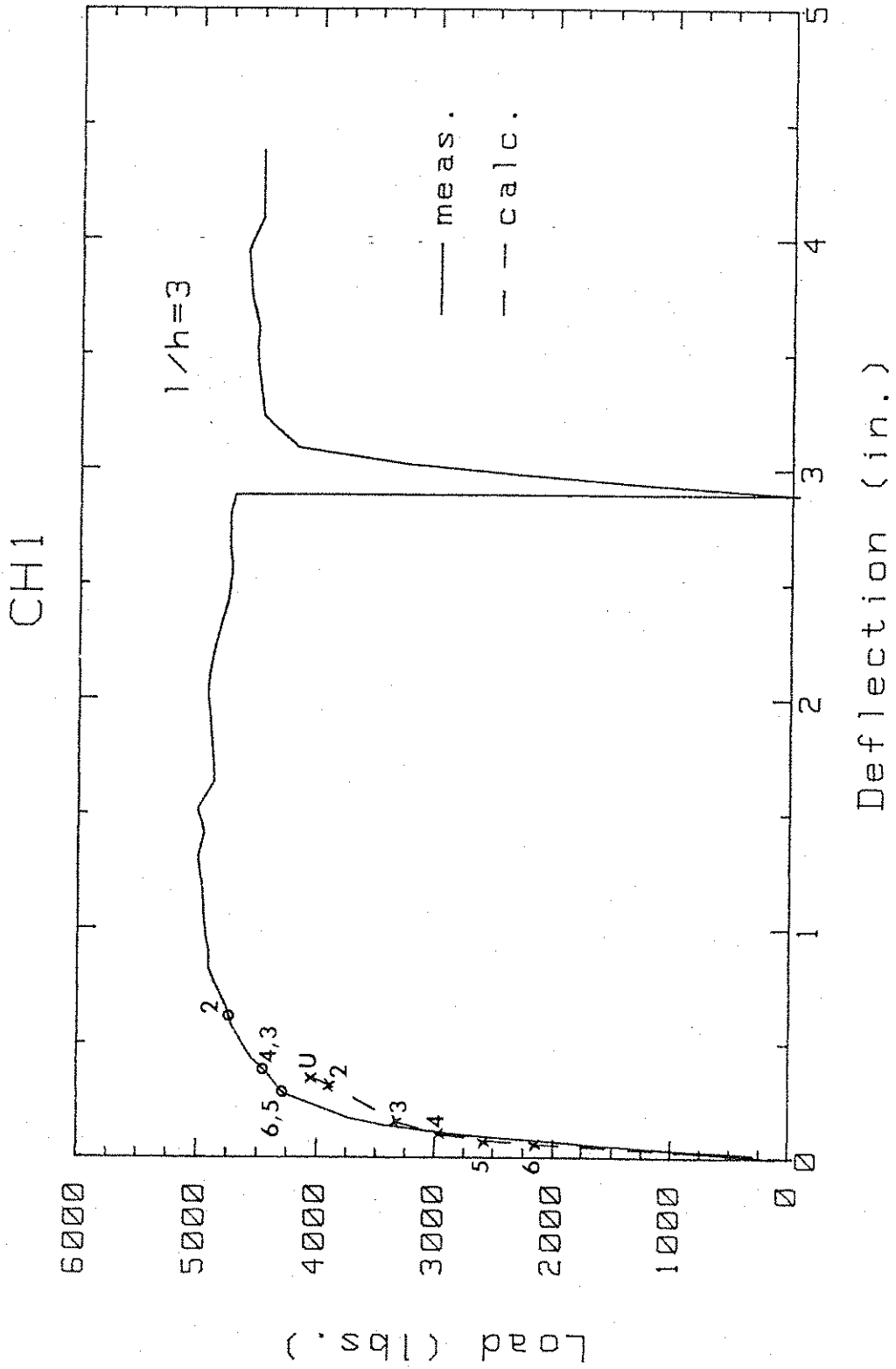


Fig. 3.1(a) Measured and Computed Load-Deflection Diagram for Specimen CH1.

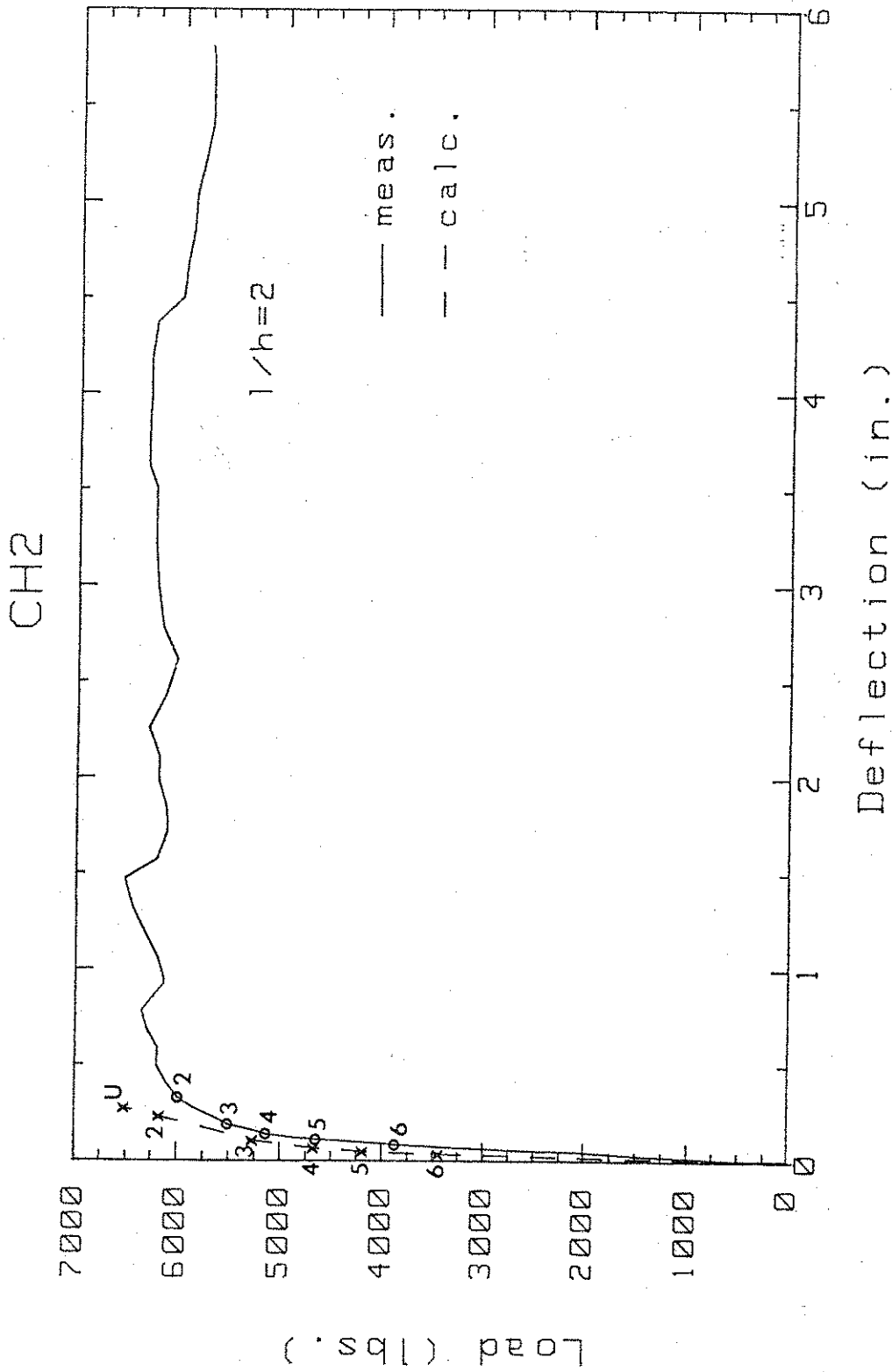


Fig. 3.1(b) Measured and Computed Load-Deflection Diagram for Specimen CH2.

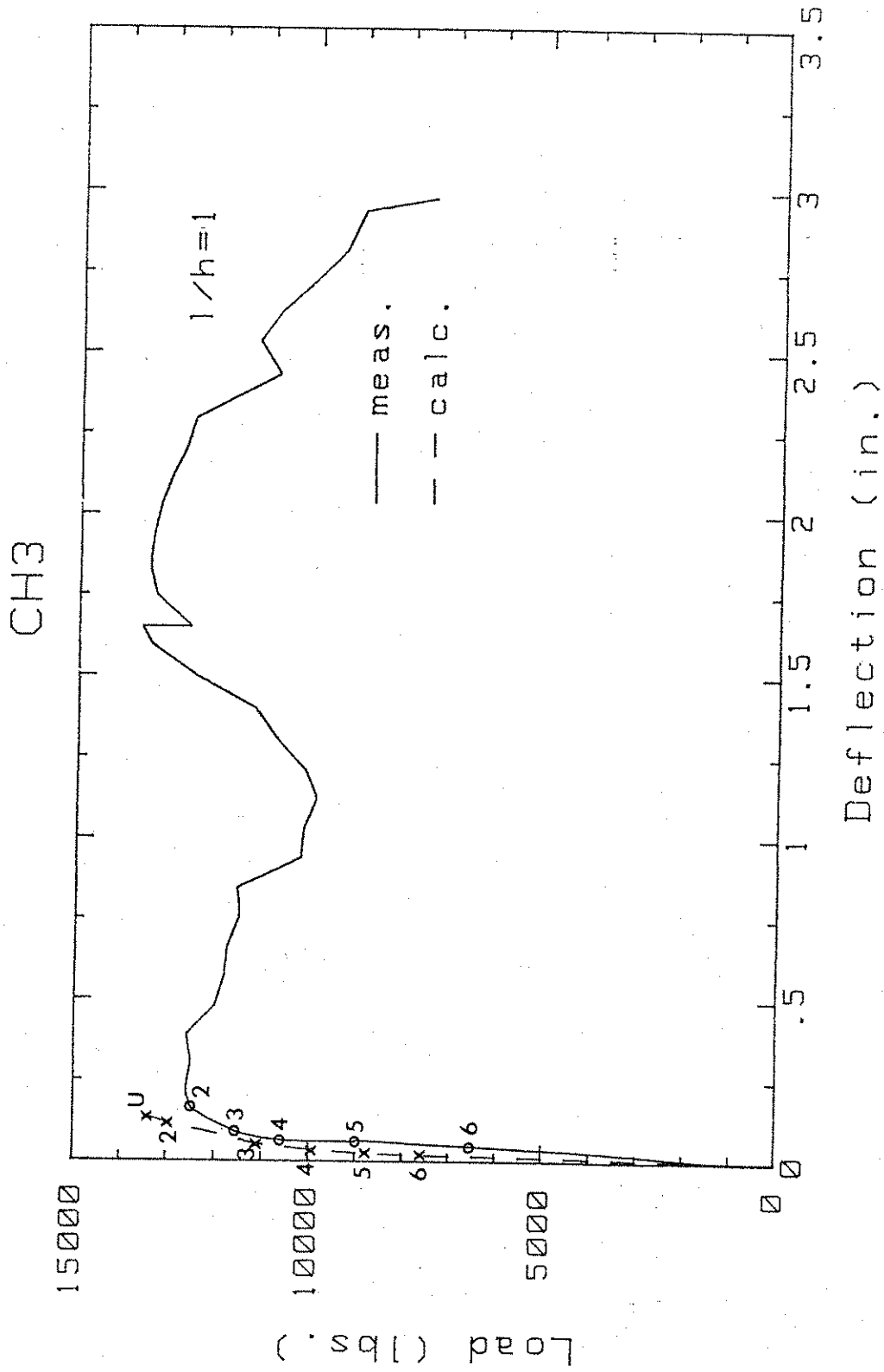


Fig. 3.1(c) Measured and Computed Load-Deflection Diagram for Specimen CH3.

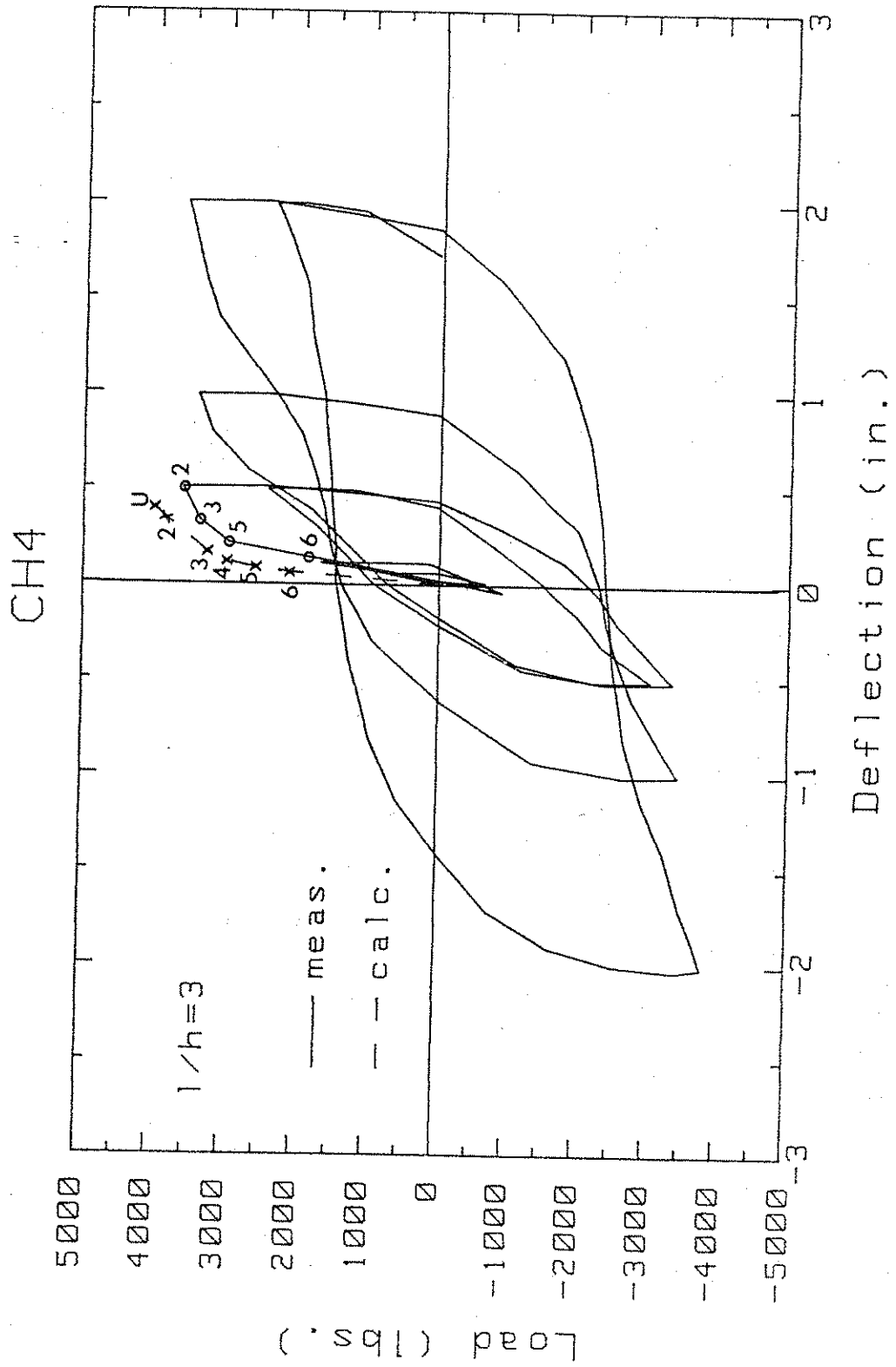


Fig. 3.1(d) Measured and Computed Load-Deflection Diagram for Specimen CH4.

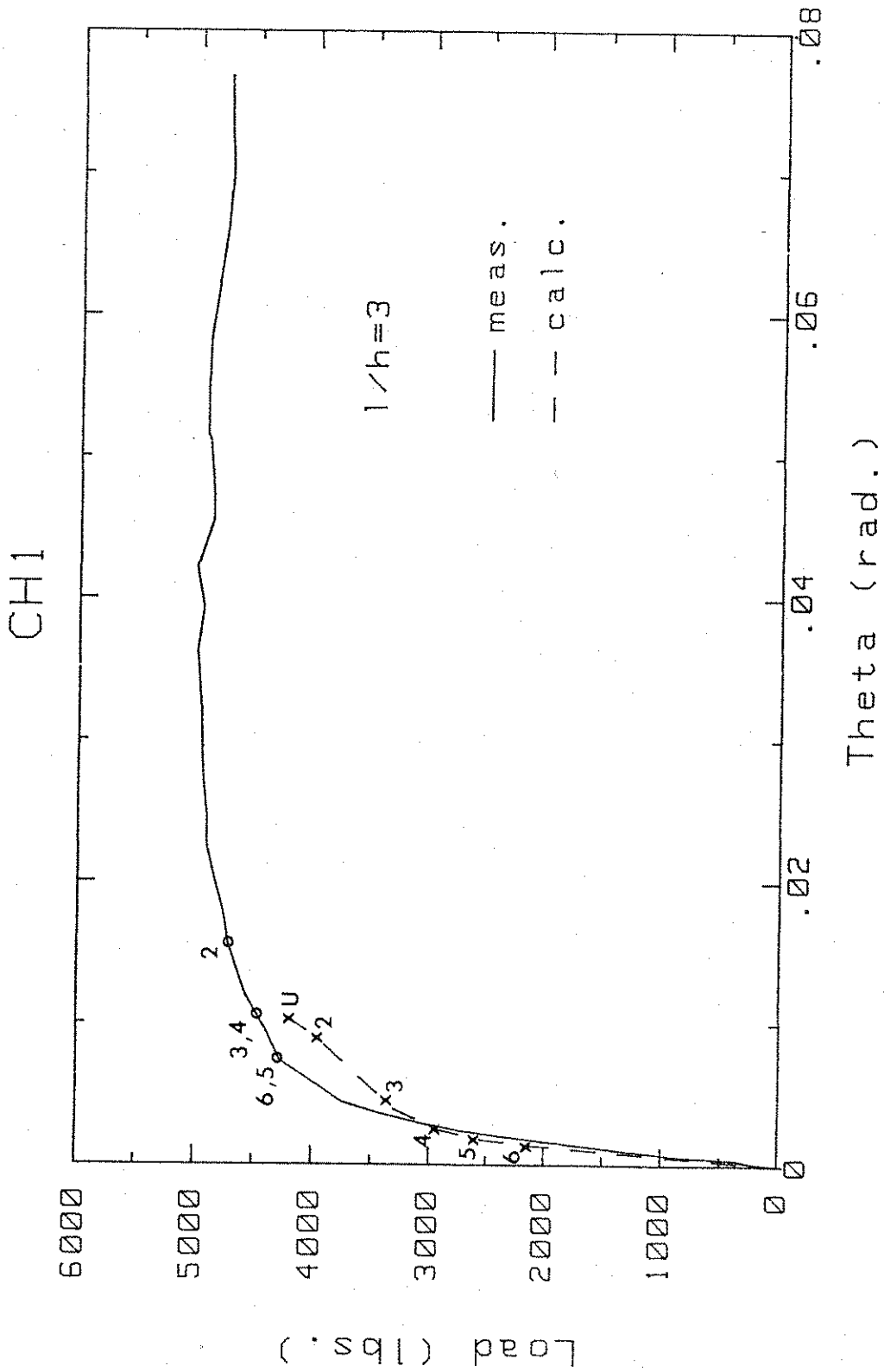


Fig. 3.2(a) Measured and Computed Load-Rotation Diagram for Specimen CH1.

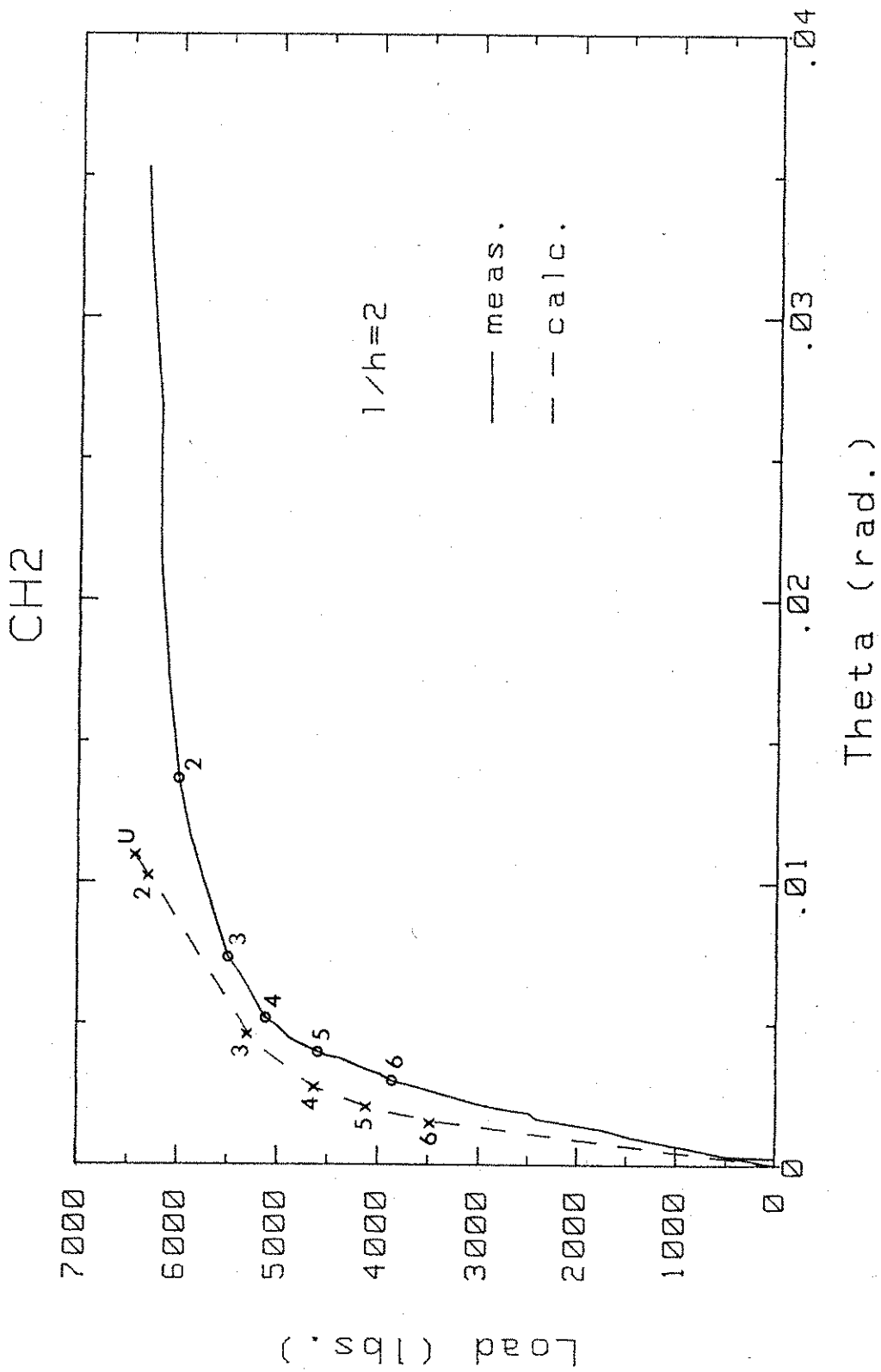


Fig. 3.2(b) Measured and Computed Load-Rotation Diagram for Specimen CH2.

CH3

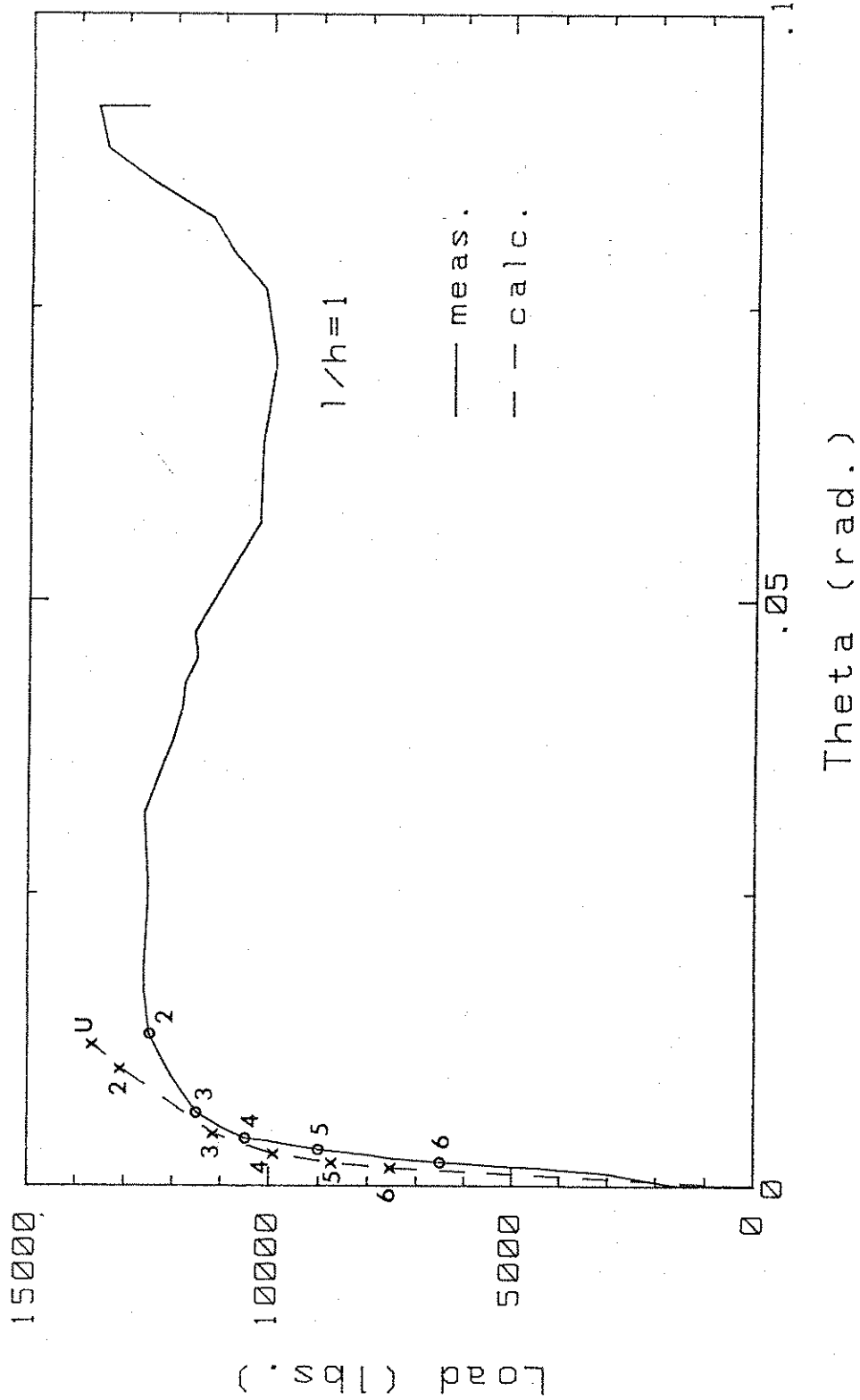


Fig. 3.2(c) Measured and Computed Load-Rotation Diagram for Specimen CH3.

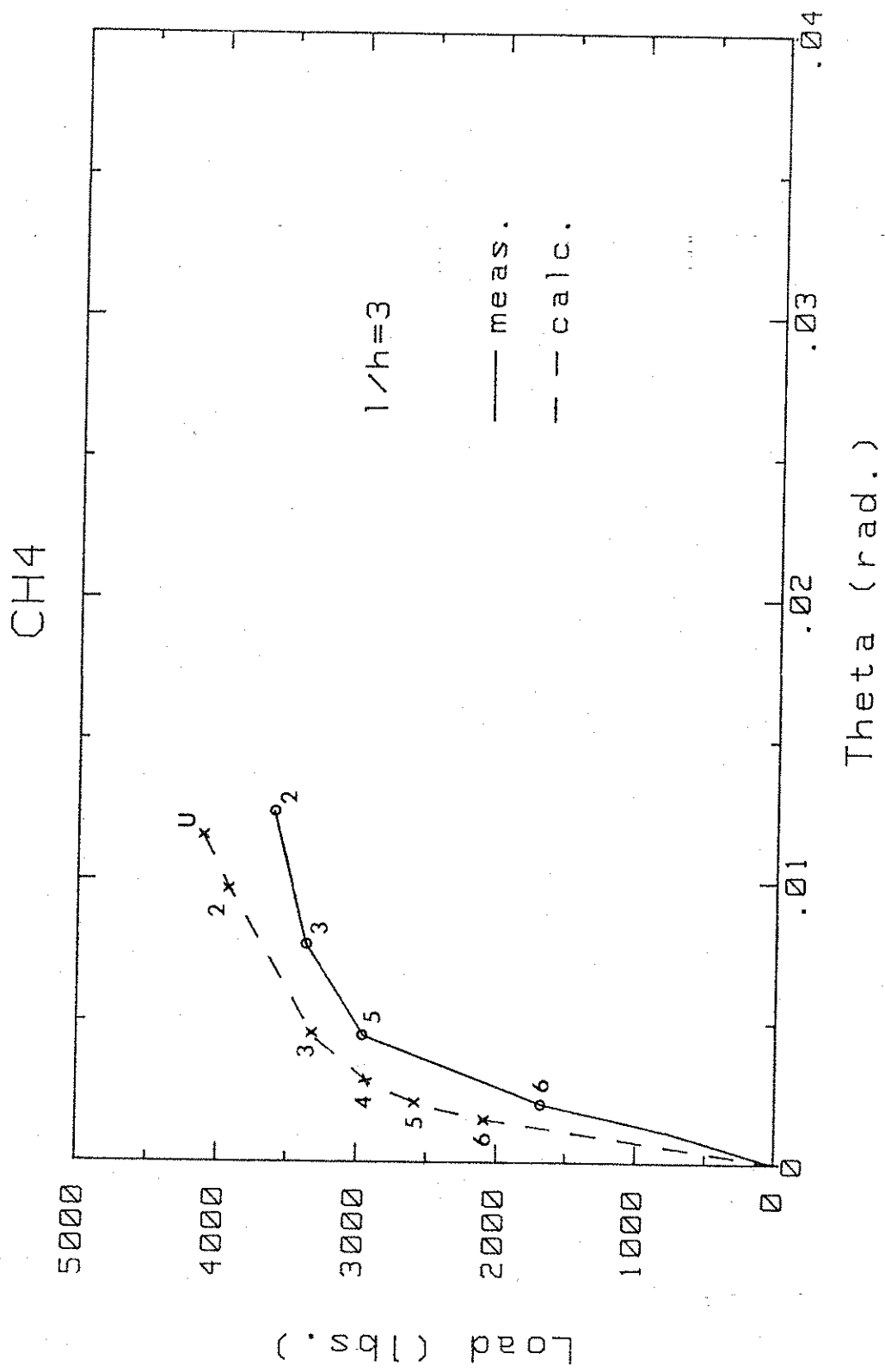


Fig. 3.2(d) Measured and Computed Load-Rotation Diagram for Specimen CH4.

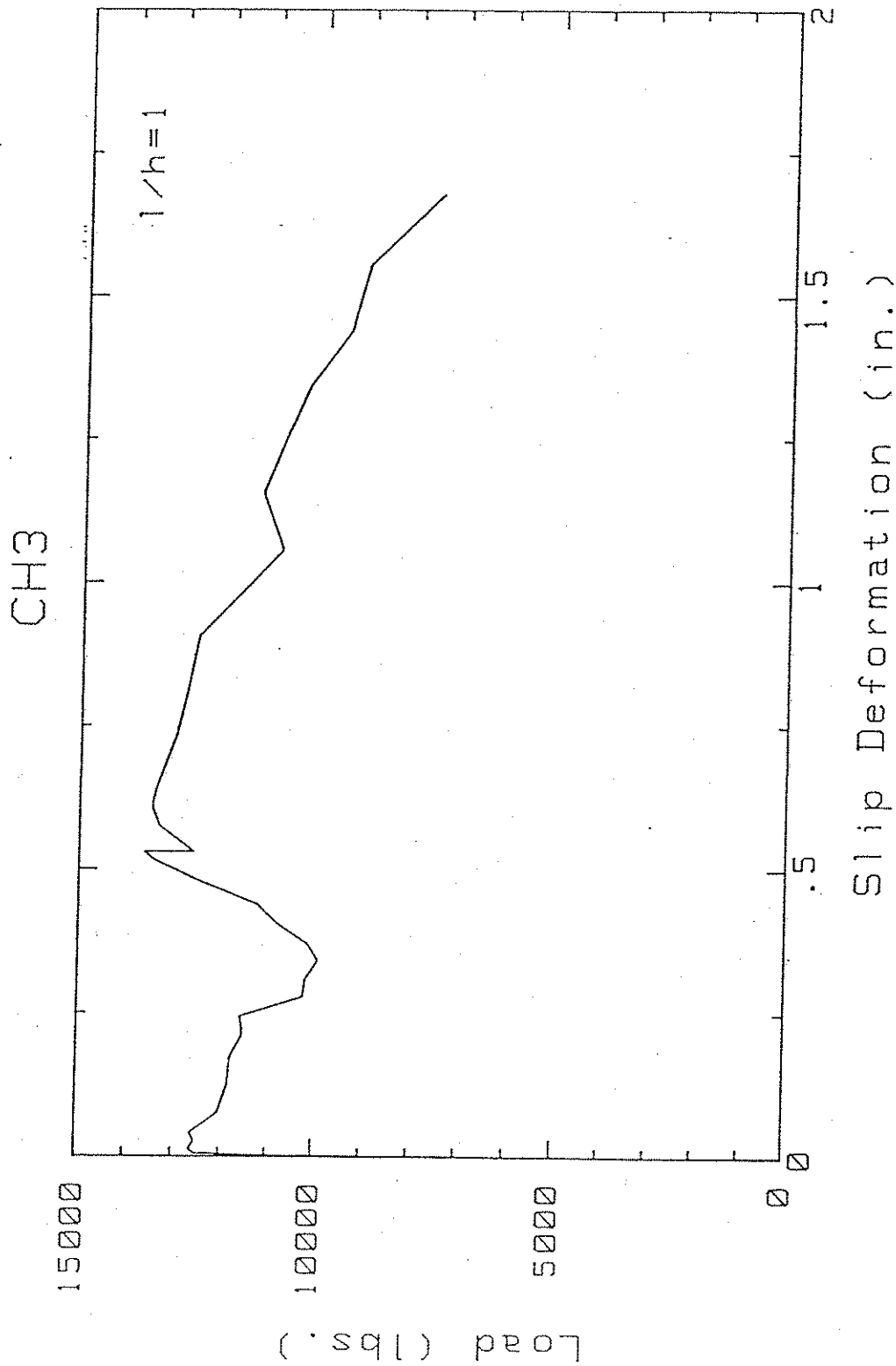


Fig. 3.3(a) Measured Load-Slip Deformation for Specimen CH3.

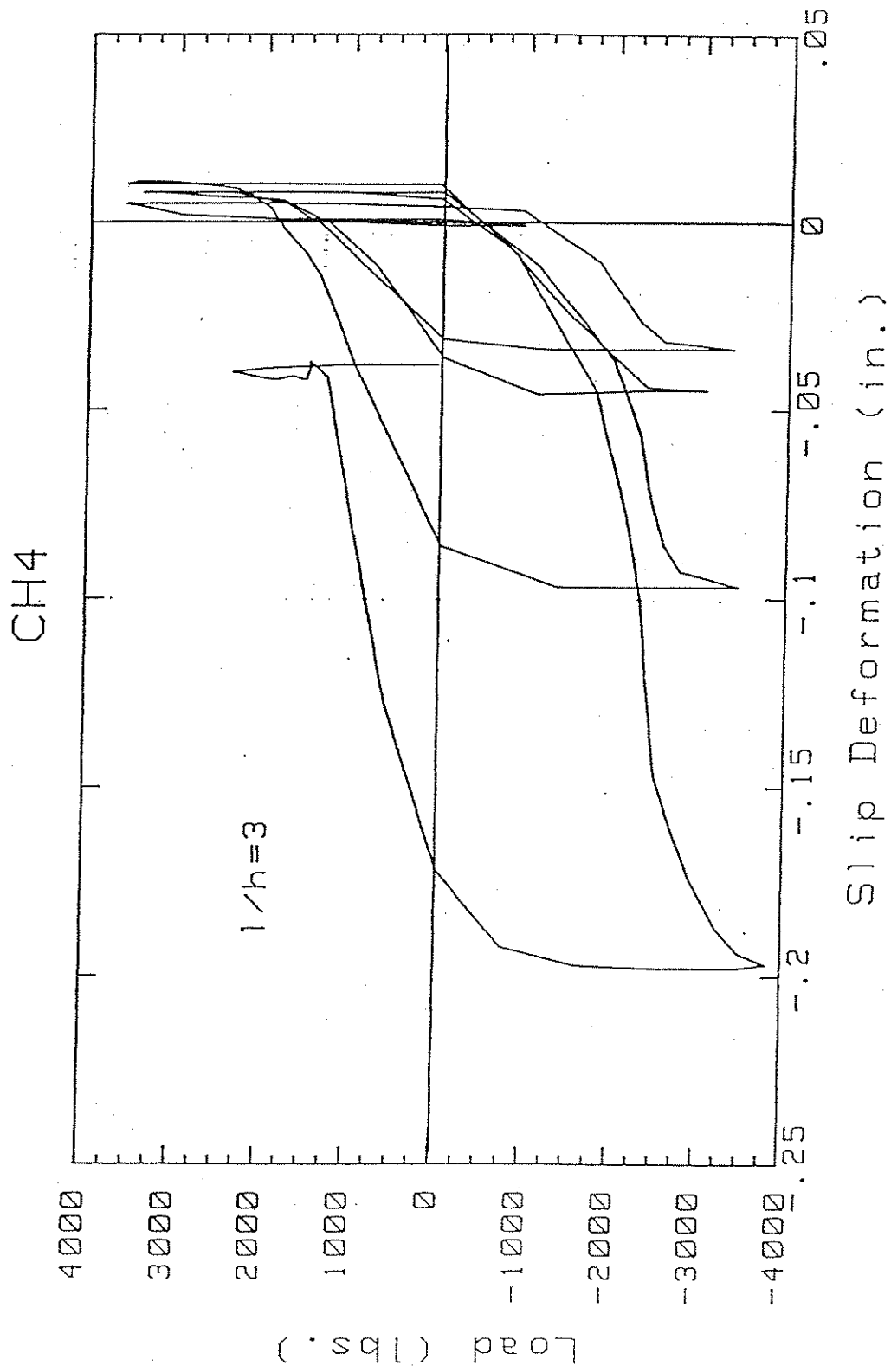
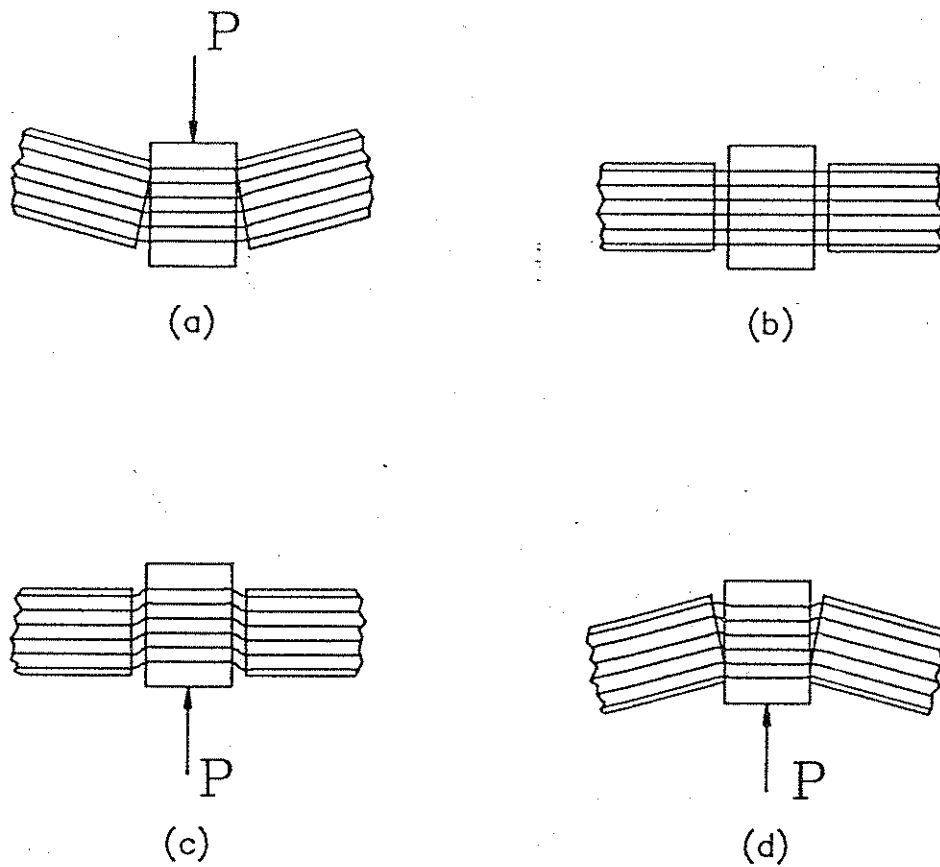


Fig. 3.3(b) Measured Load-Slip Deformation for Specimen CH4.



(a) Initial position after being loaded downward.

(b) Slight gap at hinge interface.

(c) Slight contact at interface. Relying on dowel action and slight frictional resistance for shear capacity.

(d) Crack closes, and compression is developed.

A friction force is developed in the compression zone, thus increasing shear resistance and load carrying capacity of the section.

Fig. 3.4 Response of Hinged Specimen when Subjected to Load Reversals.

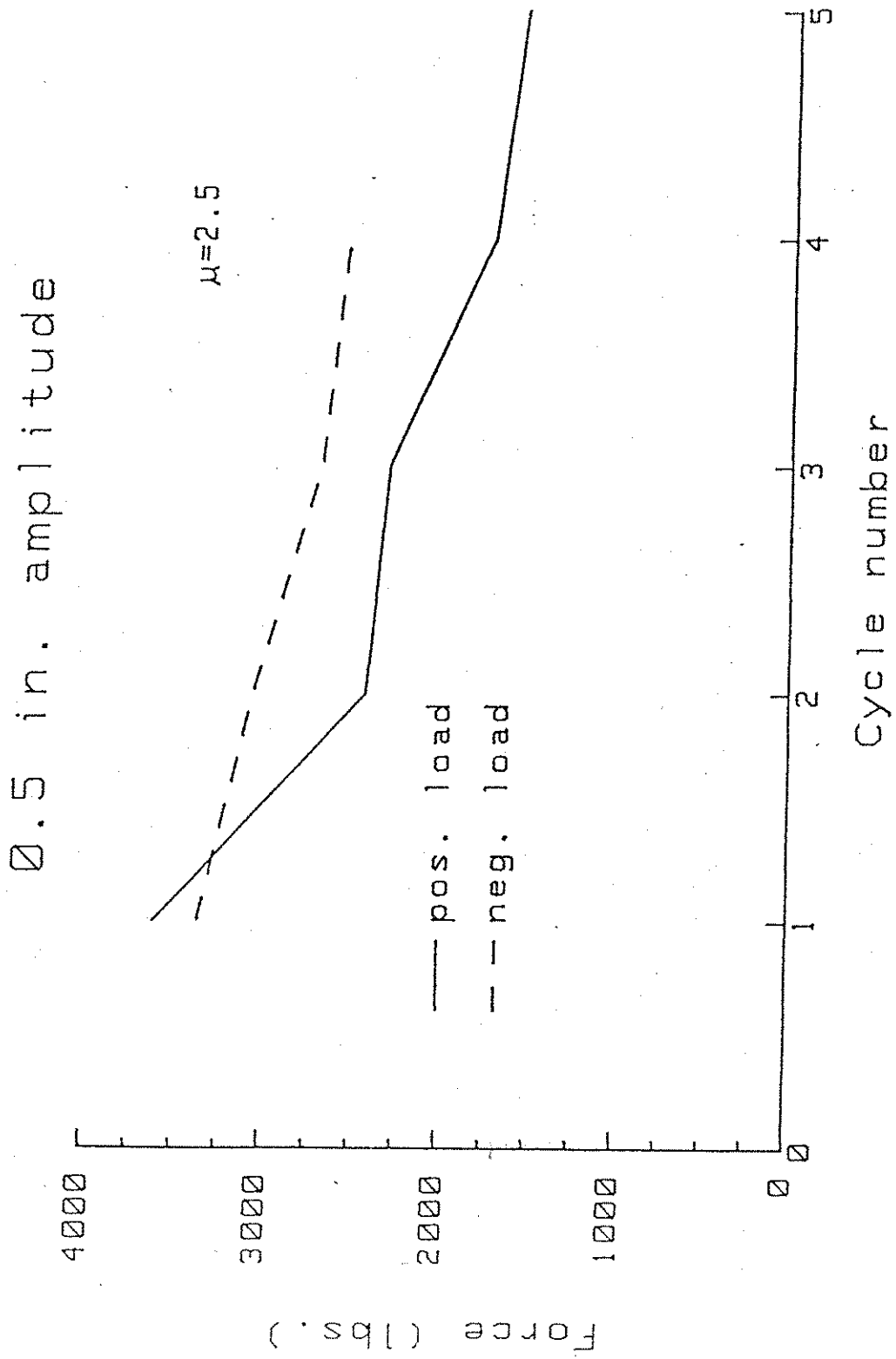


Fig. 3.5 Load vs. Cycle Number for a Ductility of 2.5.

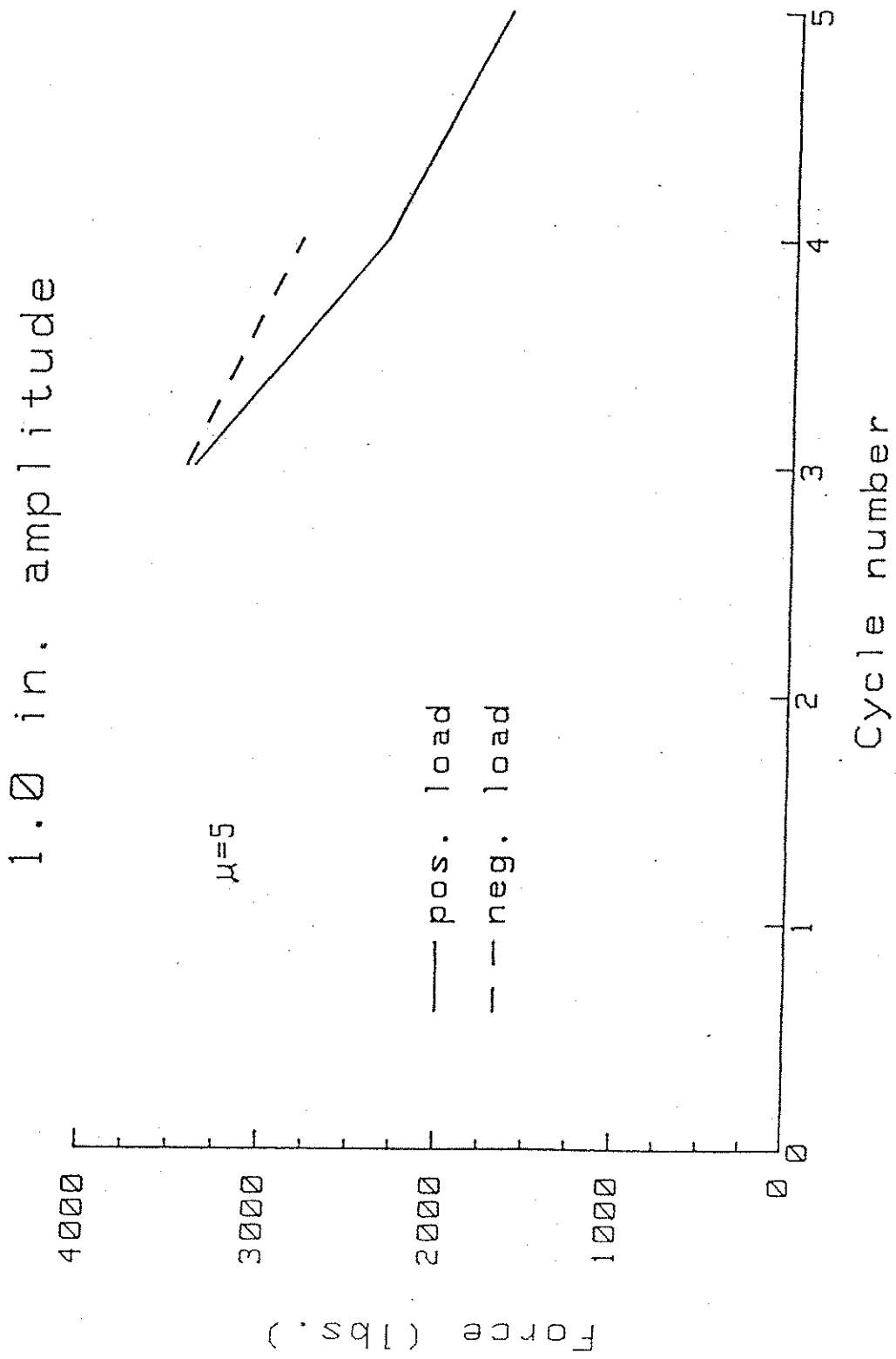


Fig. 3.6 Load vs. Cycle Number for a Ductility of 5.0.

STRAIN - RIGHT SIDE GAGES

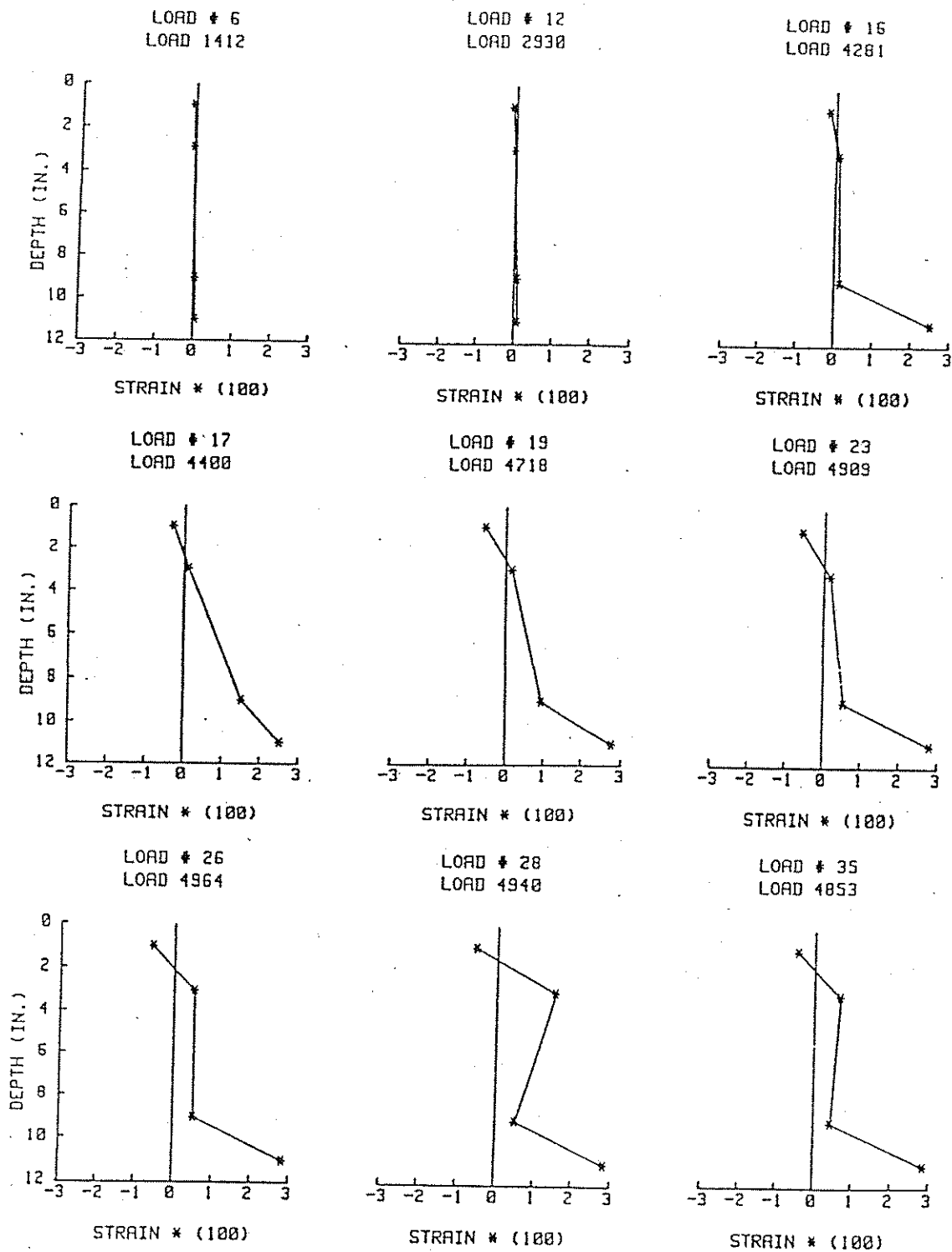


Fig. 3.7 Strain Distribution in Right Side Gages, Specimen CH1.

STRAIN - LEFT SIDE GAGES

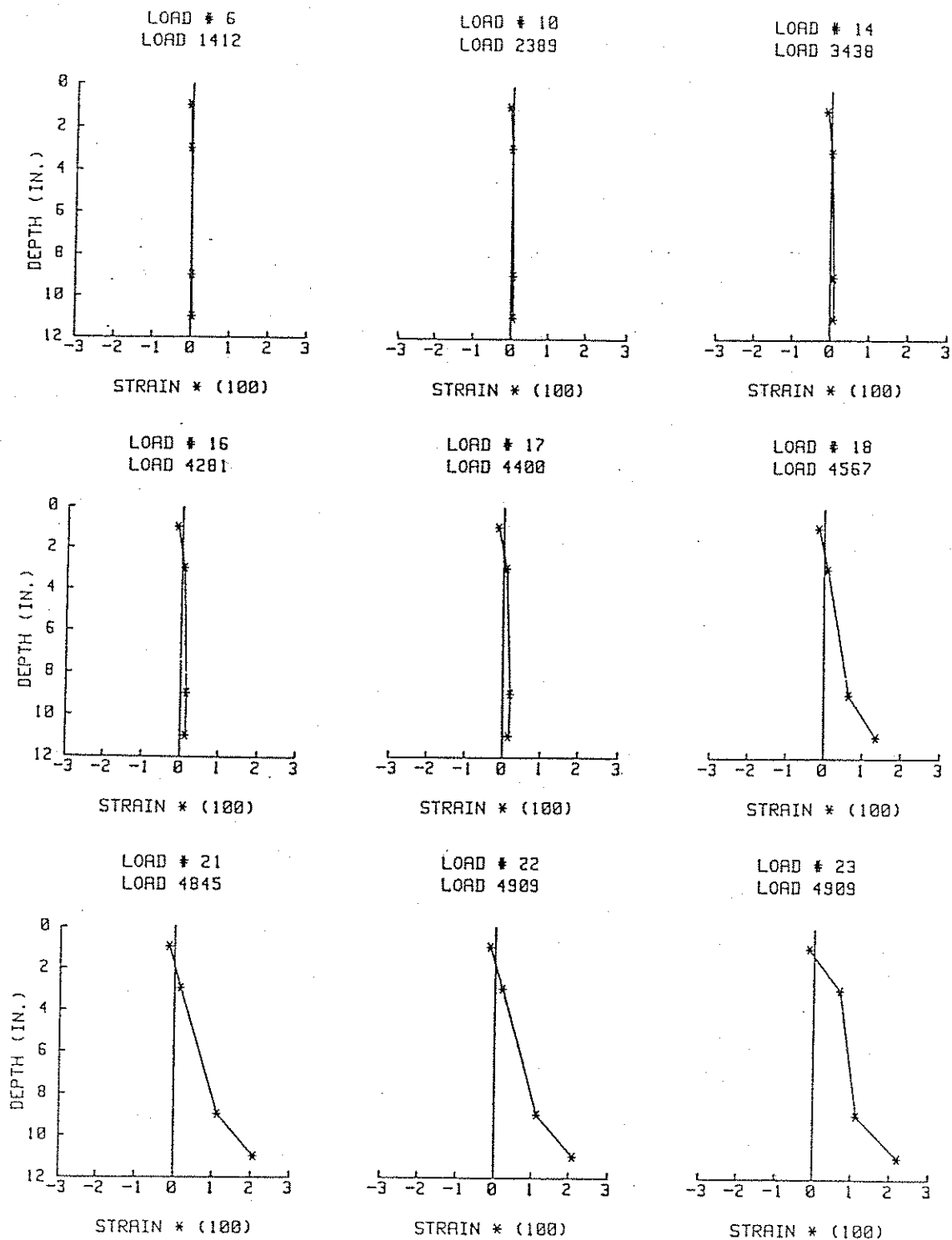


Fig. 3.8 Strain Distribution in Left Side Gages, Specimen CH1.

STRAIN - RIGHT SIDE GAGES

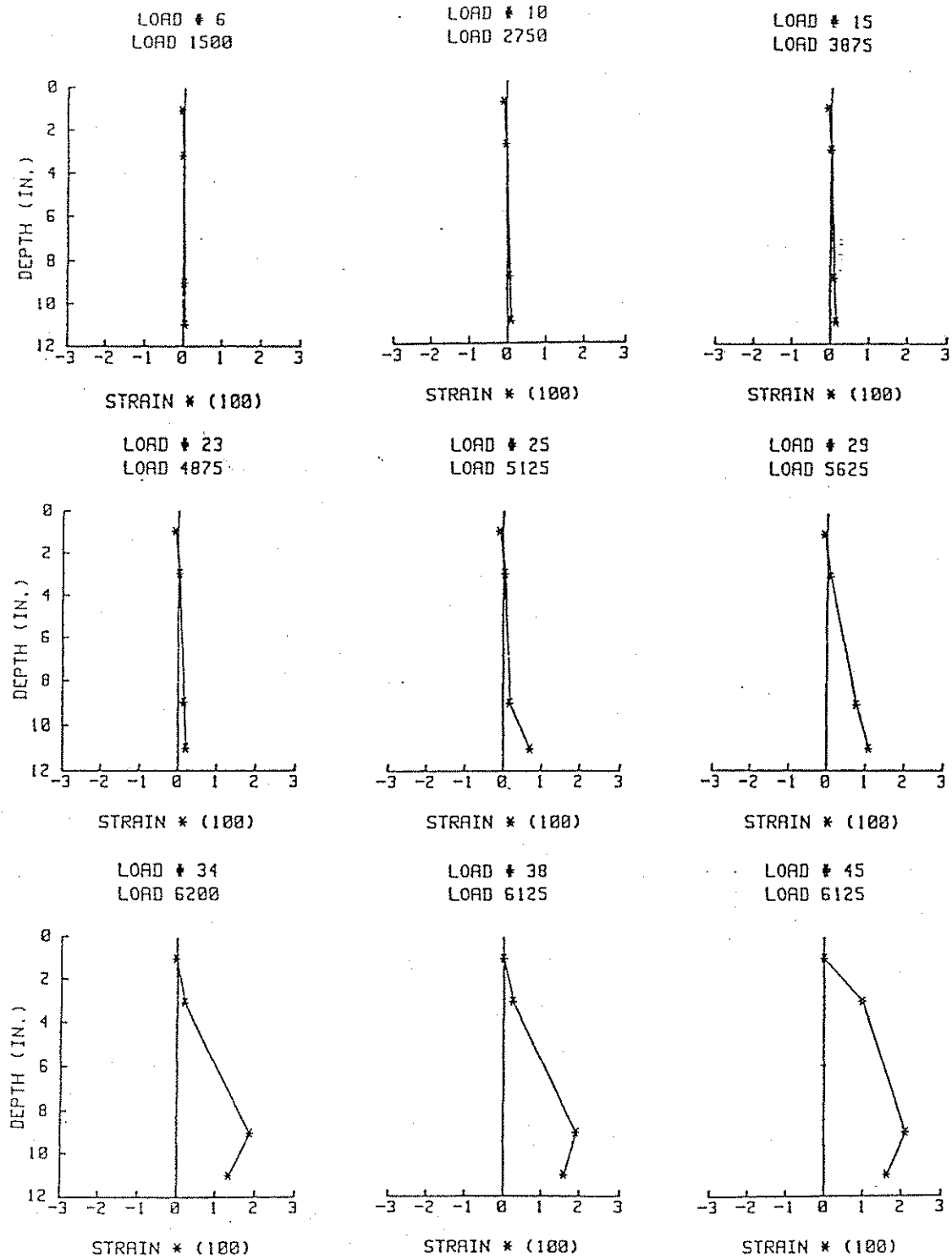


Fig. 3.9 Strain Distribution in Right Side Gages, Specimen CH2.

STRAIN - LEFT SIDE GAGES

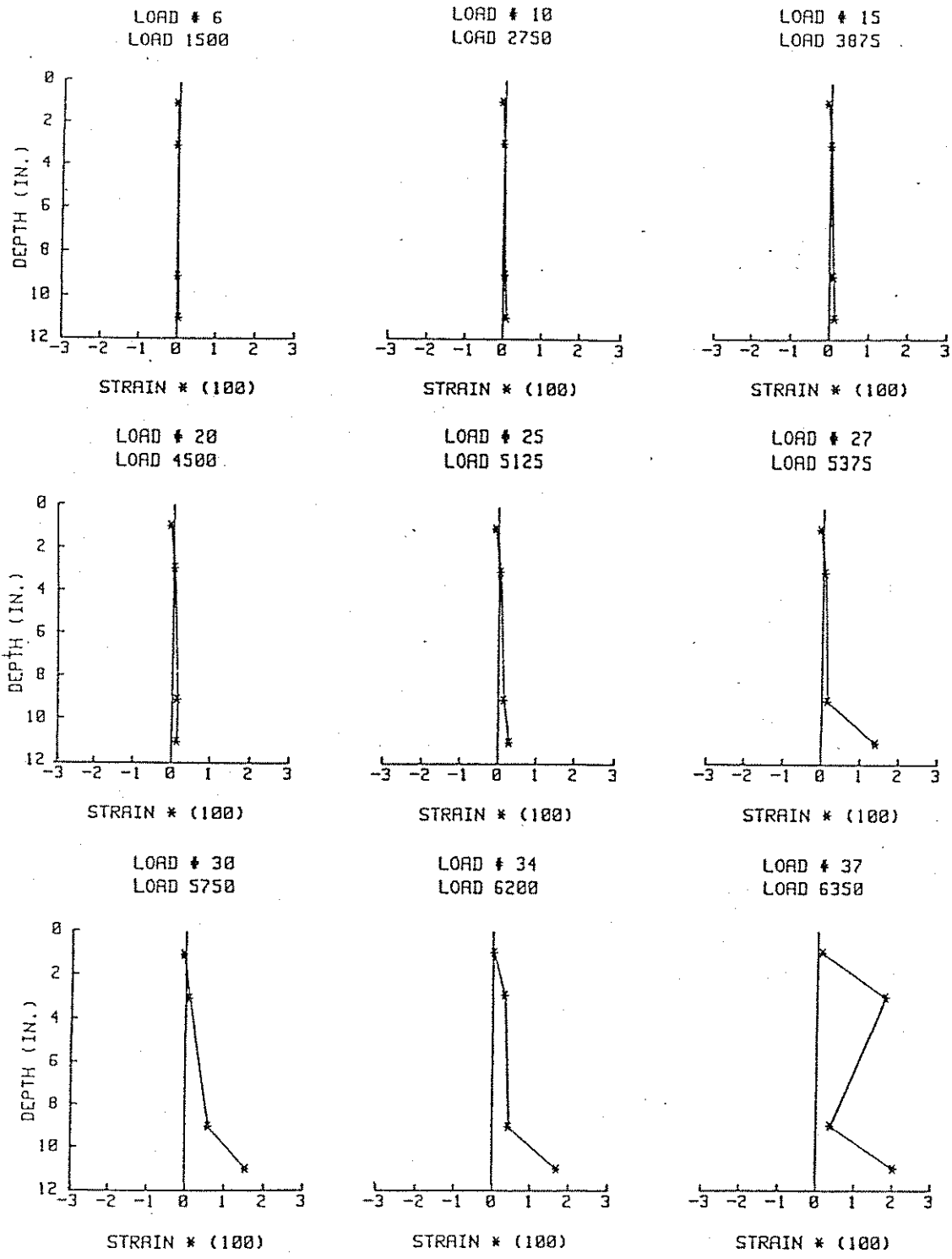


Fig. 3.10 Strain Distribution in Left Side Gages, Specimen CH2.

STRAIN - RIGHT SIDE GAGES

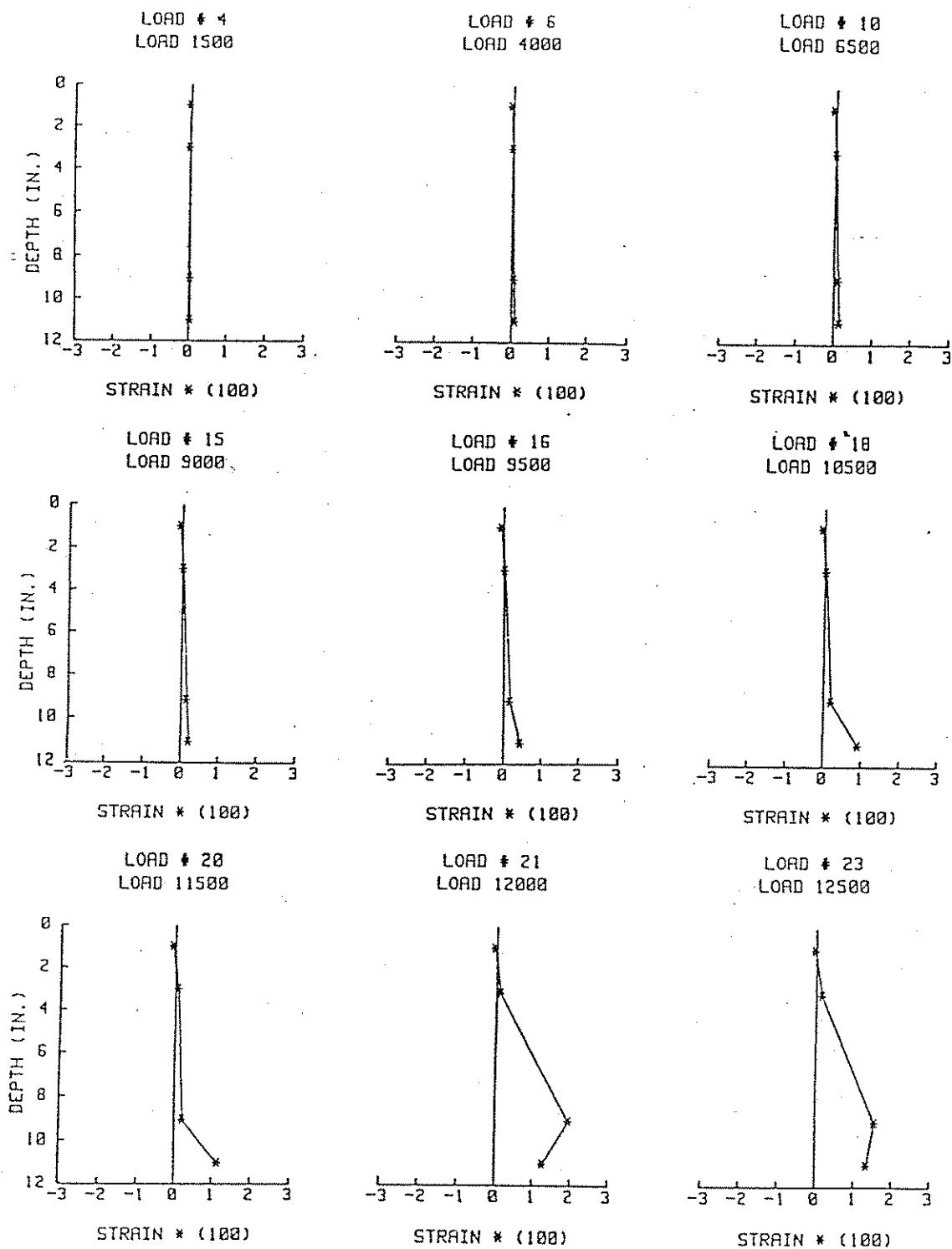


Fig. 3.11 Strain Distribution in Right Side Gages, Specimen CH3.

STRAIN - LEFT SIDE GAGES

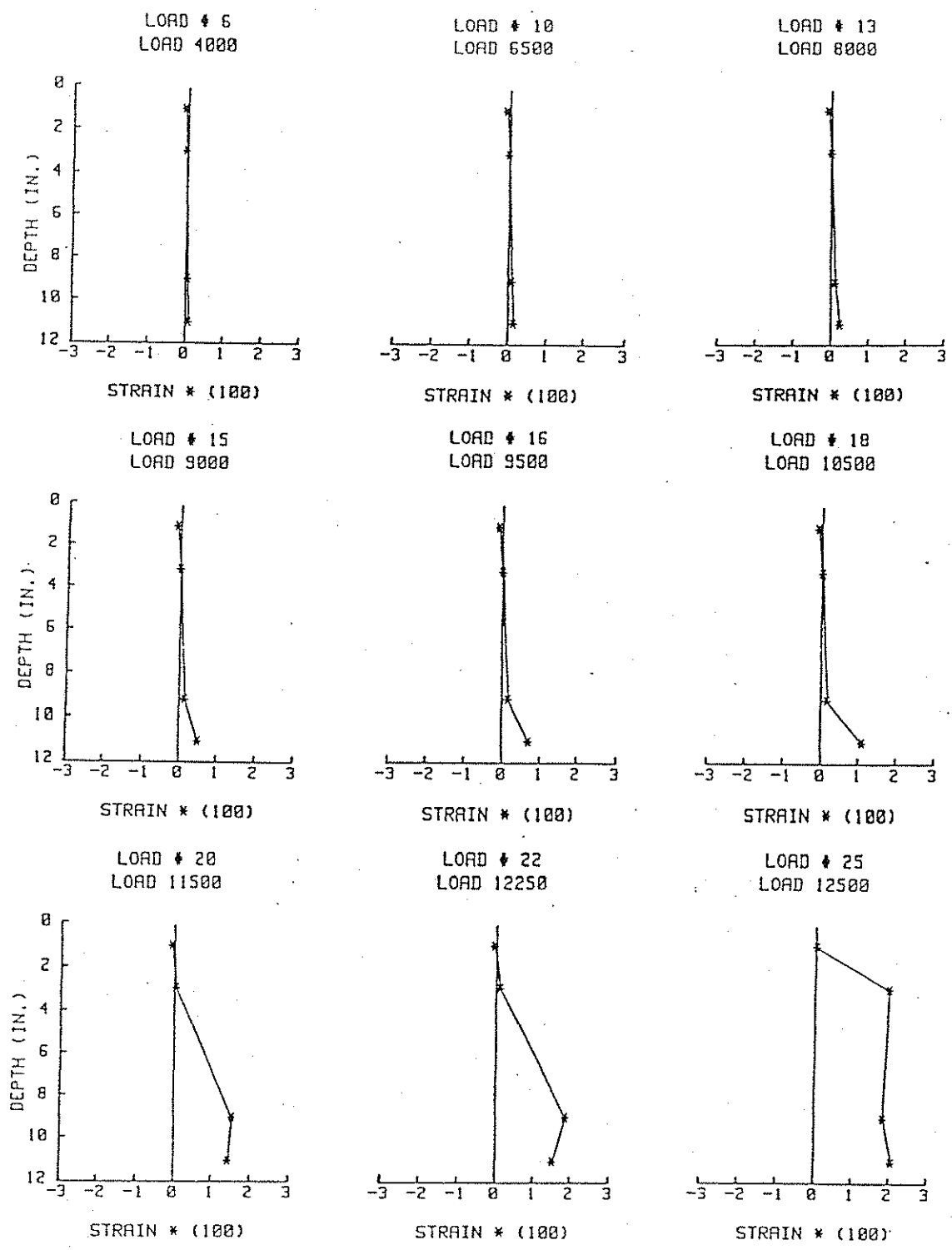


Fig. 3.12 Strain Distribution in Left Side Gages, Specimen CH3.

STRAIN - RIGHT SIDE GAGES

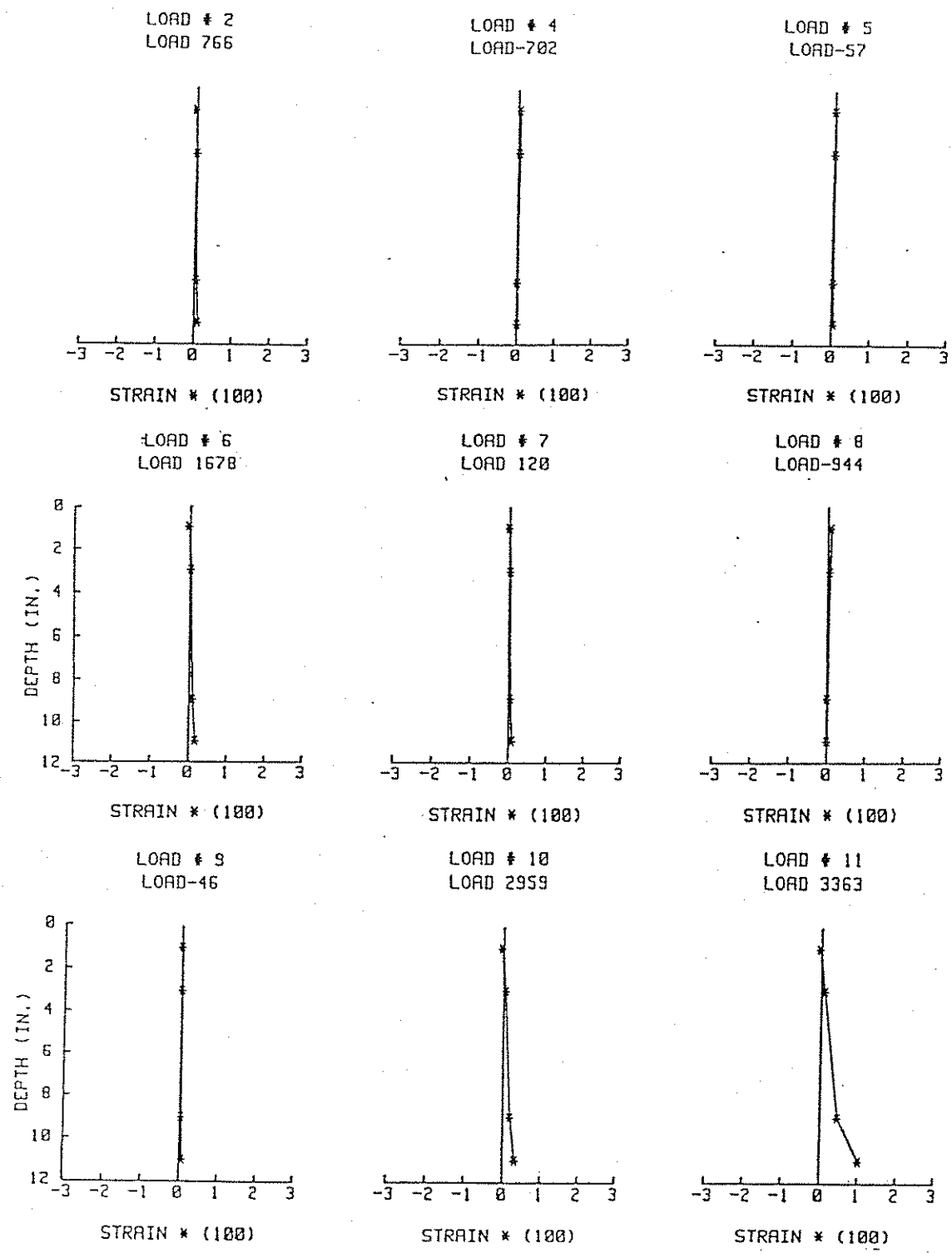


Fig. 3.13 Strain Distribution in Right Side Gages, Specimen CH4.

STRAIN - LEFT SIDE GAGES

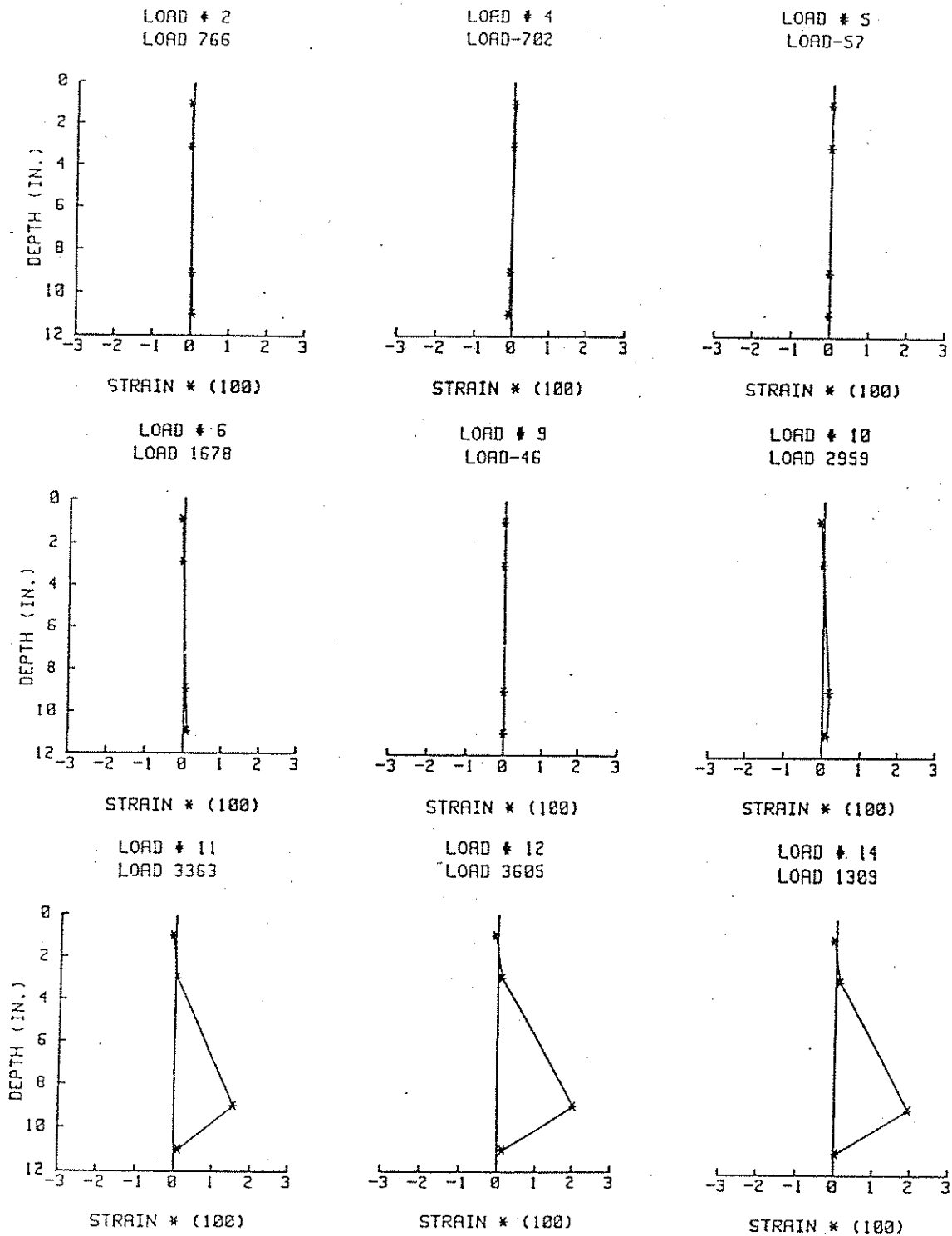


Fig. 3.14 Strain Distribution in Left Side Gages, Specimen CH4.

STRAIN - LEFT SIDE GAGES

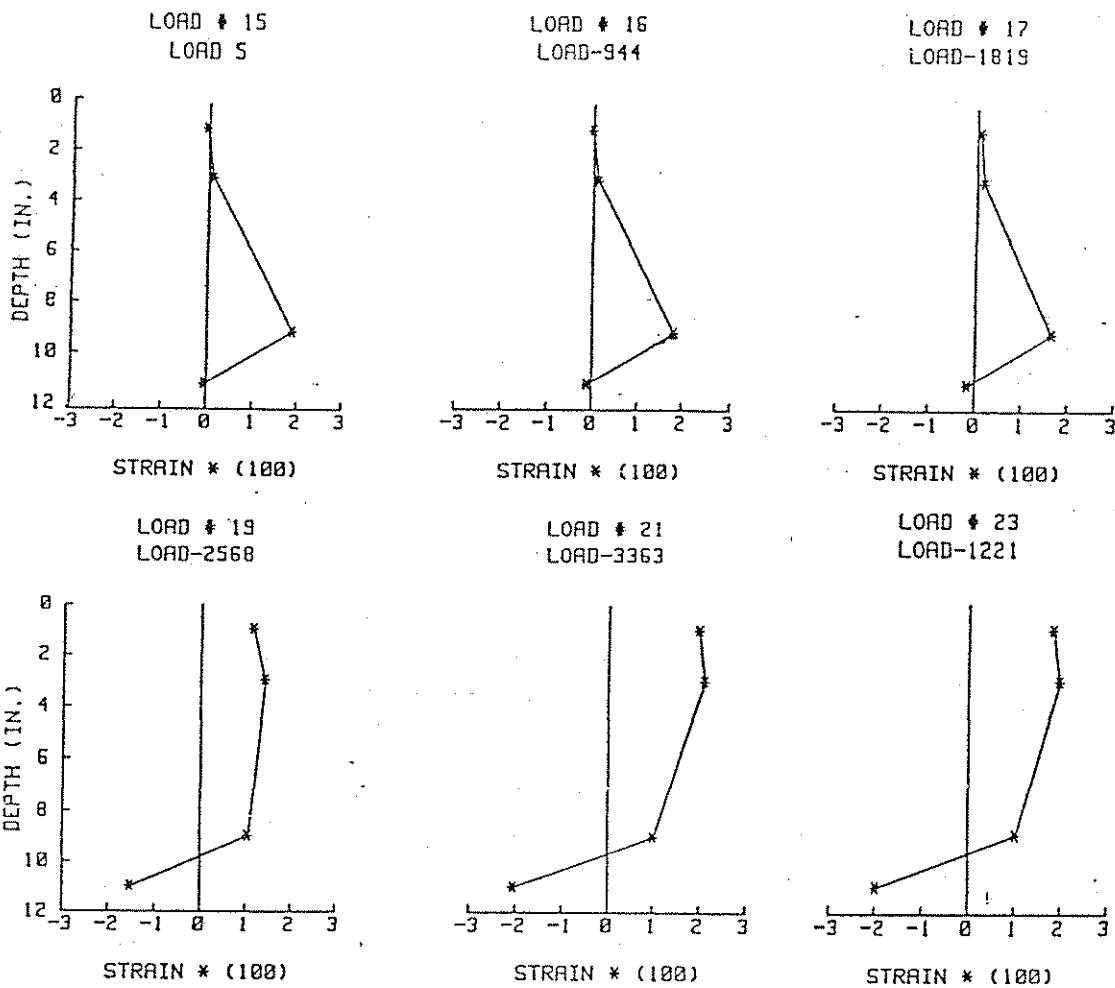


Fig. 3.15 Strain Distribution in Left Side Gages, Specimen CH4.

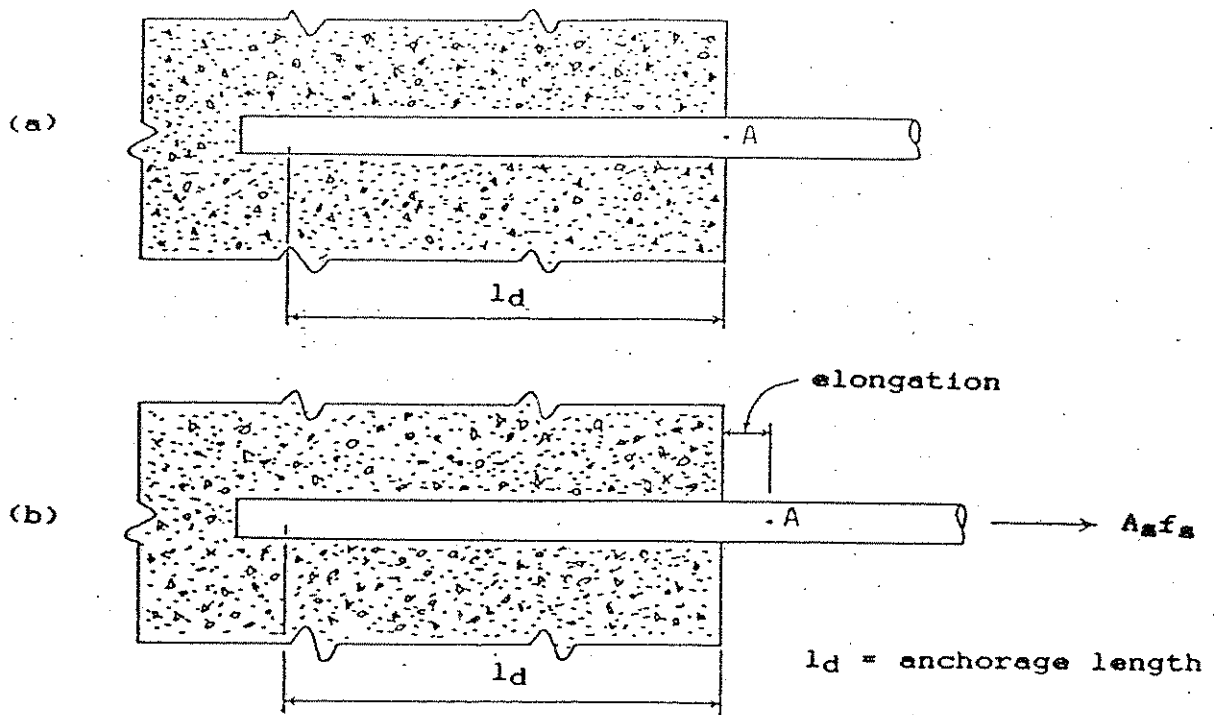


Figure 4.1 Elongation of a Steel Bar Embedded in Concrete

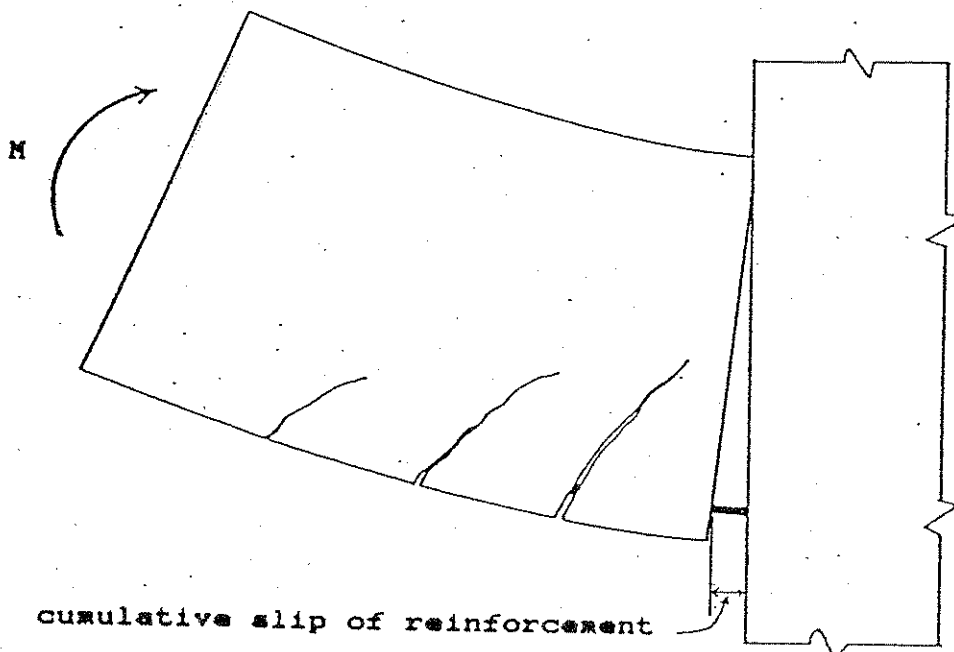


Figure 4.2 Bar Slip Mechanism in a Reinforced Concrete Element.

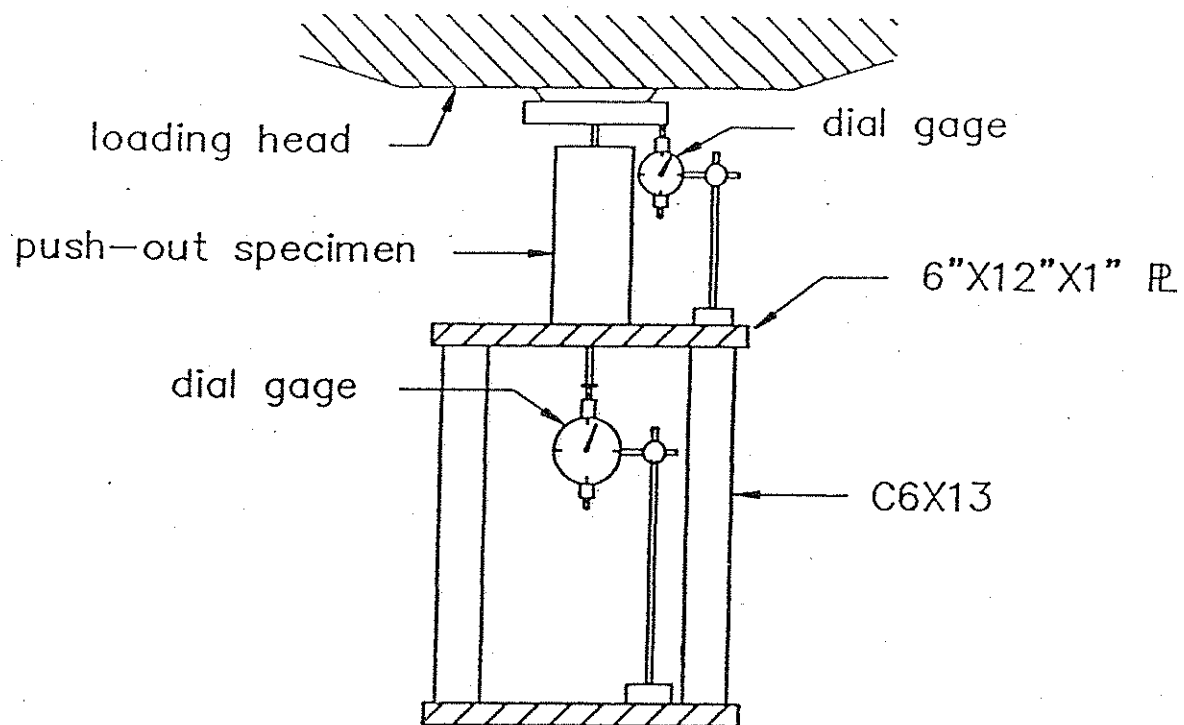


Figure 4.3 Test Set-up for Push-out Specimens.

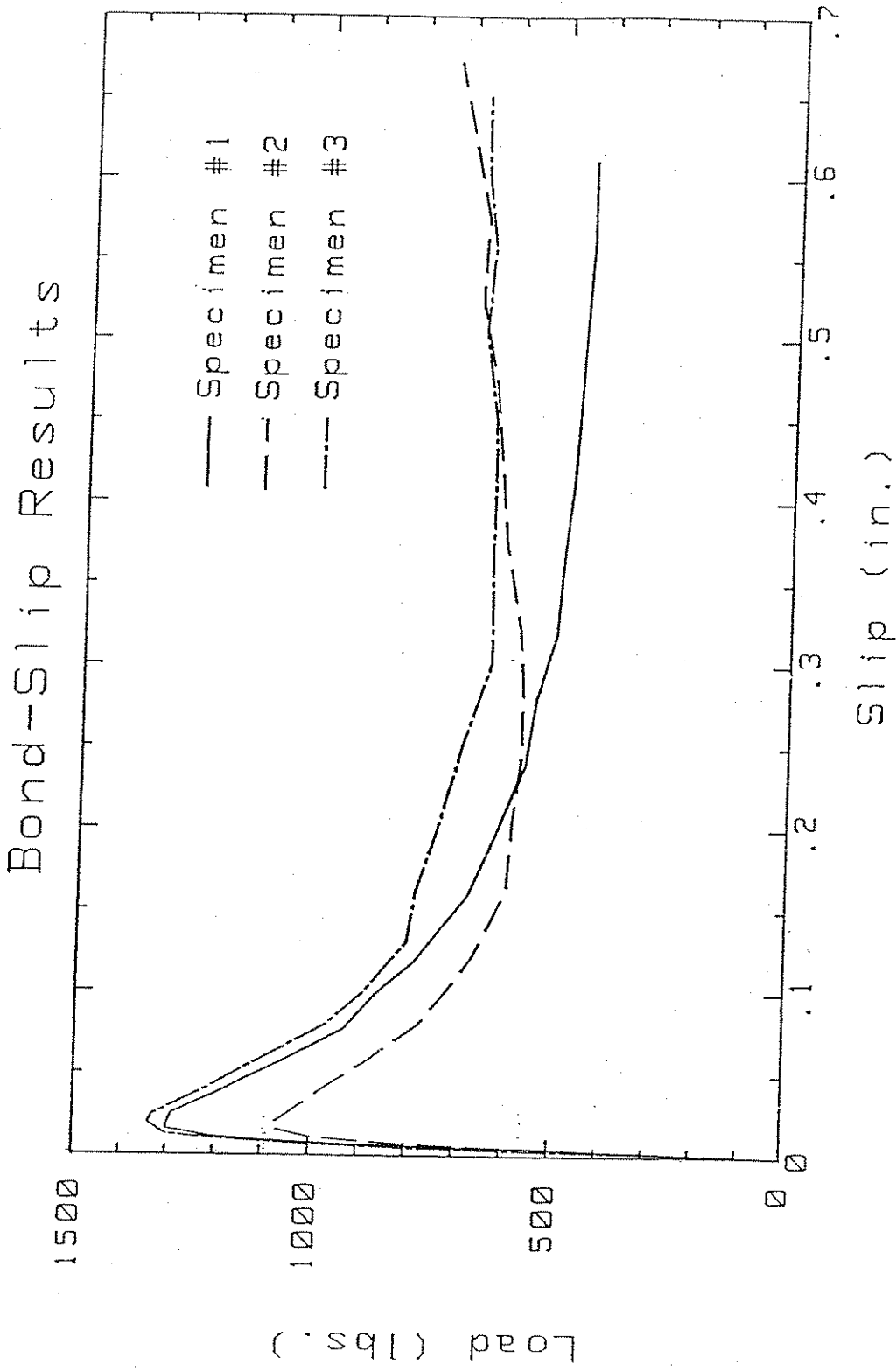


Figure 4.4 Measured Load vs. Slip Results for the Push-out Specimens.

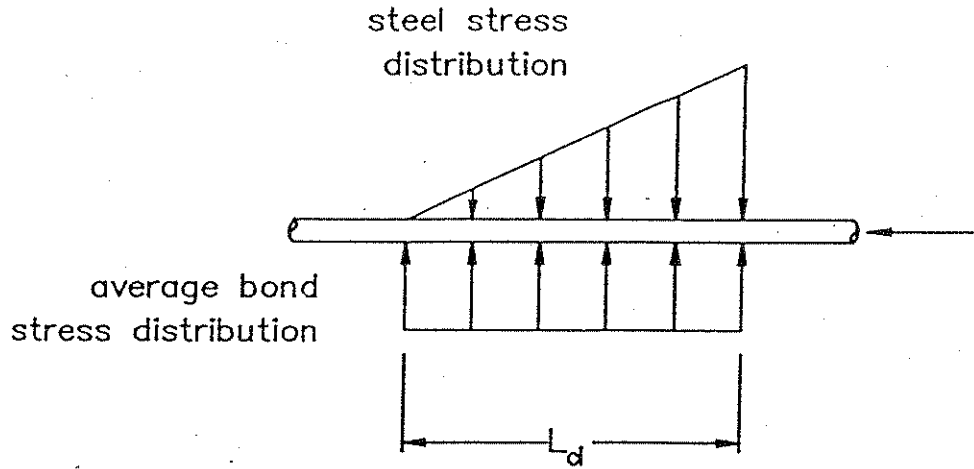


Fig. 4.5 Assumed Typical Steel Stress and Bond Stress Distribution.

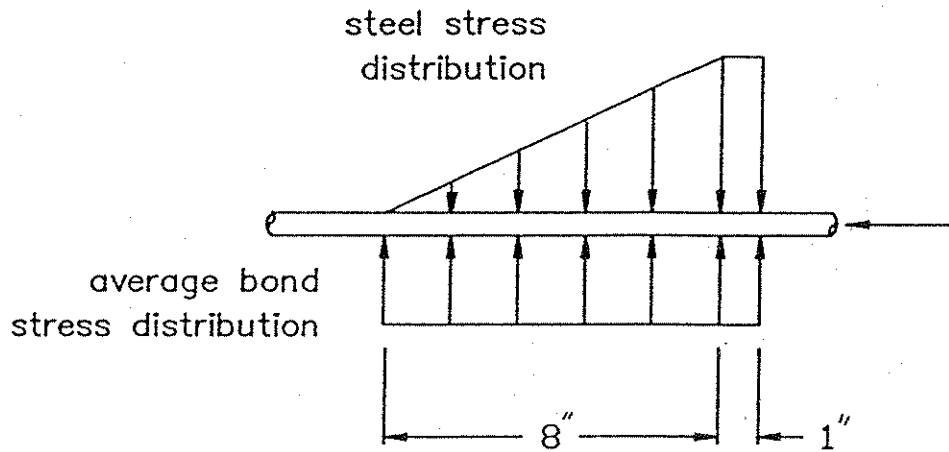


Fig. 4.6 Assumed Steel Stress and Bond Stress Distribution for Push-out Specimens.

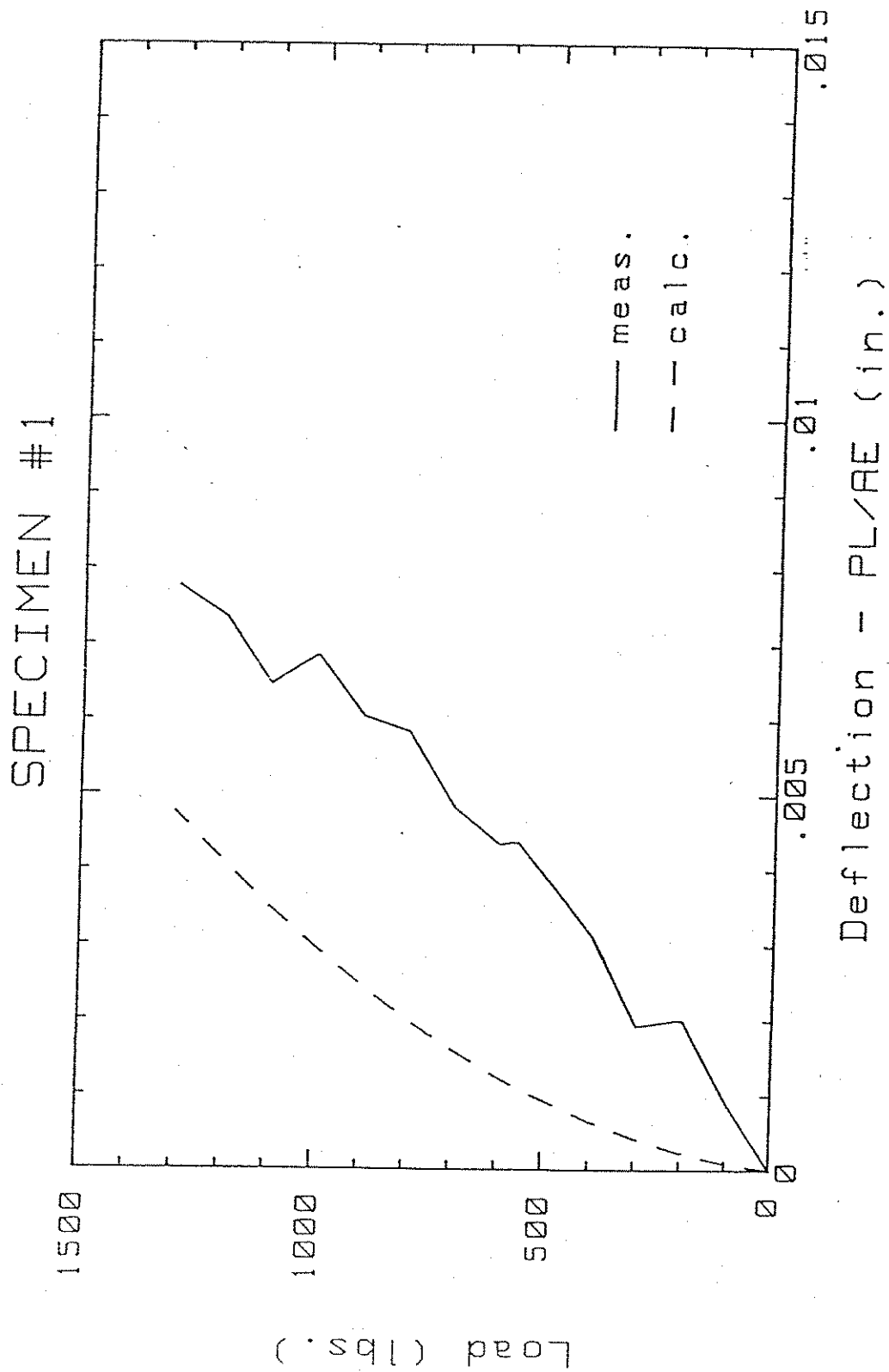


Fig. 4.7(a) Measured and Computed Load vs. Elongation, Push-out Specimen #1.

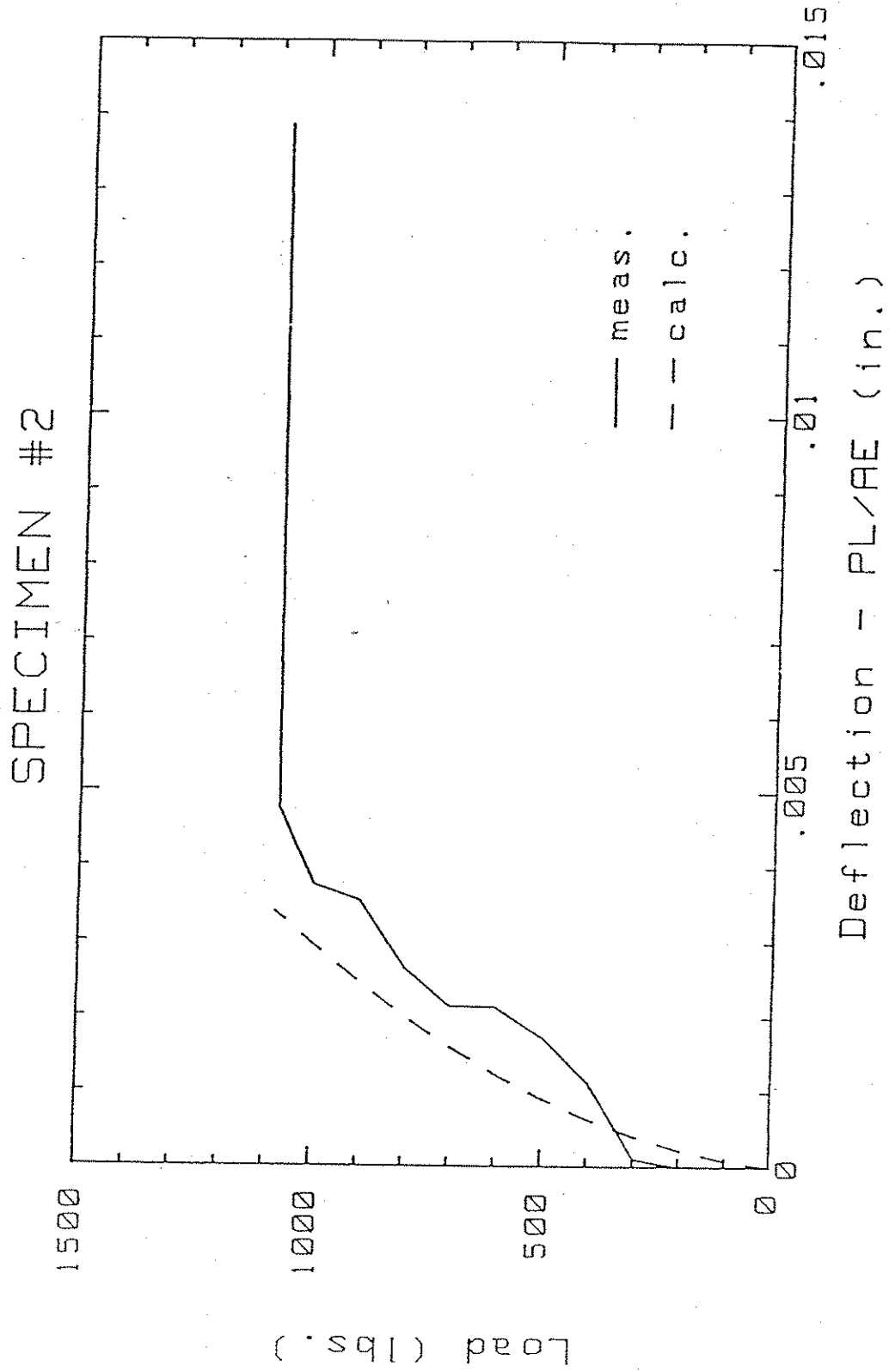


Fig. 4.7(b) Measured and Computed Load vs. Elongation, Push-out Specimen #2.

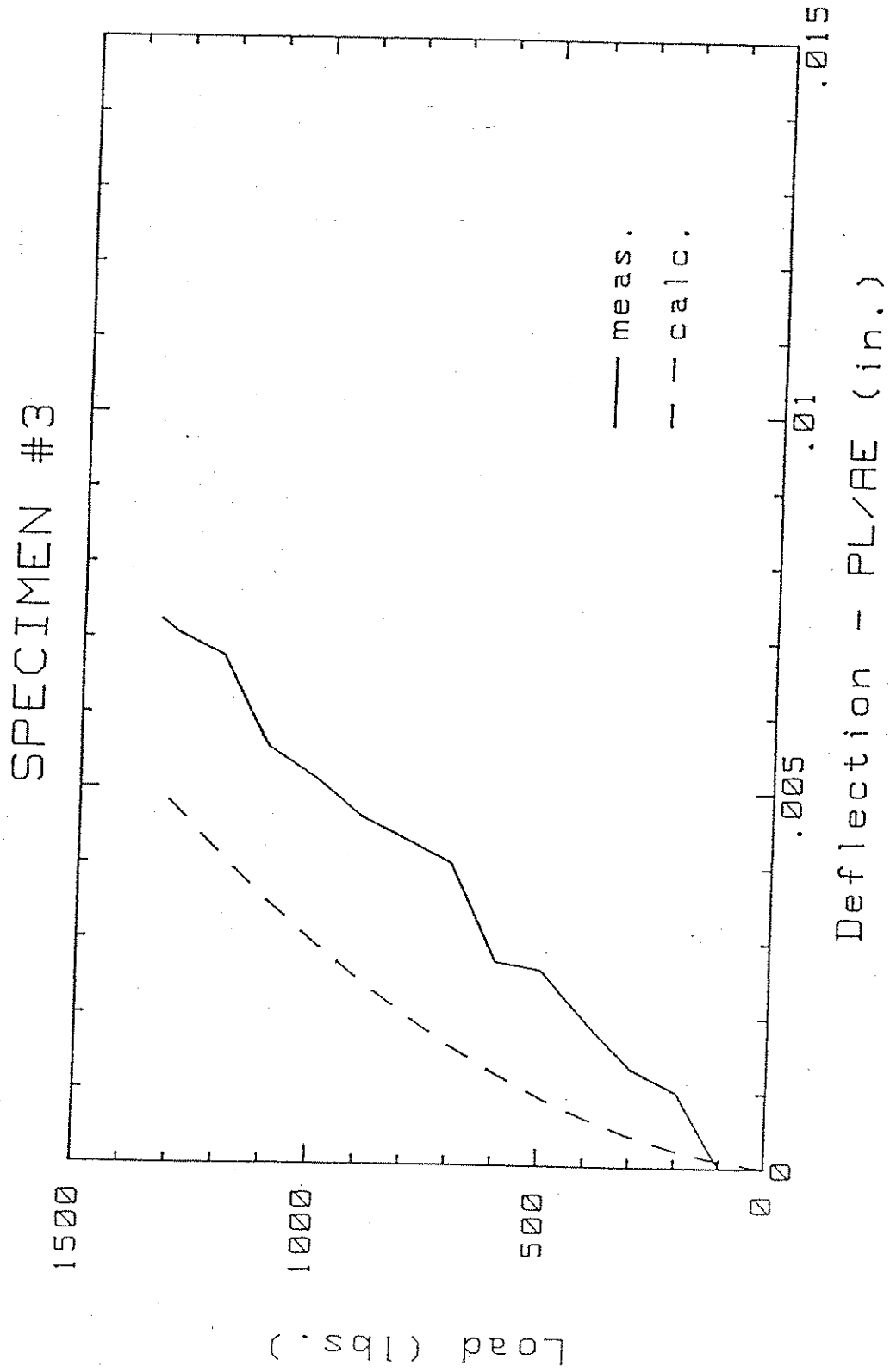


Fig. 4.7(c) Measured and Computed Load vs. Elongation, Push-out Specimen #3.

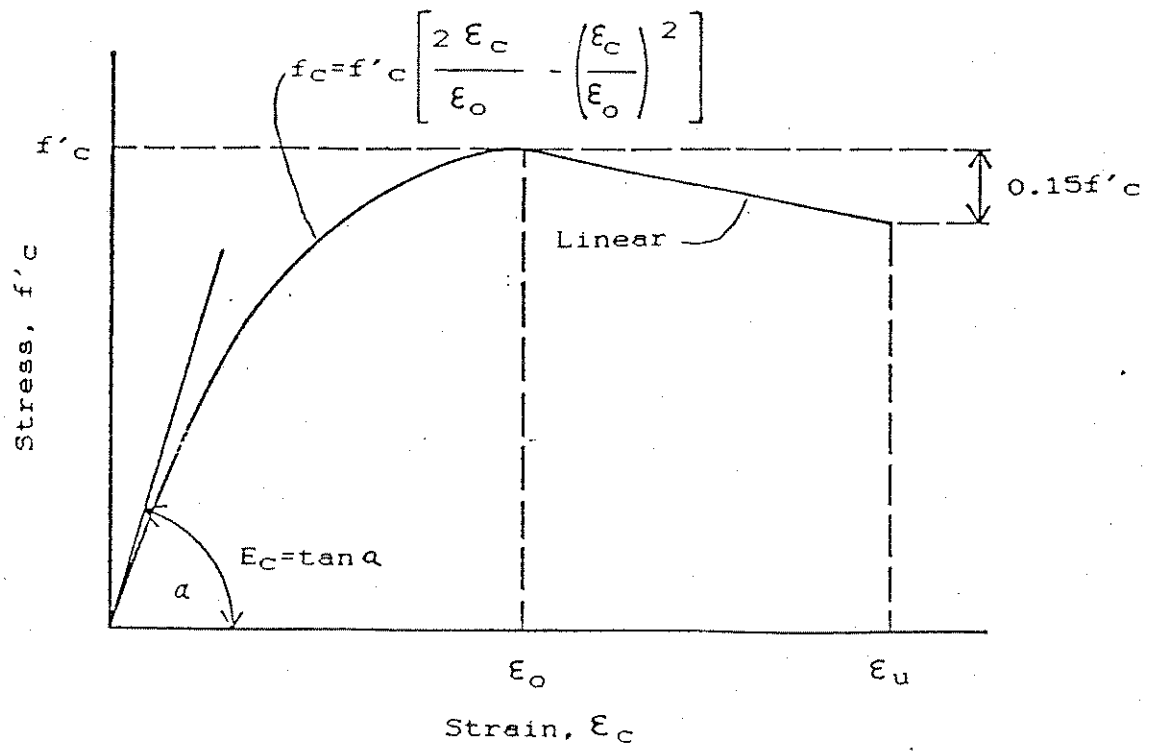


Fig. S.1 Idealized Stress-Strain Curve for Concrete [12].

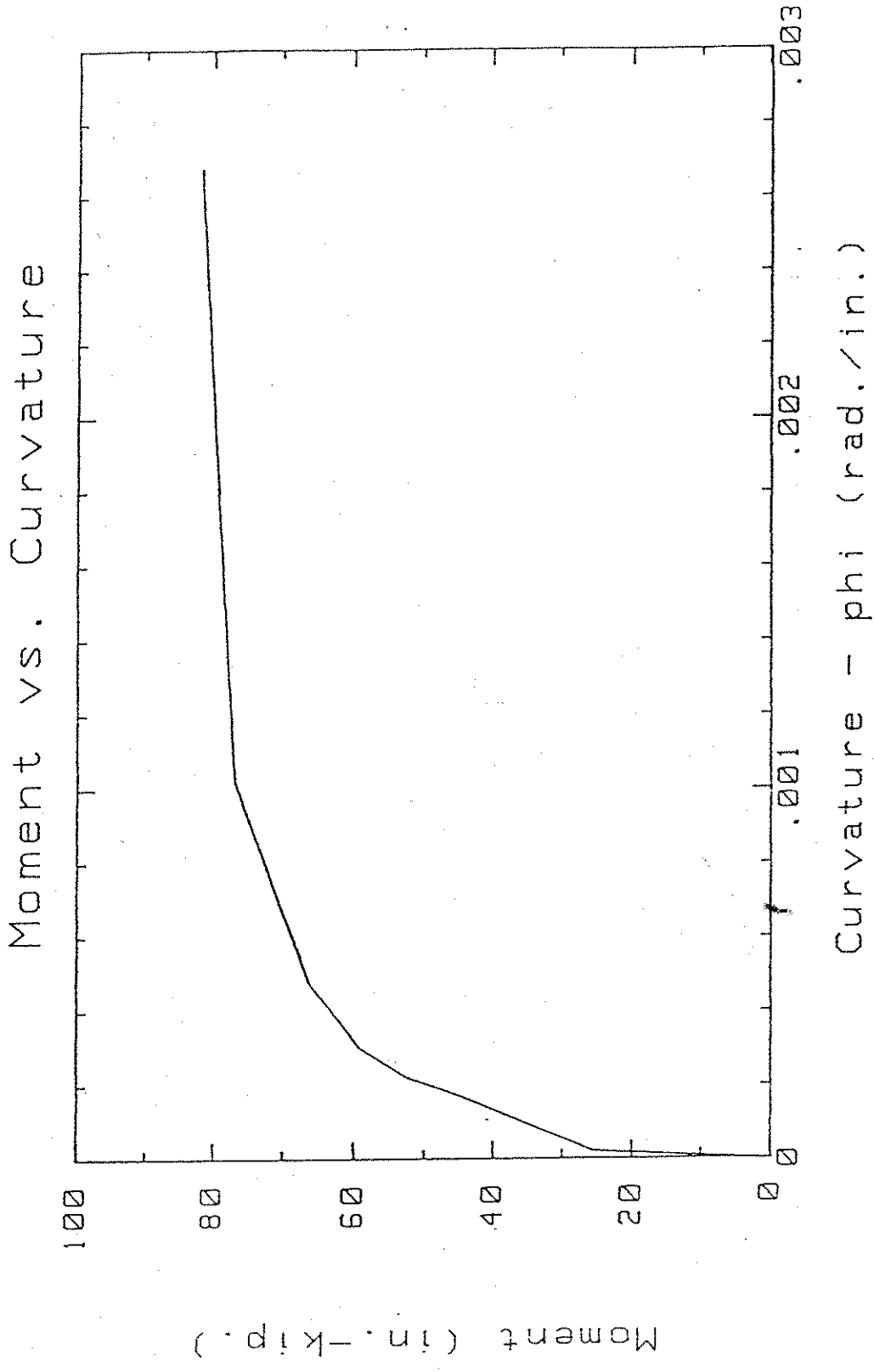


Fig. 5.2 Moment-Curvature Diagram of 2"X12" Section.

Dowel Action

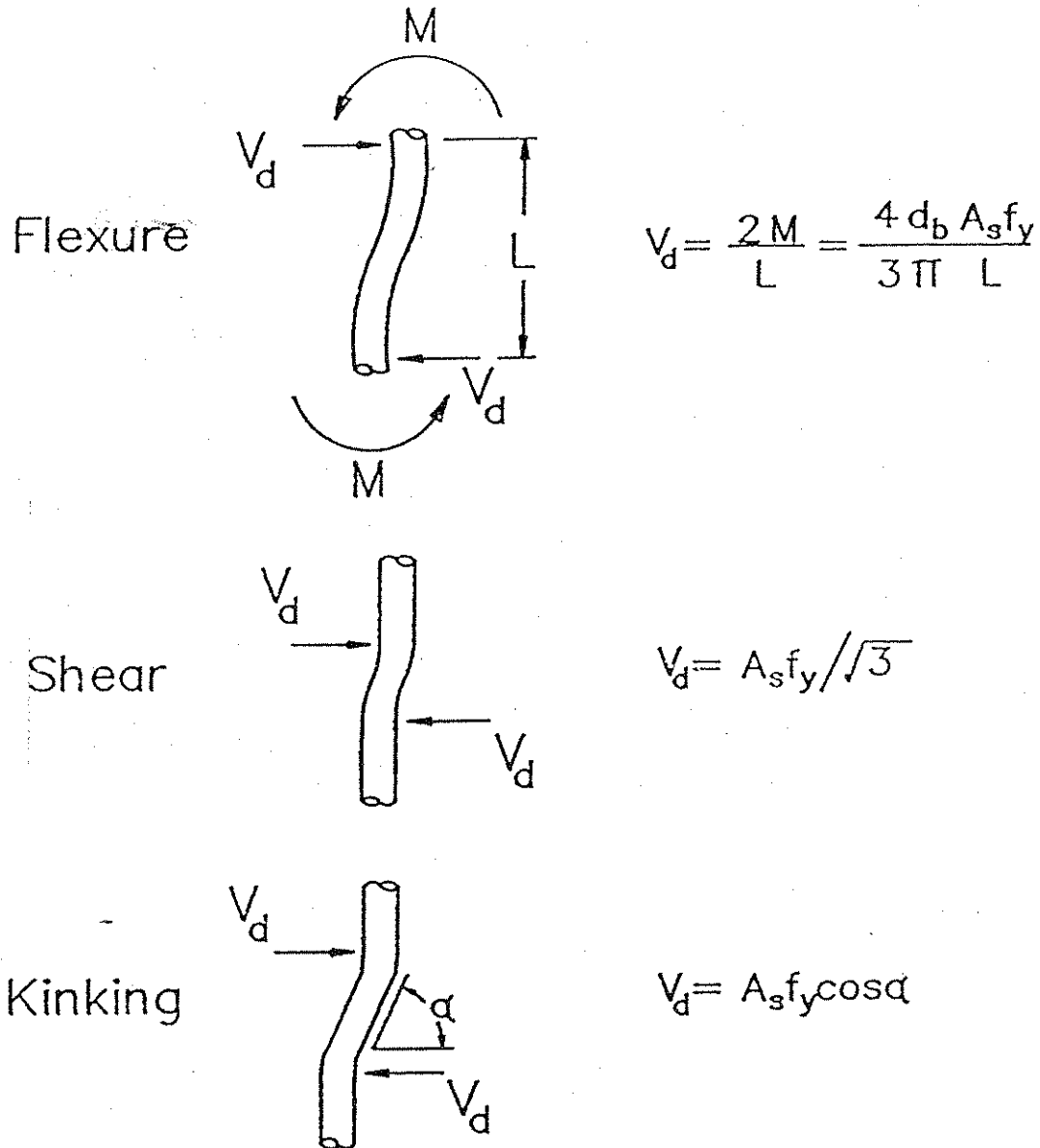


Fig. 5.3 Mechanisms for Dowel Shear.

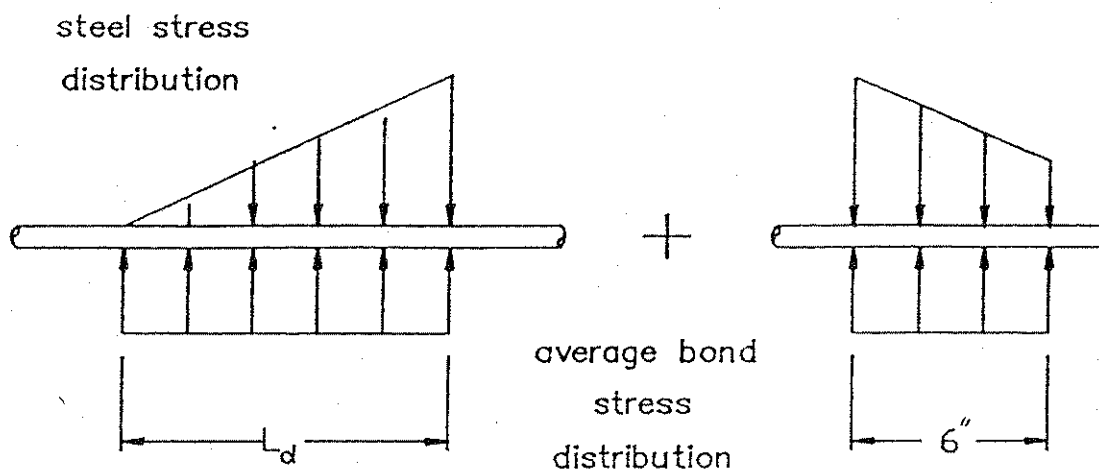


Fig. 5.4 Idealized Bond Stress Distribution for Hinged Specimens.

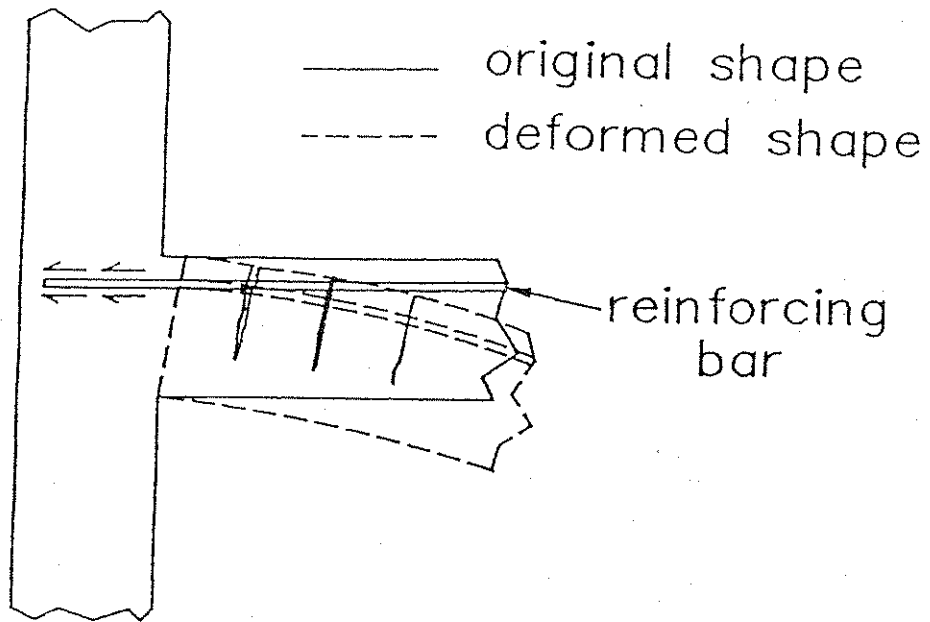


Fig. 5.5 Bar Slip Mechanism in a Typical Reinforced Concrete Beam Element.

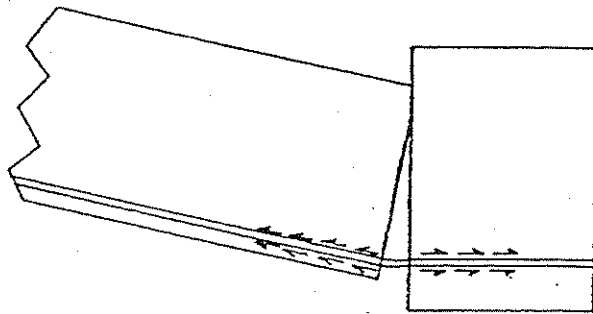


Fig. 5.6 Assumed Bar Slip Mechanism in Hinged Specimens.

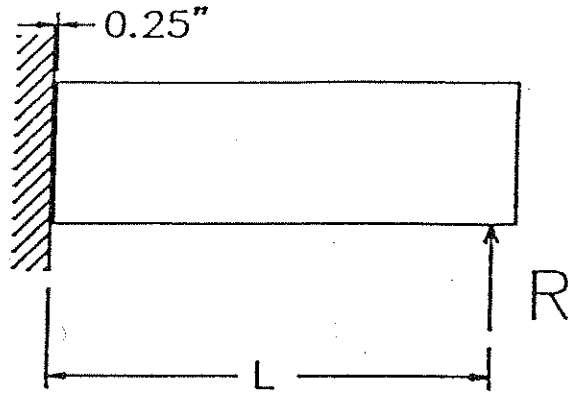


Fig. 5.7 Cantilevered End Element.

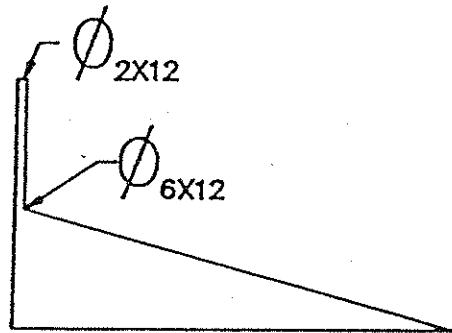


Fig. 5.8 Idealized Curvature Distribution Along the Cantilevered Element.

APPENDIX A

MIX DESIGN [18]

Estimated weights for one cubic yard of concrete were:

Coarse Aggr. (est. 2 % MC)	156 lb/yd ³
Cement	632 lb/yd ³
Coarse Aggr. (est. 2 % MC)	1459 lb/yd ³
Fine Aggr. (est. 6 % MC)	1534 lb/yd ³
	<hr/>
	3881 lb/yd ³

The above estimates were made using the Weight Method as outlined in Reference 18. The actual amount of water used varied slightly due to dry weather conditions, different aggregate moisture contents, and due to fine aggregates that were not completely washed.

APPENDIX B

MATERIAL PROPERTIES

CONCRETE PROPERTIES

		CH1	CH2	CH3	CH4
Compressive Strength, f'c (ksi)	End Element	6.03	5.18	4.97	5.12
	Middle Element	5.94	5.94	1.97*	1.97*
Slump (in.)	End	1-5/8	1-3/4	1	1-1/2
	Middle	1	1	1/2	1/2
Water/Cement	End	0.61	0.59	0.63	0.61
	Middle	0.6	0.6	0.59	0.59

The above concrete compressive strengths were taken at the time of testing.

Ratio of Cement: Fine Aggregate: Coarse Aggregate = 1.0:2.44:2.31 for all mixes.

* This appeared to be a bad cylinder. There were noticeable air voids in the concrete. The 28 day compressive strength was 2800 psi.

STEEL PROPERTIES

Bar Diameter	0.0491 in.
Yield Strength	43 ksi.
Ultimate Strength	55 ksi.
Modulus of Elasticity	29000 ksi.
Strain at Yielding	0.001483 in./in.
Strain at Ultimate	0.0124 in./in.

Stress-Strain Curve for Plain #2 Bar

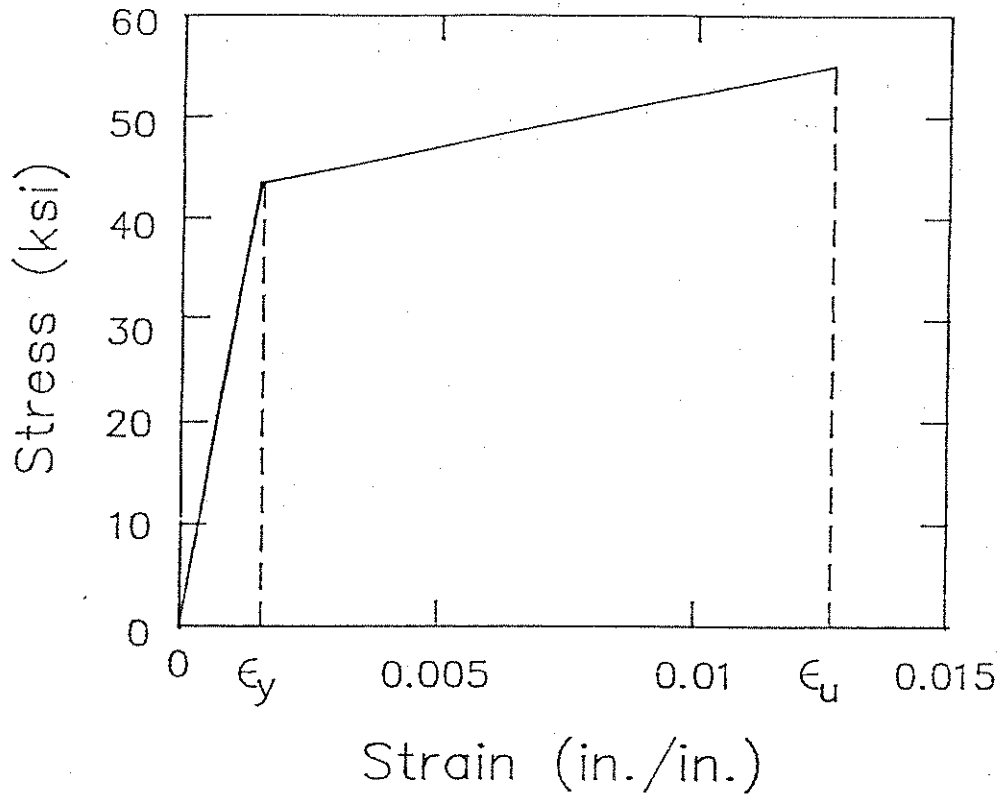


Fig. B.1 Idealized Stress-Strain Diagram for Grade 40 Plain #2 Bars.

APPENDIX C

INSTRUCTIONS FOR PROGRAM "AQUIREDAT"

AQUIREDAT is a general program for acquiring, storing, and processing data using a Hewlett Packard series 9000 computer and series 3000 data acquisition unit. The program is set up for collecting data from strain gages, Celesco displacement transducers, and linear variable differential transformers (LVDT's). The collected data is stored on a hard disk as the test proceeds and again after the test is completed. Processing involves plotting a hard copy plot of load versus displacement from a specified Celesco transducer and also includes on screen plotting of the remaining data such as load versus strain readings or load vs. LVDT readings. The program consists of a pre-processing unit, a processing unit, and a post-processing unit. Pre-processing involves inputting data for the measuring devices, such as, number of gages or gage factors. Information concerning plotting is also input in this portion. Processing involves triggering the system to take a voltage reading and converting this reading to strain or displacement. Also, the data is stored and presented to the user in the form of printed and plotted results. During the post-processing stage all of the data is stored and the user has the option of viewing on screen plotting of the final results. AQUIREDAT is designed such that the

operator controls when to trigger a single reading of the data and is not set up for continuous data scanning, such as would be required for a dynamic type of testing. ACQUIREDAT is written in Basic and comments are provided throughout the program to explain program operation and are identified by the symbol "!" which has the same function as a "REM" statement.

The following is a line by line explanation of "ACQUIREDAT" and is provided as an aid to further users. The line numbers are listed along with a brief explanation of the program's execution within these line numbers.

1-131

Contains comments concerning initial equipment set-up and basic program operation.

140-160

Necessary variables are dimensioned. The program is set up for 400 readings (i.e. 400 load increments). Storage space is provided for 20 strain gages, 4 LVDT's, and 5 Celesco displacement transducers.

280-300

The program starts by requiring the input of 3 data file names for storing data during testing. The first data file is the primary file and has all data pertaining to loads, strains, LVDT displacements, and Celesco displacements stored in it. It is important to note that this data

file is used by the program "PLOTTING" to plot results after execution of the program has been completed (i.e. Remember the name of the first file for further reference.).

310-610

This is an error trapping sequence. If a file is already present a new pathway and new file limits are created which means that the current file will be overwritten. Therefore, it is suggested that the user be aware of present files so that none are written over by mistake.

630-1160

The user is next asked a series of questions pertaining to the strain gages, LVDT's, and Celesco displacement transducers. Data that needs input is: channel numbers for each strain gage, LVDT, and Celesco. Gage factors for each strain gage including the full bridge load cell gage. The value for Poisson's ratio equals 0.29 and is used in the conversion of strain to load. Also the user needs to input the number of the Celesco displacement transducer that is to be used for the hard copy plot of load vs. displacement. In line 630 the user is asked to input the total number of strain gages in the system. This means include every strain gage that is hooked up and used in acquiring strain data. The program is currently set up for one full bridge gage on the load cell and this is hooked to channel #1. Strain can also be collected from two 1/4 bridge gages that are mounted on the load ram acting as

"mock" load cell. Line 640 asks for the number of load cell strain gages. This refers to the two gages attached to the loading ram and the strain in these gages is averaged and a load is computed in lines 1620-1670. Load from the load cell strain is computed in lines 1537 to 1542. It is assumed that the remaining strain gages are hooked up to reinforcing bars within the test specimen.

1160-1240

The total number of gages, number of load cell gages, number of LVDT's, and number of Celesco displacement transducers are stored.

1260

In line 1260 the HP-IB interface bus is initialized so that proper data communications can take place between the computer, peripherals, and data acquisition equipment. The following message will be displayed on the screen:

Equipment Present on Bus #7

3497A Mainframe	at address 09
3456A Digital Voltmeter	at address 22
3437A System Voltmeter	at address 24
System Computer	at address 21
System Printer	at address 01

1270-1360

Moments later the unstrained bridge imbalance to

excitation voltage ratio, and excitation voltage are read for each strain gage and the results are printed on the printer.

1400

The user is now asked for plotting information. In line 1400 subprogram "Plotter_i" is called and the user is asked for plot information pertaining to the Load vs. Celesco displacement plot on the HP 7470A two pen plotter. The user is asked to input the graph title, x and y plot axis limits, and number of major and minor tick marks. The plot axis limits refer to the minimum and maximum load and displacement limits. After inputting the required data the plot axes will be drawn and the graph will be labeled.

1410

The subprogram "Printerin" is then called in line 1410 and asks for plot information for an on screen plot. Plot axis limits and tick marks are required along with Viewport limits. Viewport limits define a subset of the screen in which plotting takes place. These limits can range from 0 to 1.0 but the user should limit the range to $0.1 \leq \text{LIMIT} \leq 0.9$. This allows room for labeling of the plot.

1450-1490, 1900, 2250

The user is now set to start acquiring test results. In line 1450 the user is asked "Do you want to end the test (Y/N) ?". If at this point there is something wrong with the test the user can stop (type "Y"). The data files will

be accessed and a message "YOU HAVE JUST COMPLETED THE TEST" and a question "Do you want to see any other plots (Y/N) ?" will be displayed. Type in the answer "N" and the message "<<<<<< ALL INFORMATION PROCESSING IS COMPLETED >>>>>>" will be displayed indicating that the program execution is finished. Simply press the RUN key to start the test over again. If after the question "Do you want to end the test (Y/N) ?", the user wants to continue, type in "N" and the message "APPLY STRAIN THEN CONTINUE" will be displayed. This is the indication to apply a load to the test specimen. When ready to take readings press the CONTINUE key to read strain in all of the gages.

1680-1780

Next, the LVDT readings are taken by calling the subprogram "Lvdt" in line 1680 and the Celesco displacement readings are taken by calling the subprogram "Displtrans" in line 1720. The results are then printed out by calling the subprogram "Dataprint" in line 1780. These printed results can aid the user in defining plot limits for on screen plotting of the results.

1800

In line 1800 the subprogram "Printplot" is called. It gives the user a choice of six different types of plots: (1)-Load vs. Celesco, (2)-Load vs. Strain, (3)-Load vs. Lvdt, (4)-Lvdt vs. Strain, (5)-Strain vs. Celesco, (6)-Lvdt vs. Celesco. The user is instructed to input the corre-

sponding number of the type of plot he or she would like to see and the number of the particular strain gage, LVDT, or Celesco which is to be plotted. An appropriate title and x and y axis labels are automatically chosen. The user is then asked about changing plot limits, including Viewport limits, min. and max. limits, and tick marks. After the limits are input the plot is displayed on the screen for 5 seconds. The time limit that the plot is displayed can be increased or decreased by changing the delay in line 4590.

1810-2250

When the plotting screen is cleared the user is asked "Do you want to see any other plots (Y/N) ?". If "Y" the plotting sequence is repeated, if "N" the subroutine "Plotrplot" is called in line 1850 and load vs. Celesco data is plotted on the plotter and then information is stored in the second and third files. When the disk drive light goes off indicating data storage is finished, the program execution goes back to line 1450 to ask the user "DO YOU WANT TO END THE TEST (Y/N) ?". If "Y", program execution jumps to line 1900 and all load, strain, LVDT, and Celesco data is stored in the first file. The message "YOU HAVE JUST COMPLETED THE TEST" is displayed and the final plotting portion of the program is implemented. If "N", then the data acquiring and displaying portion is again repeated.

2290-7850

The remaining portion of the program consists of the various subroutines and user defined functions that are used during program execution. These routines are listed along with corresponding line numbers and explanations of the routines that have not already been described.

2290-2800

Subroutine Plotter_i

2820-2940

Subroutine Printerin

2960-4670

Subroutine Printplot

4690-4830

Subroutine Lvdt. In line 4760 a voltage measurement for the LVDT is taken using the user defined function DEF FNDcv. The voltage is converted to displacement by dividing the voltage by an appropriate calibration factor determined from previous calibration of the LVDT.

4870-4980

Subroutine Displtrans. In line 4920 the voltage of the Celesco transducer is determined using user defined function FNDcv. This voltage is converted to displacement by multiplying by 2 volts/in. and subtracting the initial starting displacement.

5000-5150

Subroutine Plotrplot

5170-5460

Subroutine Datastore. As the test proceeds data is stored in data files 2 and 3 after each load increment.

5480-5800

Subroutine Dataprint. A hard copy of the data is printed on the Thinkjet printer after each load increment.

5801-6450

Subroutine Init. All of the system voltmeters are initialized and the HP-IB interface bus is cleared for transfer of data from the controller to the computer. This portion of the program initializes the HP-IB, assigns device names to select codes, and lists the instruments connected to the HP-IB with their address.

6452-6770

Subroutine Brmeas. Performs a strain gage bridge measurement. This program is used in conjunction with the user defined function DEF FNStrain to perform a complete strain gage measurement and calculation of strain. The subroutine Brmeas is called once before stress is applied to the gage. After stress is applied to the gage, Brmeas is called again for a second set of measurements. This information is passed to DEF FNStrain to calculate the strain.

6771-6930

User defined function DEF FNStrain.

6940-7840

Subroutine Warn. This is a subroutine for detecting errors. A common error that occurs is when a strain gage fails during testing. In this case a strain value of 9.E+19 will be recorded and an error message will be printed out. This message is printed only once when the gage initially fails. Any remaining strain readings from the failed gage will have a value of 9.E+19. It is important to note that this error will not halt program execution.

For additional information concerning the programming statements and subroutines used in the program "AQUIREDAT", the user is asked to refer to the Hewlett-Packard Basic programming manuals [8] and the HP Data Acquisition Control System Library [9].

APPENDIX D

NOTATION

a	depth of rectangular stress distribution from compression face
A_s	area of reinforcement
A_v	area of shear reinforcement
b	width of compression face of member
C	compression force within the compression zone
d	distance from the extreme compression fiber to the centroid of tension reinforcement.
d_b	diameter of the tensile and compressive reinforcement.
e	steel elongation
E_s	modulus of elasticity of steel
f'_c	measured compressive strength of concrete
f_s	steel stress
f_y	steel yield stress
h	overall depth of the section
k	general ratio of neutral axis distance measured from compression face to the effective depth, d
l or L	span length measured from the center of the support to the hinge face
l_d	development length
P	applied load
u	average bond stress
V_d	dowel shear strength of reinforcing bar
V_n	nominal shear strength
x	distance from compression face of section to neutral axis

B_1	ratio a/x ; depth of rectangular stress distribution to the depth to the neutral axis
δ	displacement at centerspan
ϵ_c	strain of concrete
ϵ_u	ultimate strain of concrete
θ_s	rotation due to bond slip
θ_y	rotation at yielding
λ	correction factor related to unit weight of concrete. = 1.0 for normal weight concrete.
ϕ_y	yield curvature
μ	coefficient of friction
μ	displacement ductility factor. $u = \delta / \delta_y$

APPENDIX E

LIST OF CCEER PUBLICATIONS

Report No.	Publication
CCEER-84-1	Saiidi, Mehdi and Rene A. Lawver, "User's Manual for LZAK-C64, A Computer Program to Implement the Q-Model on Commodore 64," Civil Engineering Department, Report No. CCEER-84-1, University of Nevada, Reno, January 1984.
CCEER-84-2	Douglas, Bruce M. and Toshio Iwasaki, "Proceedings of the First USA-Japan Bridge Engineering Workshop," held at the Public Works Research Institute, Tsukuba, Japan, Civil Engineering Department, Report No. CCEER-84-2, University of Nevada, Reno, April 1984.
CCEER-84-3	Saiidi, Mehdi, James D. Hart, and Bruce M. Douglas, "Inelastic Static and Dynamic Analysis of Short R/C Bridges Subjected to Lateral Loads," Civil Engineering Department, Report No. CCEER-84-3, University of Nevada, Reno, July 1984.
CCEER-84-4	Douglas, B. "A Proposed Plan for A National Bridge Engineering Laboratory," Civil Engineering Department, Report No. CCEER-84-4, University of Nevada, Reno, December 1984.
CCEER-85-1	Norris, Gary M. and Pirouze Abdollaholiaee, "Laterally Loaded Pile Response: Studies with the Strain Wedge Model," Civil Engineering Department, Report No. CCEER-85-1, University of Nevada, Reno, April 1985.
CCEER-86-1	Ghusn, George E. and Mehdi Saiidi, "A Simple Hysteretic Element for Biaxial Bending of R/C Columns and Implementation in NEABS-86," Civil Engineering Department, Report No. CCEER-86-1, University of Nevada, Reno, July 1986.
CCEER-86-2	Saiidi, Mehdi, Renee A. Lawver, and James D. Hart, "User's Manual for ISADAB and SIBA, Computer Programs for Nonlinear Transverse Analysis of Highway Bridges Subjected to Static and Dynamic Lateral Loads," Civil Engineering Department, Report No. CCEER-86-2, University of Nevada, Reno, September 1986.
CCEER-87-1	Siddharthan, Raj, "Dynamic Effective Stress Response of Surface and Embedded Footings in Sand," Civil Engineering Department, Report No. CCEER-86-2, University of Nevada, Reno, June 1987.

-2-

- CCEER-87-2 Norris, Gary and Robert Sack, "Lateral and Rotational Stiffness of Pile Groups for Seismic Analysis of Highway Bridges," Civil Engineering Department, Report No. CCEER-87-1, University of Nevada, Reno, June 1987.
- CCEER-88-1 Orie, James and Mehdi Saiidi, "A Preliminary Study of One-Way Reinforced Concrete Pier Hinges Subjected to Shear and Flexure," Civil Engineering Department, Report No. CCEER-87-3, University of Nevada, Reno, December 1987.